Viscoelastic Properties of Symmetric Poly(styrene-b-2-vinylpyridine)s in the Disordered and Ordered States

方, 龍

https://doi.org/10.15017/1398399

出版情報：九州大学, 2013, 博士（工学）, 課程博士
バージョン：

Viscoelastic Properties of Symmetric Poly(styrene-*b*-2-vinylpyridine)s in the Disordered and Ordered States

Long Fang

Department of Molecular & Material Sciences

Interdisciplinary Graduate School of Engineering Sciences

Kyushu University

Contents

Chapter 1 Introduction

1.1 Structure and Physical Properties of Block Copolymers

1.1.1 Definition and Synthesis of Block Copolymers

A block copolymer is a copolymer formed when the same monomers cluster together and form “blocks” of repeating units. For example, a polymer made up of X and Y monomers joined together like:

-Y-Y-Y-Y-Y-X-X-X-X-X-Y-Y-Y-Y-Y-X-X-X-X-X-

is a block copolymer where –Y-Y-Y-Y-Y- and –X-X-X-X-X- groups are the blocks. Each block is long enough to be regarded as a polymer.

The architecture of copolymers can be controlled by the synthesis procedure, and it is possible to prepare diblock, triblock, multiblock, star block and graft copolymers as shown in Figure 1-1. The architectures seem to be limitless depending on chemist’s imagination. Here, we just give some examples which have been widely investigated by many researchers.

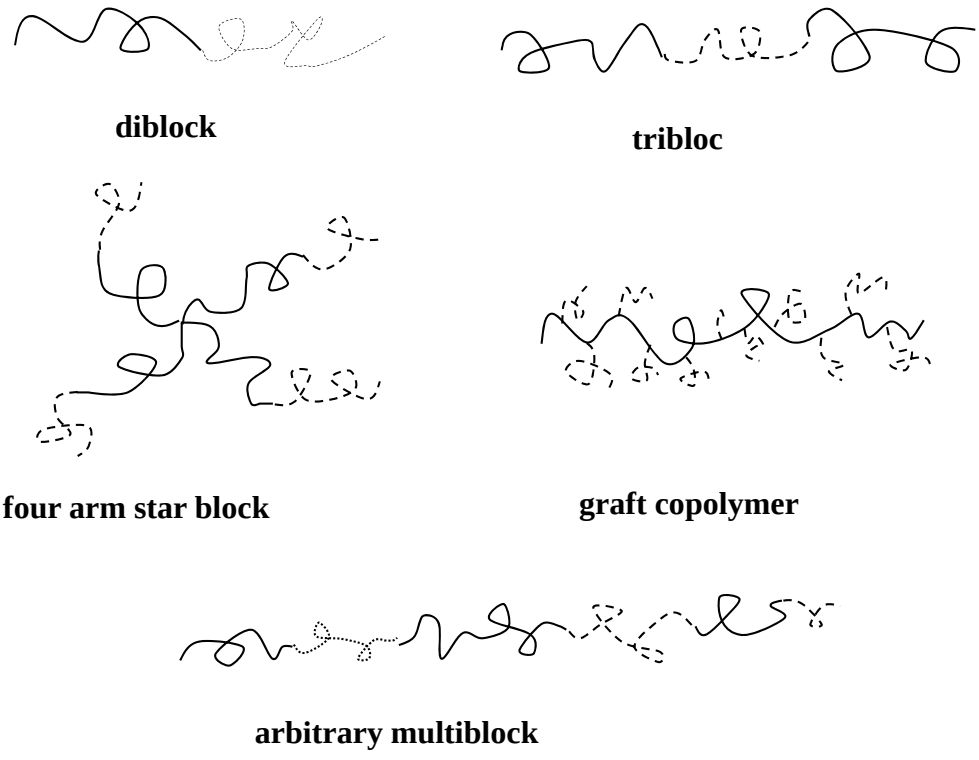

Figure 1-1 Some block copolymer architectures

Block copolymers can be polymerized by various types of polymerization methods. To obtain well characterized block copolymers with narrow molecular weight distribution, best way is to utilize living polymerization of anionically reactive polymers. In the living anionic polymerization, the polymer grows by addition of monomers to the living anionic chain end. The first anionic block copolymerization was achieved as early as the 1950s [1]. Industrially, block copolymers such as triblock copolymers of polystyrene-polybutadiene-polystyrene (PS-PB-PS, known as SBS), which are used as synthetic rubbers, are prepared by anionic polymerization [2]. The most common class of copolymer in terms of tonnage produced is the styrenic copolymers, largely PS-PB-PS and PS-PI-PS triblocks, where PI denotes polyisoprene. Copolymers containing poly(ethylene oxide) and poly(propylene oxide) or poly(butylene oxide) are extensively used as surfactants.

1.1.2 Melt Phase Behavior of Block Copolymers

Block copolymers in the melt state can self assemble into a variety of ordered structures via the process of so-called microphase separation when temperature is

reduced as shown Figure 1-2 [3-13], which is called as order-disorder transition (ODT). Concerning the length scale of the ordered structure, it is appropriate to call as nanophase separated structure as used in recent papers. Nanophase separation is driven by the enthalpy of demixing of the constituent components of the block copolymers, while macrophase separation is prevented by the chemical connectivity of the blocks. This enthalpy is proportional to the Flory-Huggins segmental interaction parameter χ, which is found to be inversely proportional to temperature T, and is usually parameterized as $\chi = A/T + B$ [14], where A and B are constants. The entropy penalty associated with the chain stretching is proportional to the degree of polymerization N. The product χN that expresses the enthalpy-entropy balance is then used to parameterize block copolymer phase behavior, along with the composition of the copolymers ϕ [15]. Depending on the degree of incompatibility χN, two regimes can be identified: the weak segregation regime (WSR) corresponding to χN close to $(\chi N)_{ODT}$ and the strong segregation regime (SSR) extending to high incompatibility. In the WSR, the composition profile is essentially sinusoidal whereas components are essentially pure and the interphase between them is narrow in the SSR [16].

Symmetric diblock copolymers form a lamellar phase with alternating layers of the constituent blocks. For more asymmetric copolymers it becomes energetically more favorable for phases with curved interfaces to form, including gyroid, cylinder and sphere as shown in Figure 1-3 [17-22]. $(\chi N)_{ODT}$ shows the lowest value 10.5 for symmetric diblock copolymers and lamellar ordered structure will form when χN>10.5 [19]. For asymmetric diblock copolymers, however, $(\chi N)_{ODT}$ becomes larger as diblock copolymers change from symmetric to asymmetric. Furthermore, order-order transition (OOT) occurs among different ordered structures for asymmetric diblock copolymers [23-28]. On the other hand, gyroid structure can be formed only in a very narrow composition region and χN region near ϕ = 0.4 [19], while it is only observed for a few cases experimentally.

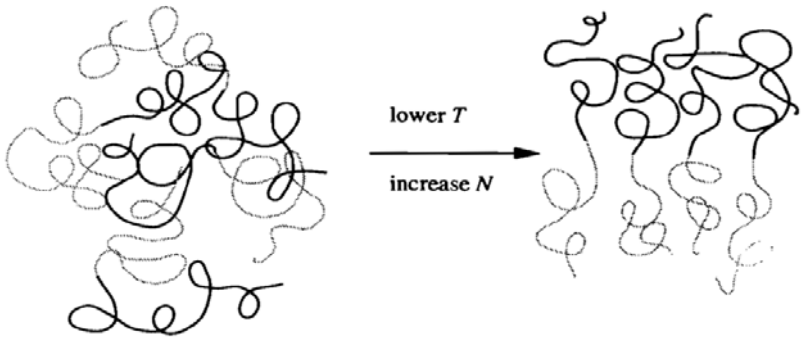

Figure 1-2 Nanophase separation in a block copolymer melt

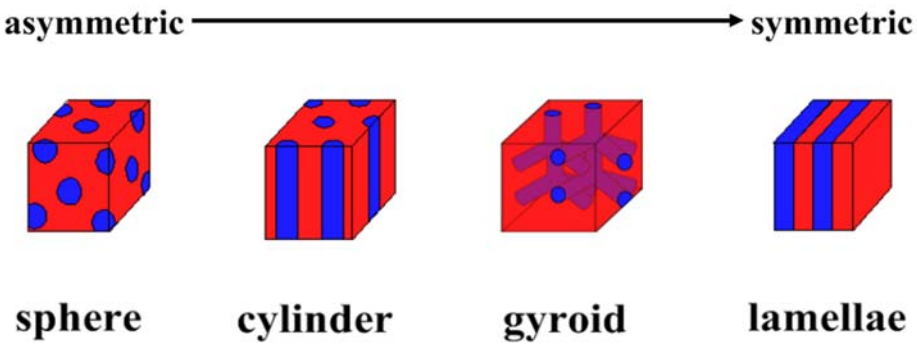

Figure 1-3 Different ordered structures for diblock copolymers via the nanophase separation as a function of the component composition ϕ.

1.1.3 Experimental Studies of Phase Behaviors

The ordered structures of the block copolymers can be determined by experimental methods such as small-angle X-ray scattering (SAXS), small-angle neutron scattering (SANS) [29-36] and transmission electron microscopy (TEM) [37-42]. It is possible to assess the ordered structures of block copolymers just from SAXS or SANS powder pattern if enough reflections are sampled for the pattern to be indexed unambiguously. TEM is useful because it provides a direct picture of the morphology, though it only probes very small area of the sample. Dynamic mechanical analysis (DMA) [43-46] can be used to locate order-order and order-disorder phase transition, but not to unambiguously identify the structures. However, the low frequency dynamic shear moduli sometimes can provide an indication of the type of structures for bulk samples. Therefore, combination of different experimental assessments is needed to

identify the structure unambiguously. General points of the above mentioned methods are summarized below.

SAXS and SANS are ideal for the investigation of morphology of ordered phases in block copolymer melts, solids and gels because length scales probed are typical of those of block copolymer microstructures, i.e. 1-100 nm. In contrast to TEM, the structure of the sample averaged over macroscopic size of the beam is probed. Scattering data are presented as a function of the scattering vector $\boldsymbol{q}$ or its magnitude:

$$q = |q| = \frac{4\pi \sin\theta}{\lambda} \tag{1.1}$$

The relative positions of a sufficient number of reflections arising from microstructural periodicities enable unambiguous identification of morphology. For example, in an oriented lamellar phase with the beam incident parallel to the layers, Bragg reflections at q^*, $2q^*$, $3q^*$,…, where q^* is the first order reflection, are observed along a direction parallel to the layer normal.

SAXS is appropriate where the electron density contrast between blocks is sufficient for the polymer to diffract X-rays [47]. SANS is valuable for studies of polymer structure because of the opportunity for contrast variation via isotope labeling [48]. Typically, hydrogen atoms are selectively replaced by deuterium with changing the scattering contrast, which can be used to obtain information on chain conformation in block copolymer melts or intramicellar structure in block copolymer solutions [49].

The most direct method for the investigation of block copolymer morphology is TEM. In this technique a thin section of block copolymer or a solvent-cast film is first microtomed. For soft samples, ultrathin sections are obtained at low temperatures (typically -100 ^{o}C), via cryo-ultramicrotoming (i.e. slicing of the sample at low temperature). Contrast between rubbery and glassy components in the section is then achieved by exposing the sample to osmium tetraoxide vapour, which selectively stains the rubbery component [50, 51]. In polyolefin diblock copolymers containing poly(ethylene) it has recently been shown that ruthenium tetraoxide (RuO_4) can be used as a staining agent, and the amorphous component (e.g. poly(ethylethylene) or

poly (ethylene-propylene)) is selectively stained due to reduced diffusivity of RuO_4 in the semicrystalline microdomains [52]. However, the disadvantages of TEM are that misidentification of morphology is possible based on inspection of only a projection of a small region of the sample [53-55]. Difficulty in the preparation of the sample is also a disadvantage.

The flow properties of block copolymer melts depend on the state of order in the system, which has been exploited to locate the ODT. For homopolymers, terminal region behavior (storage modulus, $G' \sim \omega^2$ and loss modulus, $G'' \sim \omega^1$) is observed at high temperature, where ω is frequency. For block copolymers in the ordered state, however, above terminal region behavior cannot be observed due to the presence of ordered structures. By the difference, it has been revealed that there is a sharp decrease in both G' and G'' at the ODT by temperature sweep measurements at a fixed frequency [43-46]. Of course, OOT can be also observed by temperature sweep measurements.

Large scale responses from reorientation and deformation of multigrain dominate at lower frequency end and frequency dependence behaviors depend on multigrain types. Due to these large scale structural heterogeneity and component heterogeneity, viscoelastic behaviors of block copolymers in the ordered state become very complicated [56-62], even for the simplest diblock copolymers. To overcome the above problem, block copolymers with components having almost same thermo rheological properties are needed. Poly(styrene-*b*-2-vinylpyridine) (SP) is such kind of model polymer since polystyrene (PS) and poly(2-vinylpyridine) (P2VP) have almost same thermo rheological properties. Direct comparison of viscoelastic properties between SP and corresponding PS homopolymers become possible and such study will elucidate dynamics of block copolymers. Characterization features of SP copolymers are summarized in next section.

1.2 Physical Properties of Poly(styrene-*b*-2-vinylpyridine)s

1.2.1 Physical Properties of Poly(2-vinylpyridine)

Table 1-1 Critical molecular weights and limiting values of J_e and G_N^0 at 160 °C

	M_e	M_c	M_c'	J_e	G_N^0
P2VP	2.9×10^4	$3.5\text{-}4.5\times10^4$	$9\text{-}10\times10^4$	2.4×10^{-5}	$1.3_2\times10^5$
PS	1.8×10^4	$3.3\text{-}4.0\times10^4$	$13\text{-}14\times10^4$	1.9×10^{-5}	2.0×10^5

Dilute solution properties of poly(2-vinylpyridine) (P2VP) were studied by Matsushita *et al* [63-65] and it was reported that P2VP and polystyrene (PS) have almost the same Kuhn segment length and other physical properties. Viscoelastic properties of P2VP over a wide range of molecular weight (M) were studied in bulk and solution by Takahashi *et al* [66, 67]. It was found that the absolute values of zero shear viscosity (η^0) of P2VP in bulk and in α–chloronaphtharene (αCN) are practically the same as those of PS over whole experimental range of M. Glass transition temperature T_g and the temperature dependence of η^0 in bulk is also the same. It is concluded that among various polymers so far studied, P2VP and PS have very similar viscoelastic properties in both bulk and a good solvent (αCN), though the plateau modulus G_N^0 and J_e of P2VP are slightly different from those of PS as shown in Table 1-1 [66].

1.2.2 Polymerization Method of Poly(styrene-*b*-2-vinylpyridine)s

The poly(styrene-*b*-2-vinylpyridine)s (SP) diblock copolymers were prepared by anionic polymerizations [64, 65] in THF at -78 °C under high vacuum (10^{-5} mmHg) using break-seal method to add second monomer (P) in stepwise. Cumyl-K was used as an initiator and typical polymerization time was about 6 hrs for 100k dalton.

1.2.3 Phase Behaviors of SP Copolymers

Figure 1-4 shows the variations of morphologies of nanophase separated structures with the volume fractions of polystyrene block chain, ϕ_S, for the block and graft copolymers of different types determined by TEM and SAXS [68-74].

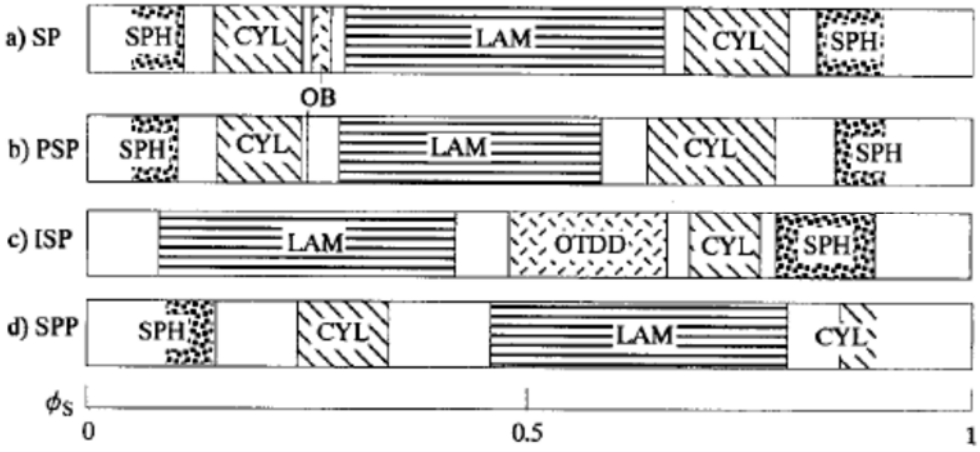

Figure 1-4 Variations of morphologies with compositions for the block and graft copolymers of different types. SPH: spherical structure, CYL: cylindrical structure, OB: ordered bicontinuous structure, LAM: lamellar structure, OTDD: ordered tricontinuous double diamond structure.

As shown in the figure, the typical morphologies such as spherical, cylindrical and lamellar structures appear for all types of copolymers. The appearances of these typical morphologies for diblock copolymers are well explained by the theories of nanophase separated structures in the strong segregation limit presented by Meier [75-77], Helfand *et al*. [78-81], Semenov [82], Kawasaki *et al*. [83, 84] The composition ranges of SP diblock and poly(2-vinylpyridine-*b*-styrene-*b*-2-vinylpyridine) (PSP) triblock copolymers are similar, reflecting the fact that PSP triblock copolymers are symmetric. In comparison with SP diblock or PSP triblock copolymers, the composition range of each structure shifts to the lower ϕ_S value and ordered tricontinuous structures identified as ordered tricontinuous double diamond (OTDD) structures appear in a wide range of composition for poly(isoprene-*b*-styrene-*b*-2-vinylpyridine) (ISP) triblock copolymers. On the other hand, the order of morphological change with composition is the same, but the

composition range of each structures shifts to the higher ϕ_S value for poly(styrene-*b*-2-vinylpyridine-*b*-2-vinylpyridine) (SPP) graft copolymers.

1.2.4 Chain Conformations of SP Copolymers

Chain conformations of block copolymers can be studied by intrinsic viscosity [85-92], light scattering [93-97], SANS [98, 99] measurements and Monte Carlo calculations [96-97, 100]. It is found that chain conformation of diblock copolymer does not differ much from that of homopolymer in dilute solutions by using viscosity, light scattering and Monte Carlo calculations. To examine nanophase separated structures at the molecular level, studies on the molecular weight dependence of lamellar domain size become of vital importance by SAXS and SANS. The lamellar domain sizes of SP copolymers D_{SP} is expressed by the following empirical equation [101, 102]:

$$D_{SP} = 0.0337 M_n^{0.64} \quad \text{(nm)} \tag{1.2}$$

The data are in good agreement with the theories of Helfand-Wasserman (eqs 1.3) [78-81] and Semenov (eq 1.4) [82] for lamellar domain sizes of AB diblock copolymers, D_{AB}.

$$-(2/6^{1/2})\chi^{1/2} bN + D_{AB} + (0.353/2^{1/4}) D_{AB}^{3.5} / (bN^{1/2})^{2.5} = 0 \tag{1.3a}$$

$$D_{AB} = 1.34 \chi^{1/7} bN^{9/14} \tag{1.3b}$$

$$D_{AB} = (4/6^{1/2})(3/\pi^2)^{1/3} \chi^{1/6} bN^{2/3} \tag{1.4}$$

Where b is the segment length, which is 0.68 nm for SP diblock copolymers, N is the degree of polymerization of block copolymer and χ is the interaction parameter, which is 0.073 for SP diblock copolymers [101].

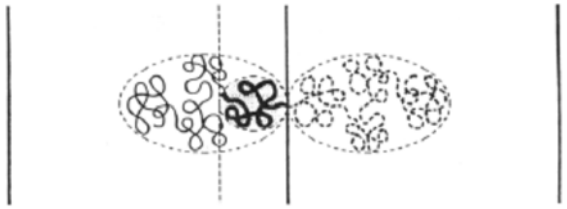

(a)

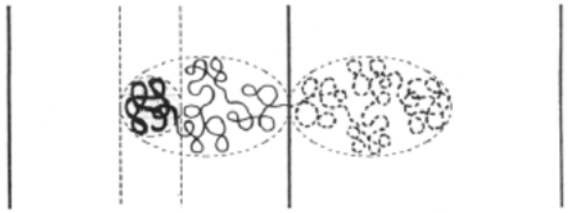

(b)

Figure 1-5 Schematic drawing of the chain conformations of parts of block chains from the edge-view: (a) a part of a chain adjacent to the junction point; (b) a part of a chain at the free end.

Moreover, the radii of gyration of a block chain along the directions parallel (x and z), R_{gx}(=R_{gz}) and perpendicular (y), R_{gy} to the lamellae can be obtained by SANS measurement from the film specimens perpendicular and parallel to incident beams, respectively, using the contrast matched samples [103]. The empirical equation of molecular weight dependence of radius of gyration of PS along any direction at unperturbed states is shown as follows:

$$R_{g0} = 0.0165M^{0.5} \quad \text{(nm)} \tag{1.5}$$

The empirical equations of R_{gx}(=R_{gz}) and R_{gy} for the S block chains of SP diblock copolymers are given by following equations [68, 102, 104]:

$$R_{gx} = R_{gz} = 0.0289M^{0.43} \quad \text{(nm)} \tag{1.6}$$

$$R_{gy} = 0.00453M^{0.64} \quad \text{(nm)} \tag{1.7}$$

As a result, block chains in lamellae are extended along the direction perpendicular to lamellae, while they are contracted along the parallel direction. The junction points between different block chains are localized near the interface between the domains, and they are contracted along the direction parallel to lamellae at the same extent as the whole block chain with the same molecular weight as shown in Figure 1-5(a), while chains at the free-ends of block copolymers are widely distributed within the lamellar domain with the distribution maximum at the center of domain and they are unperturbed as shown in Figure 1-5(b) [105-107]. Furthermore, the experimental distribution of chains at the free-ends of block polymers is well explained by the mean field theories of nanophase separated structure [105-106, 108-109].

1.3 Dynamics of Block Copolymers

In this section, important points of dynamics of block copolymers, which are closely related to this study, are summarized.

1.3.1 Viscoelastic Properties of Block Copolymers

The viscoelastic behaviors of polymeric liquids are strongly dependent on temperature. However, for non-associating flexible chains in homogeneous liquids, temperature dependence is nearly remarkably simple: linear viscoelastic functions translate parallel to the coordinate axes, expressed logarithmically, without changing shape. Moreover, shift along a modulus or compliance axis are usually so small as to be virtually undetectable. This behavior can be used to develop a master curve for the response being measured, greatly extending the span of coverage beyond what can be covered by measurements at a single temperature [110-114]. This is what called time temperature superposition (TTS) principle.

For non-entangled homopolymers, G' and G'' can be approximately expressed by Rouse like modes as shown in Figure 1-6 for PS (M_w=19.6K). For entangled homopolymers, master curves of G' and G'' show that plateau region appear in the intermediate frequency region followed by terminal region behavior at lower frequency end as shown in Figure 1-7.

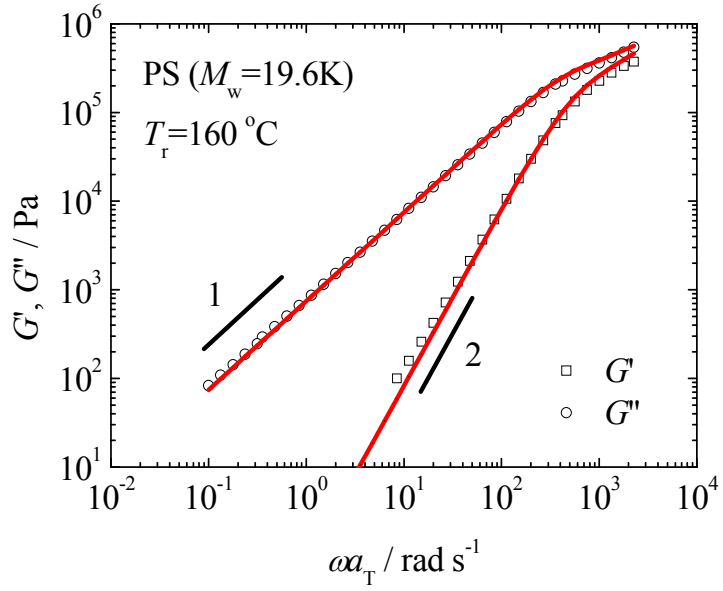

Figure 1-6 Viscoelastic properties of PS (M_w=19.6K) with Rouse fitting results at T_r = 160 °C

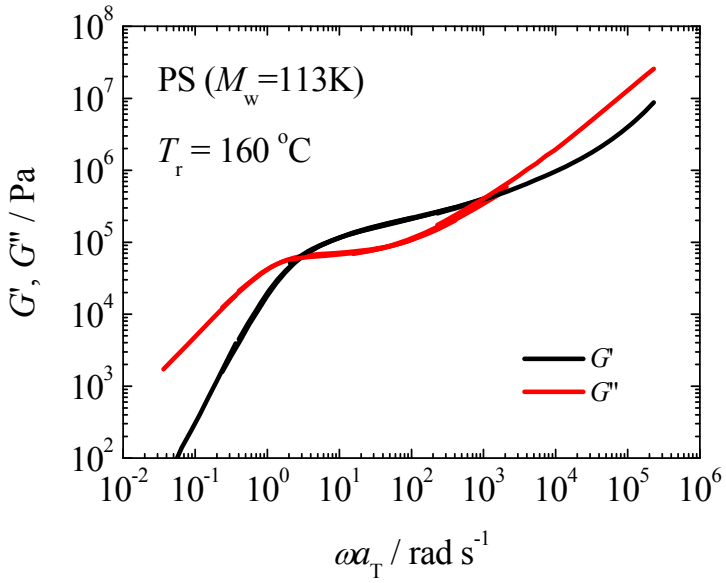

Figure 1-7 Master curve of viscoelastic properties for PS (M_w=113K) at T_r = 160 °C

For block copolymers, in the strong segregation regime, nanophase separated structure of block copolymers reaches equilibrium states in chain length scale. In the larger scale, however, the structure is randomly oriented multigrain structure which is dependent on thermal and flow history. These structural characters and the viscoelastic heterogeneity of components are the reasons for very complicated rheological properties of block copolymers. Relationships between structures and viscoelastic properties of block copolymers are also summarized in some review

articles [115-121]. Among these studies, it can be easily found that the situation is very complicated for the simplest case, i.e., diblocks. The storage modulus G' and the loss modulus G'' have a power law like frequency dependence at lower ω end:

$$G'(\omega) \sim G''(\omega) \sim \omega^{\alpha} \tag{1.8}$$

where α slowly changes between 0.3 and 0.7 in the frequency range of over 10 decades. This response is intermediate between that of a elastic liquid (with low frequency end behavior $G'(\omega) \sim \omega^2$ and $G''(\omega) \sim \omega^1$) and that of a solid with nonzero low frequency end ($G'(\omega) \rightarrow \text{const} \neq 0$ as $\omega \rightarrow 0$) as shown in Figure 1-8.

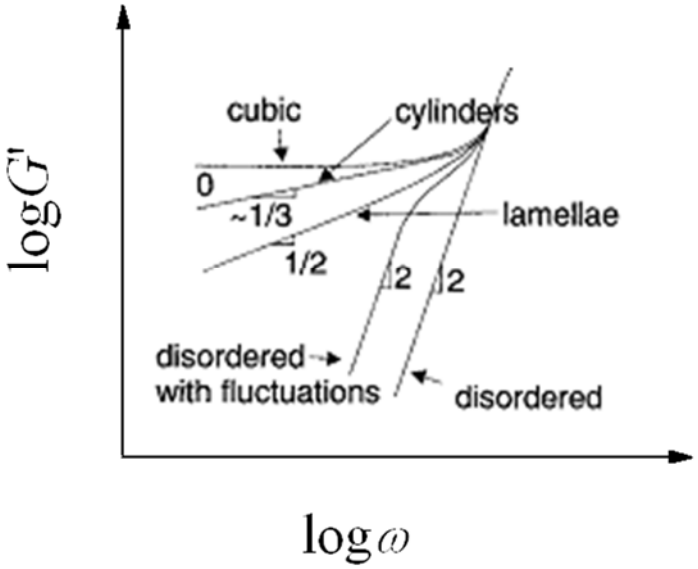

Figure 1-8 Power law like behaviors for block copolymers in the disordered and ordered states

Master curves cannot be generated by TTS due to thermo rheological heterogeneities between the component blocks. This point is revisited in section 1.3.2. On the other hand, power law like behavior at lower frequency end in Figure 1-8 are common to most ordered diblock samples.

There are two possible mechanisms of this anomalous behavior: microscopic and mesoscopic. It is believed that both are responsible for the power law like behavior for high molecular weight block copolymers, but in different frequency ranges. The microscopic mechanism of this unusual relaxation behavior is due to nontrivial disentanglement processes, while the mesoscopic mechanism is due to the

deformation and displacement of domains (lamellae, cylinders, spheres, etc.) [60].

The most well studied relationships between structure and rheology of block copolymers are those for lamellar forming diblock copolymers. In the quiescent disordered states, it is reported that the fluctuation effects are more pronounced on the viscoelastic properties than those on scattering data [32]. Both *G*' and *G*" are enhanced due to the fluctuation effects at lower ω, that is in terminal region. The enhancement by the fluctuation effects is more obvious for *G*' than *G*" [122, 123]. In a few studies, flow induced ordering are reported in the quiescent disordered states close to the ODT [124-126].

In the quiescent ordered states, *G*' and *G*'' show power law dependence (*G*', *G*" ~ $\omega^{1/2}$) at low ω end [32, 43, 122]. This behavior can be theoretically explained by the large scale motions of randomly oriented grains/defects [84] and/or by chain relaxation mechanism of entangled component polymers (chain retraction modes) [60]. It is observed that *G*' and *G*" values in the power law region become smaller when lamellae are preferentially aligned parallel and perpendicular to the flow direction in which lamellar normals are parallel to shear gradient and vorticity directions, respectively [127-132]. The effect of alignment is more pronounced in the latter case. When the structure is well aligned, ω dependencies of *G*' and *G*" become similar to those of uniform polymeric liquids.

It is widely considered that the relaxation perpendicular to lamellar plane is restricted in SSR, since energy cost of A block penetrating into B-rich domain should be comparable to entropy gain (~*kT*), and vice versa. For AB diblock copolymers in the non-entangled state in Figure 1-9(a), there is no entanglement between the chains from opposite brushes. In SSR, block A and B relax independently with Rouse like modes along the lamellar plane [133]. In the entangled state in Figure 1-9(b), however, entanglements not only occur between neighboring chains, but also the chains from the opposite brushes entangle with each other at the center of lamellar domains, referred as interpenetration zones. The thickness of interpenetration zones, ξ_A and ξ_B are estimated by eq. (1.9) [60]:

$$\xi_i/(2h_i) = 3^{-1/9}\pi^{2/9}(\chi N)^{-2/9} f_i^{-2/3}, \qquad i = \text{A or B} \tag{1.9}$$

Where h_i are the heights of brushes A or B, which can be estimated by eq. (1.10) [60]:

$$h_i = bf_i(8\chi/3\pi^4)^{1/6} N^{2/3}, \qquad i = \text{A or B} \tag{1.10}$$

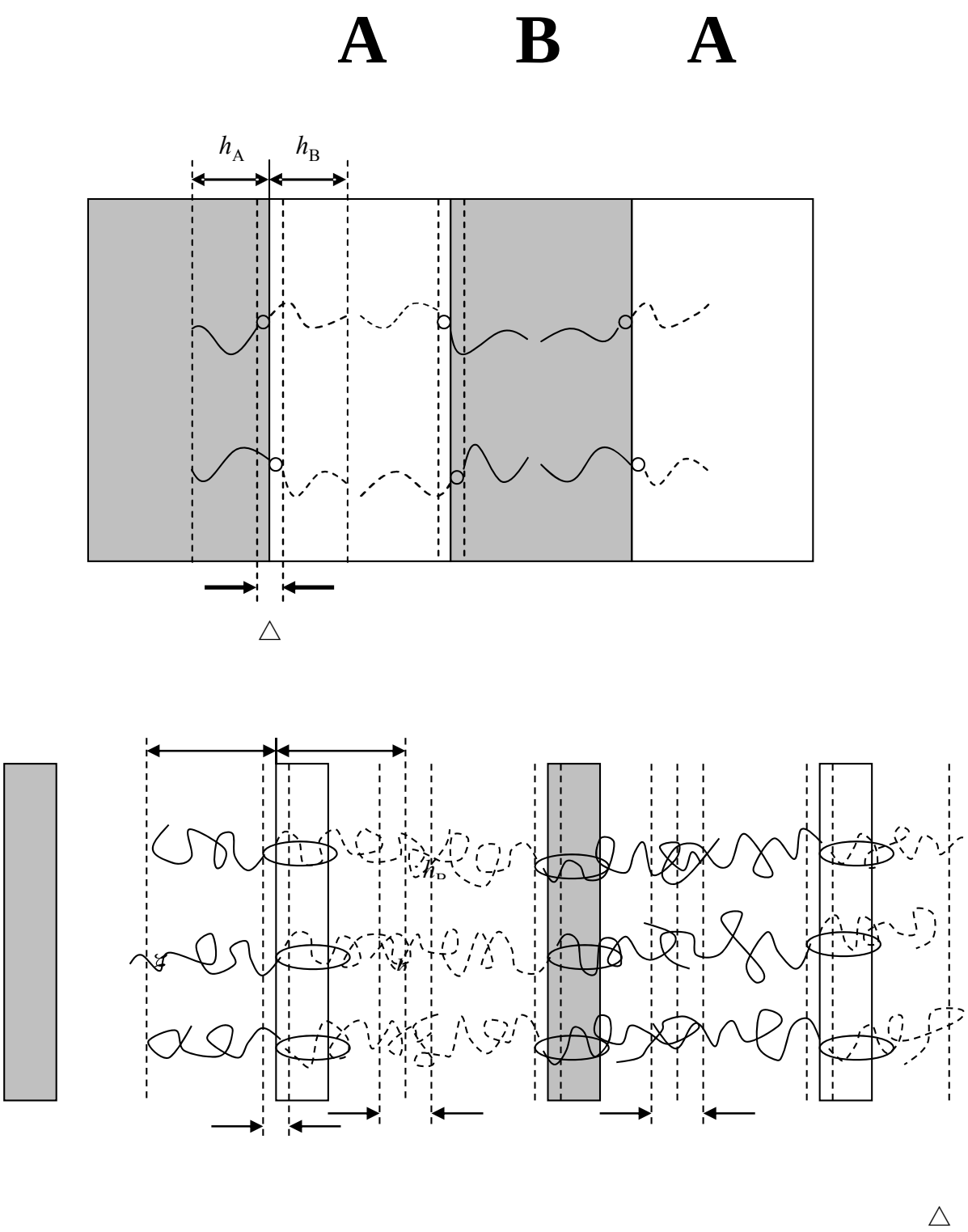

Figure 1-9 Chain conformation of AB diblock copolymer in a lamellar mesophase. (a)

Non-entangled state and (b) Entangled state. The thickness of A and B lamellaes are $2h_A$ and $2h_B$, respectively. The thickness of interpenetration zones for A and B are ξ_A and ξ_B, respectively. The thickness of interface between A and B regions is Δ. Symbols are denoted in the figures.

For AB diblock copolymers in the entangled state, interpenetration zones are of vital importance to chain relaxation since interpenetration zones nearly occupy half of lamellae when χNreaches up to 400 according to eq. (1.9). In such case, block chains cannot relax along the lamellar plane with Rouse like modes freely. Before this kind of relaxation mode, block chains have to escape from interpenetration zones by gradual retraction of dangling segments toward junction points, which has been described by modified reptation theory [134, 135] with introduction of contour-length fluctuations and constraint release. Chain ends in the interpenetration zones entangle with those from opposite brushes and entanglements can be considered as a constraining tube around the chains by Doi-Edwards model [136]. With the progression of chain relaxation, block chains escape from the constraining tube step by step and leave the constraining tube completely at last as shown in Figure 1-10.

Above all, chain conformation in a lamellar mesophase and block retraction mechanism are discussed by assuming that junction points between two blocks cannot move along or normal to lamellar interface. Actually, however, junction points between blocks can relax and move along lamellar interface, especially in WSR. To see corresponding experimental observations, the following part will focus on the diffusion of block copolymers in the disordered state and ordered state.

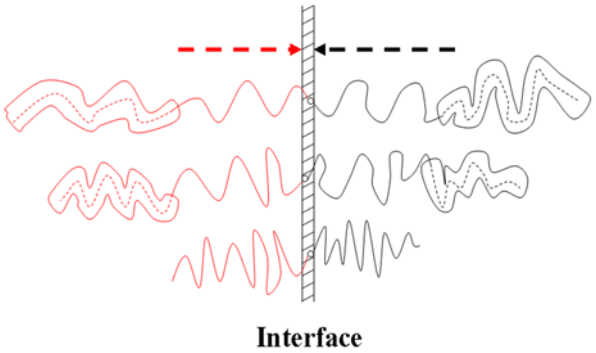

Figure 1-10 Block retraction mechanism for AB diblock copolymer in a lamellar mesophase. The solid lines are chains without entanglements, while the dashed lines are those with entanglements.

The tubes outside the dashed lines describe the existence of entanglements.

1.3.2 Diffusion Mechanisms of Block Copolymers

Diffusion mechanisms in disordered block copolymer melts and in the vicinity of ODT have been attracting a great deal of attention. Self-diffusion in disordered state block copolymer melts can be referred to excellent reviews [137-139]. The total friction of a copolymer chain is not the simple sum of the frictions of component monomers, especially when two monomers have completely different friction coefficients [140-147]. Therefore, it is not always possible to predict the diffusion coefficient of block copolymers based on the knowledge of monomeric friction of the blocks. The complexity of monomeric friction coefficients in block copolymers is not only a problem in block copolymers but also in miscible polymer blends. The monomeric frictions of blends and copolymers have been generalized using the concept called "self concentration" [148], which was introduced to understand concentration dependent friction coefficients and viscosities [149-152]. The self concentration concept assumes with inhomogeneous mixing of two polymers even in disordered block copolymers or miscible polymer blends due to the connectivity of the polymer.

With increasing segregation strength, block copolymers undergo an ODT. The ODT has been successfully monitored through the change of structure factors by X-ray and neutron scattering. Viscoelastic properties are even more sensitive to the ODT [139] and such properties are often used to locate the ODT. However, it has been found surprisingly that the self-diffusion is not sensitive to the ODT [153-161]. This insensitivity of diffusivity on the ODT does not depend on the structures to which the block copolymers form at the ODT. Examples of this insensitivity are seen for the bcc [156-157, 162], hexagonal [157, 163] and lamellar [149, 155-157, 160-161] morphologies. Besides the insensitivity of diffusion coefficients to ODT, it has been reported that the distribution of diffusion coefficients increases at the onset of ODT [156-157, 162-163]. The origin of this broadening cannot be simply assigned to anisotropy of the structure nor different diffusion mechanisms, since this broadening is also pronounced in sphere forming

system [157] as the same with cylinder or lamellar domains.

Table 1-2 Diffusion mechanisms for various systems

Symmetry	Anisotropy	Diffusion mechanism
Sphere	Isotropic	Hopping diffusion
Cylinder	Anisotropic	Interface diffusion (cylinder axis)
		Hopping diffusion (normal to cylinder axis)
Gyroid	Isotropic	Interface diffusion
Lamellae	Anisotropic	Interface diffusion (in plane)
		Hopping diffusion (normal to lamellar plane)

In the ordered state, however, depending on the symmetry of the domains and molecular weight, various diffusion mechanisms have been proposed. The diffusion mechanism observed is either hopping diffusion or interface diffusion depending on the symmetry of the structure as shown in Table 1-2 [133].

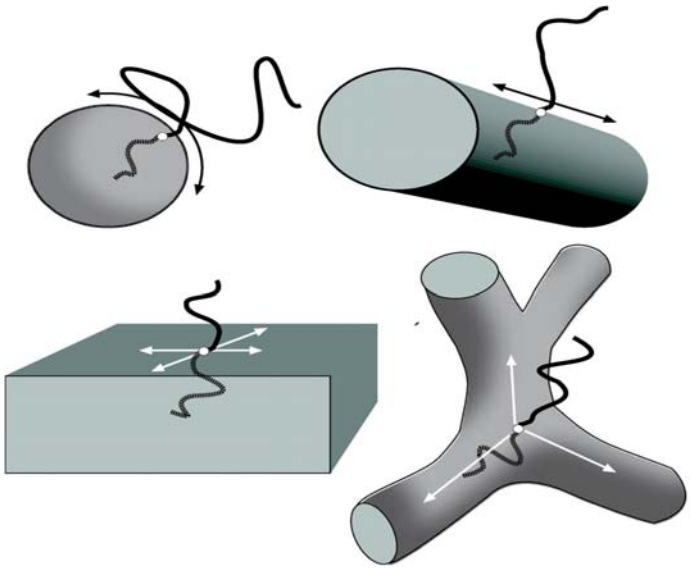

Figure 1-11 Schematic pictures of possible interface diffusion of block copolymer chains in spherical, cylindrical, lamellar and gyroid domains. The arrows indicate the directions of undisturbed interface diffusion.

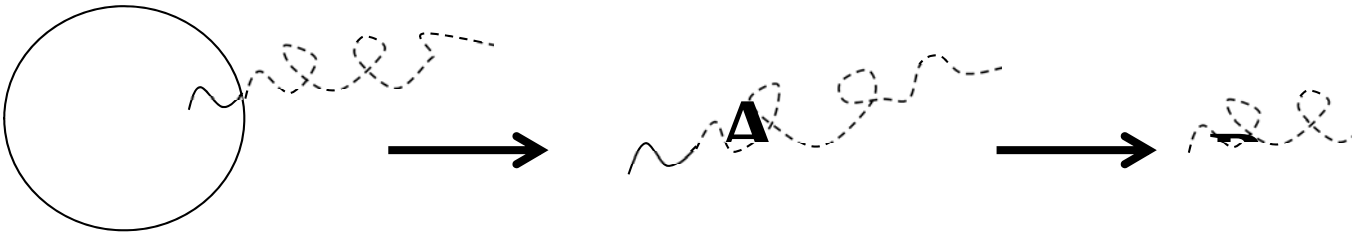

Figure 1-12 A schematic picture of hopping diffusion process controlled by thermodynamic interaction.

Table 1-3 Diffusion mechanisms of interface diffusion

	$M<M_C$	$M>M_C$
Weak segregation	Rouse	Activated reputation
Strong segregation	Rouse	Block retraction

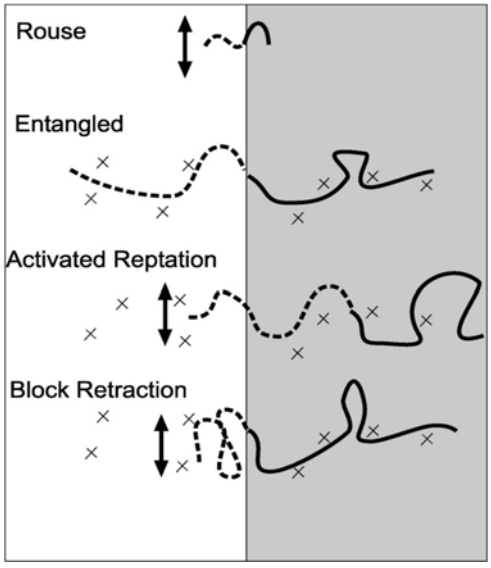

Figure 1-13 Diffusion mechanisms of interface diffusion.

The joints between the blocks of block copolymer chains, especially in strong segregation, are localized at the interface of domains so that each block is mostly contained in its respective domain [105-106, 164-166]. Block copolymer chains can diffuse along the interfaces without disturbing this localization of the joints at the interface, which is called as "interface diffusion" as shown in Figure 1-11 [133].

Interface diffusion is expected to be the dominating self-diffusion mechanism in block copolymer melts. In the strong segregation limit, no other diffusion may be allowed. In the large but finite χN regime, the possibility of a block copolymer chain leaving one domain and diffusing to another domain cannot be ruled out. This kind of self-diffusion is called as "hopping diffusion". Hopping diffusion should be strongly influenced by the incompatibility of the blocks: one of the blocks must be exposed to being surrounded by the other block during the elementary step in the hopping diffusion mechanism as shown in Figure 1-12 [167, 168].

Hopping diffusion of block copolymers is believed to be controlled by segregation strength alone, and entanglement does not have significant influence on diffusion mechanism as suggested by simulation of a single chain in static potential fields [169]. However, entanglements are very important for interface diffusion as summarized in Table 1-3 and Figure 1-13. Rouse diffusion of non-entangled block copolymer chain showing no thermodynamic slowing down. Two possible saddle points for interfacial diffusion in entangled block copolymers: activated reptation and block retraction.

One of the diffusion mechanisms proposed above, block retraction, is consistent with the speculation in theory for lamellar forming entangled system. However, most parts of rheological measurements are limited to apparent frequency dependence behaviors for block copolymers in the ordered state. Chain relaxation mechanisms have not been well examined by rheological measurements in melt state due to thermo rheological heterogeneity between components. However, viscoelastic properties and chain conformation of SP copolymers have been investigated in solution according to almost the same physical properties including thermo rheological properties between PS and P2VP. Some results can be explained without conflict by the diffusion

mechanisms proposed above. Hence, it may be possible and it is very essential to investigate the viscoelastic properties of SP copolymer melts and elucidate chain relaxation mechanisms to promote the understanding in dynamics of block copolymers.

1.4 Research Objectives

Despite of many experimental studies as partly mentioned in section 1.3.1, chain relaxations of block component polymers have not been well understood due to the difficulties in separating and specifying relaxation modes in dynamic viscoelastic properties of block copolymers. The main reason preventing such study is the fact that TTS is not valid for viscoelastic properties of nanophase separated block copolymers in principle. Different relaxation modes from different components are overlapped at a certain temperature and frequency for general diblock copolymer samples.

As mentioned in section 1.2.1, since PS and P2VP have almost thermo rheological properties, comparison of viscoelastic properties between diblock copolymers and component homopolymers become possible. In this thesis, hence, viscoelastic properties of symmetric SP copolymers in the disordered and ordered states are widely investigated and block chain relaxation mechanisms are speculated by analyzing the separation method of responses from large scale motions and chain relaxations. The structure of this thesis can be mainly divided into three parts as follows:

I. Examine the viscoelastic properties of SP copolymers with lower molecular weights in the disordered and ordered states by combining dynamic and steady shear measurements based on SANS and SAXS results (Chapter 2).

II. Examine a separation method of responses from large scale motions and chain relaxations in viscoelastic properties for symmetric SP copolymers in the ordered state including the effects of flow history (Chapter 3).

III. Investigate M dependence of viscoelastic properties for symmetric SP copolymers with wide M range in the ordered state and elucidate the relaxation

mechanism of block chains in a lamellar mesophase by analyzing M dependencies of η^0, J_e and the relaxation time ($<\tau>_w$) in comparison with corresponding PS homopolymers (Chapter 4).

References

[1]Scwarc M, Levy M, Milkovich R, *J. Am. Chem. Soc.*, **78**, 2656 (1956)

[2]Aggarwal SL, Introduction and overview. In "*Processing, structure and properties of block copolymers*", Folkes MJ (ed.), London: Elsevier (1985)

[3]Gehlsen MD, Almdal K, Bates FS, *Macromolecules*, **25**, 939 (1992)

[4]Almdal K, Bates FS, Mortensen K, *J. Chem. Phys.*, **96**, 9122 (1992)

[5]Stuhn B, Mutter R, Albrecht T, *Europhys. Lett.*, **18**, 427 (1992)

[6]Balsara NP, Perahia D, Safinya CR, Tirrell M, Lodge TP, *Macromolecules*, **25**, 3896 (1992)

[7]Winey KL, Gobran DA, Xu Z, Fetters LJ, Thomas EL, *Macromolecules*, **27**, 2392 (1994)

[8]Hashimoto T, Ogawa T, Han CD, *J. Phys. Soc. Japan*, **63**, 2206 (1994)

[9]Adams JL, Graessley WW, Register RA, *Macromolecules*, **27**, 6026 (1994)

[10]Karis TE, Russell TP, Gallot Y, Mayes AM, *Macromolecules*, **28**, 1129 (1995)

[11]Han CD, Baek DM, Kim JK, Ogawa T, Sakamoto N, Hashimoto T, *Macromolecules*, **28**, 5043 (1995)

[12]Floudas G, Vlassopoulos D, Pitsikalis M, Hadjichristidis N, Stamm M, *J. Chem. Phys.*, **104**, 2083 (1996)

[13]Balsara NP, Dai HJ, Watanabe H, Sato T, Osaki K, *Macromolecules*, **29**, 3507 (1996)

[14]Brandrup J, Immergut EH (eds.), *Polymer Handbook*, 2nd ed., New York: Wiley (1975)

[15]Leibler L, *Macromolecules*, **13**, 1602 (1980)

[16]Hamley IW, *The Phyics of Block Copolymers,* Oxford: Oxford University Press (1998)

[17]Bates FS, Fredrickson GH, *Annu. Rev. Phys. Chem.*, **41**, 525 (1990)

[18]Bates FS, Fredrickson GH, Phys. Today, **52**, 32 (1999)

[19]Matsen MW, Bates FS, *Macromolecules*, **29**, 1091 (1996)

[20]Lodge TP, *Macromol. Chem. Phys.*, **204**, 265 (2003)

[21]Matsen MW, *J. Phys.: Condens. Matter*, **14**, R21 (2002)

[22]Binder K, Muller M, *Curr. Opin. Colloid Interface Sci.*, **5**, 315 (2000)

[23]Almdal K, Koppi KA, Bates FS, Mortensen K, *Macromolecules*, **25**, 1743 (1992)

[24]Hamley IW, Koppi KA, Rosedale JH, Bates FS, Almdal K, Mortensen K, *Macromolecules*, **26**, 5959 (1993)

[25]Koppi KA, Tirrell M, Bates FS, Almdal K, Mortensen K, *J. Rheol.*, **38**, 999 (1994)

[26]Forster S, Khandpur AK, Zhao J, Bates FS, Hamley IW, Ryan AJ, Bras W, *Macromolecules*, **27**, 6922 (1994)

[27]Khandpur AK, Forster S, Bates FS, Hamley IW, Ryan AJ, Bras W, Almdal K, Mortensen K, *Macromolecules*, **28**, 8796 (1995)

[28]Zhao J, Majumdar B, Schulz MF, Bates FS, Almdal K, Mortensen K, Hajduk DA, Gruner SM, *Macromolecules*, **29**, 1204 (1996)

[29]Almdal K, Rosedale JH, Bates FS, Wignall GD, Fredrickson GH, *Phys. Rev. Lett.*, **65**, 1112 (1990)

[30]Bates FS, Fredrickson GH, *Annu. Rev. Phys. Chem.*, **41**, 525 (1990)

[31]Bates FS, Rosedale JH, Fredrickson GH, Glinka CJ, *Phys. Rev. Lett.*, **61**, 2229 (1988)

[32]Bates FS, Rosedale JH, Fredrickson GH, *J. Chem. Phys.*, **92**, 6255 (1990)

[33]Mai SM, Fairclough JPA, Hamley IW, Denny RC, Liao B, Booth C, Ryan AJ, *Macromolecules*, **29**, 6212 (1996)

[34]Rosedale JH, Bates FS, Almdal K, Mortensen K, Wignall GD, *Macromolecules*, **28**, 1429 (1995)

[35]Sakamoto N, Hashimoto T, *Macromolecules*, **28**, 6825 (1995)

[36]Stuhn B, Mutter R, Albrecht T, *Europhys. Lett.*, **18**, 427 (1992)

[37]Aggarwal SL, *Polymer*, **17**, 938 (1976)

[38]Forster S, Khandpur AK, Zhao J, Bates FS, Hamley IW, Ryan AJ, *et al.*, *Macromolecules*, **27**, 6922 (1994)

[39]Hajduk DA, Harper PE, Gruner SM, Honeker CC, Kim G, Thomas EL, *et al.*, *Macromolecules*, **27**, 4063 (1994)

[40]Khandper AK, Forster S, Bates FS, Hamley IW, Ryan AJ, Bras W, *et al.*, *Macromolecules*, **28**, 8796 (1955)

[41]Pochan DJ, Gido SP, Pispas S, Mays JW, Ryan AJ, Fairclough JPA, *et al.*, *Macromolecules*, **29**, 5091 (1996)

[42]Schulz MF, Khandpur AK, Bates FS, Almdal K, Mortensen K, Hajduk DA, *et al.*, *Macromolecules*, **29**, 2857 (1996)

[43]Rosedale JH, Bates FS, *Macromolecules*, **23**, 2329 (1990)

[44]Han CD, Kim J, *J. Polym. Sci. Polym. Phys.*, **25**, 1741 (1987)

[45]Kim J, Han CD, *J. Polym. Sci. Polym. Phys.*, **26**, 677 (1988)

[46]Han CD, Kim J, Kim JK, *Macromolecules*, **22**, 383 (1989)

[47]Balta-Calleja FJ, Vonk CG, *X-ray scattering of synthetic polymers*, London: Elsevier (1989)

[48]Higgins JS, Benoit HC, *Polymers and neutron scattering*, Oxford: Oxford University Press (1994)

[49]Richards RW, *Adv. Polym. Sci.*, **71**, 1 (1985)

[50]Kato K, *J. Electron Microsc. Japan*, **14**, 220 (1965)

[51]Kato K, *Polym. Eng. Sci.*, **7**, 38 (1967)

[52]Khandpur AK, Macosko CW, Bates FS, *J. Polym. Sci. Polym. Phys.*, **33**, 247 (1995)

[53]Alward DB, Kinning DJ, Thomas EL, Fetters LJ, *Macromolecules*, **19**, 215 (1986)

[54]Thomas EL, Alward DB, Kinning DJ, Martin DC, Handlin DL, Fetters LJ, *Macromolecules*, **19**, 2197 (1986)

[55]Thomas EL, Electron microscopy, In "*Encyclopedia of Polymer Science and Engineering*", Vol.5, Mark HF, Bikales NM, Overberger CG, Menges (eds.), New York: Wiley (1989)

[56]Koppi KA, Tirrell M, Bates FS, Almdal K, Colby RH, *J. Phys. II*, **2**, 1941 (1992)

[57]Okamoto S, Saijo K, Hashimoto T, *Macromolecules*, **27**, 3753 (1994)

[58]Kawasaki K, Onuki A, *Phys. Rev. A*, **42**, 3664 (1990)

[59]Witten TA, Leibler L, Pincus PA, *Macromolecules*, **23**, 824 (1990)

[60]Rubinstein M, Obukhov SP, *Macromolecules*, **26**, 1740 (1993)

[61]Semenov AN, *Langmuir*, **11**, 3560 (1995)

[62]Johnson JM, Allgaier JB, Wright SJ, Young RN, Buzza M, McLeish TCB, *Chem. Soc. Faraday Trans.*, **91**, 2403 (1995)

[63]Matsushita Y, Shimizu K, Nakao H, Choshi H, Noda I, Nagasawa M, *Polym. J.*, **18**, 361 (1986)

[64]Matsushita Y, Nakao Y, Saguchi R, Choshi H, Nagasawa M, *Polym. J.*, **18**, 493, (1986)

[65]Matsushita Y, Nakao Y, Shimizu K, Noda I, Nagasawa M, *Macromolecules*, **21**, 2790 (1988)

[66]Takahashi Y, Ochiai N, Matsushita Y, Noda I, *Polym. J.*, **28**, 1065 (1996)

[67]Takahashi Y, Noda I, Nagasawa M, *Macromolecules*, **18**, 2220 (1985)

[68]Matsushita Y, Nomura M, Watanabe J, Mogi Y, Noda I, Imai M, *Macromolecules*, **28**, 6007 (1995)

[69]Mogi Y, Mori K, Matsushita Y, Noda I, *Macromolecules*, **25**, 5412 (1992)

[70]Mogi Y, Kotsuji H, Kanebo Y, Mori K, Matsushita Y, Noda I, *Macromolecules*, **25**, 5408 (1992)

[71]Mogi Y, Nomura M, Kotsuji H, Ohishi K, Matsushita Y, Noda I, *Macromolecules*, **27**, 6755 (1994)

[72]Matsushita Y, Watanabe J, Katano F, Yoshida Y, Noda I, *Polymer*, **37**, 321 (1996)

[73]Matsushita Y, Noda I, *Macromol. Symp.*, **106**, 251 (1996)

[74]Matsushita Y, *Polym. Preprints, Japan*, **45**, No.1, 103 (1996)

[75]Meier DJ, *J. Polym. Sci. Part C*, **28**, 81 (1969)

[76]Meier DJ, In "*Block and Graft Copolymers*", Burke JJ, Weiss V (eds.), P. 105, New York: Syracuse University Press (1973)

[77]Meier DJ, *Polym. Prep.*, **15**, 171 (1974)

[78]Helfand E, *Macromolecules*, **8**, 552 (1975)

[79]Helfand E, Wasserman ZR, *Macromolecules*, **9**, 879 (1976)

[80]Helfand E, Wasserman ZR, *Macromolecules*, **11**, 960 (1978)

[81]Helfand E, Wasserman ZR, *Macromolecules*, **13**, 994 (1980)

[82]Semenov AN, *Sov. Phys. JETP (Engl. Transl.)*, **61**, 733 (1985)

[83]Ohta T, Kawasaki K, *Macromolecules*, **19**, 2621 (1986)

[84]Kawasaki K, Ohta T, Kohrogi M, *Macromolecules*, **21**, 2972 (1988)

[85]Utracki LA, Simha R, *Macromolecules*, **1**, 505 (1968)

[86]Dondos A, Froelich D, Rempp P, Benoit H, *J. Chem. Phys.*, **64**, 1012 (1967)

[87]Dondos A, Rempp P, Benoit H, *Macromol. Chem.*, **130**, 233 (1969)

[88]Kotaka T, Ohnuma H, Inagaki H, *Polymer*, **10**, 517 (1969)

[89]Kotaka T, Tanaka T, Inagaki H, *Polym. J.*, **3**, 327 (1972)

[90]Ogawa E, Sato M, Shima M, *Eur. Polym. J.*, **17**, 497 (1981)

[91]Matsushita Y, Nakao Y, Shimuzu K, Noda I, Nagasawa M, *Macromolecules*, **21**, 2790 (1988)

[92]Ogawa E, Sato M, Yamaguchi N, Shima M, *Eur. Polym. J.*, **18**, 257 (1982)

[93]Tanaka T, Kotaka T, Inagaki H, *Macromolecules*, **7**, 311 (1974)

[94]Tanaka T, Omoto M, Inagaki H, *Macromolecules*, **12**, 146 (1979)

[95]Prud'homme J, Bywater S, *Macromolecules*, **4**, 543 (1971)

[96]Tanaka T, Kotaka T, Inagaki H, *Macromolecules*, **9**, 561 (1976)

[97]Tanaka T, Kotaka T, Ban K, Hattori M, Inagaki H, *Macromolecules*, **10**, 960 (1977)

[98]Han CC, Mozer B, *Macromolecules*, **10**, 44 (1977)

[99]Ionescu L, Picot C, Duplessix R, Duval M, Benoit H, Lingelser JP, Gallot Y, *J. Polym. Sci. Polym. Phys.*, **19**, 1033 (1981)

[100]Bendler J, Solc K, Gobush W, *Macromolecules*, **10**, 635 (1977)

[101]Matsushita Y, Mori K, Saguchi R, Nakao Y, Noda I, Nagasawa M, *Macromolecules*, **23**, 4313 (1990)

[102]Matsushita Y, Noda I, Torikai N, *Macromol. Symp.*, **124**, 121 (1997)

[103]Matsushita Y, Nakao Y, Saguchi R, Mori K, Choshi H, Muroga Y, Noda I,

Nagasawa M, Chang T, Glinka CJ, Han CC, *Macromolecules*, **21**, 1802 (1988)

[104]Matsushita Y, Mori K, Mogi Y, Saguchi R, Noda I, Nagaswa M, Chang T, Glinka CJ, Han CC, *Macromolecules*, **23**, 4317 (1990)

[105]Torikai N, Matsushita Y, Noda I, Karim A, Satija SK, Han CC, *Physica B*, **213&214**, 694 (1995)

[106]Torikai N, Noda I, Karim A, Satija SK, Han CC, Matsushita Y, Kawakatsu T, *Macromolecules*, **30**, 2907 (1997)

[107]Matsushita Y, Mori K, Saguchi R, Noda I, Nagasawa M, Chang T, Glinka CJ, Han CC, *Macromolecules*, **23**, 4387 (1990)

[108]Anastasiadis SH, Russell TP, Satija SK, Majkrzak CF, *J. Chem. Phys.*, **92**, 5677 (1990)

[109]Shull KR, Mayes AM, Russell TP, *Macromolecules*, **26**, 3929 (1993)

[110]Markovitz H, *J. Polym. Sci.: Symp.*, **50**, 431 (1975)

[111]Kraft M, Meissner J, Kaschta J, *Macromolecules*, **32**, 751 (1999)

[112]Colby RH, Fetters LJ, Graessley WW, *Macromolecules*, **20**, 2226 (1987)

[113]Plazek DJ, *J. Polym. Sci.*, *A2*, **6**, 621 (1968)

[114]Williams ML, Landel RF, Ferry JD, *J. Am. Chem. Soc.*, **77**, 3701 (1955)

[115]Colby RH, *Curr. Opin. Colloid Interface Sci.*, **1**, 454 (1996)

[116]Watanabe H, "*Rheology of Multiphase Polymeric Systems*", In: Araki T, Qui TC, Shibayama M, "*Structure and Properties of Multiphase Polymeric Materials*", (1998), Marcel Dekker, New York.

[117]Kossuth MB, Morse DC, Bates FS, *J. Rheol.*, **43**, 167 (1999)

[118]Spontak RJ, Patel NP, *Curr. Opin. Colloid Interface Sci.*, **5**, 334 (2000)

[119]Hamley IW, *Curr. Opin. Colloid Interface Sci.*, **5**, 342 (2000)

[120]Hamley IW, *J. Phys. Condens. Matter*, **13**, R643 (2001)

[121]Lodge TP, *Macromol. Chem. Phys.*, **204**, 265 (2003)

[122]Bates FS, *Macromolecules*, **17**, 2607 (1984)

[123]Jin X, Lodge TP, *Rheol. Acta*, **36**, 229 (1997)

[124]Koppi KA, Tirrell M, Bates FS, *Phys. Rev. lett.*, **70**, 1449 (1993)

[125]Balsara NP, Hammouda B, Kesani PK, Jonnalagadda SV, Straty GC,

Macromolecules, **27**, 2566 (1994)

[126]Balsara NP, Dai JH, Kesani PK, Garetz BA, Hammouda B, *Macromolecules*, **27**, 7406 (1994)

[127]Tepe T, Hajduk DA, Hillmyer MA, Weimann PA, Tirrell M, Bates FS, *et al.*, *J. Rheol.*, **41**, 1147 (1997)

[128]Winey KI, Patel SS, Larson RG, Watanabe H, *Macromolecules*, **26**, 2542 (1993)

[129]Kannan R, Kornfield JA, *Macromolecules*, **27**, 1177 (1994)

[130]Gupta VK, Krishnamoorti R, Kornfield JA, Smith SD, *Macromolecules*, **28**, 4464 (1995)

[131]Patel SS, Larson RG, Winey KI, Watanabe H, *Macromolecules*, **28**, 4313 (1995)

[132]Riise BL, Fredrickson GH, Larson RG, Pearson DS, *Macromolecules*, **28**, 7653 (1995)

[133]Yokoyama H, *Mater. Sci. Eng. R,* **53**, 199 (2006)

[134]Ball RC, McLeish TCB, *Macromolecules*, **22**, 1911 (1989)

[135]Yurasova TA, McLeish TCB, Semenov AN, *Macromolecules*, **27**, 7205 (1994)

[136]Doi M, Edwards SF, In "*The Theory of Polymer Dynamics*", 2nd ed., Oxford University Press: Oxford (1988**)**

[137]Anastasiadis SH, *Curr. Opin. Colloid Interface Sci.*, **5**, 324 (2000)

[138]Papadakis CM, Ritting F, *J. Phys.: Condens. Matter*, **17**, R551 (2005)

[139]Fredrikson GH, Bates FS, *Annu. Rev. Mater. Sci.*, **26**, 501 (1996)

[140]Chapman BR, Hamersky MW, Milhaupt JM, Kostelecky C, Lodge TP, von Meerwall ED, Smith SD, *Macromolecules*, **31**, 4562 (1998)

[141]Milhaupt JM, Chapman BR, Lodge TP, Smith SD, *J. Polym. Sci. Polym. Phys.*, **36**, 3079 (1998)

[142]Composto RJ, Kramer EJ, White DM, *Polymer*, **31**, 2320 (1990)

[143]Kim E, Kramer EJ, Osby JO, *Macromolecules*, **28**, 2320 (1995)

[144]Green RF, Adolf DB, Gilliom LR, *Macromolecules*, **24**, 3377 (1991)

[145]Colby RH, *Polymer*, **30**, 1275 (1989)

[146]Roovers J, Toporowski PM, *Macromolecules*, **25**, 1096 (1992)

[147]Chung GC, Kornfield JA, Smith SD, *Macromolecules*, **27**, 964 (1994)

[148]Lodge TP, Mcleish TC, *Macromolecules*, **33**, 5278 (2000)

[149]Hamersky MW, Tirrell M, Lodge TP, *J. Polym. Sci. Polym. Phys.*, **34**, 2899 (1996)

[150]Milhaupt JM. Lodge TP, *J. Polym. Sci. Polym. Phys.*, **39**, 843 (2001)

[151]He YY, Lutz TR, Ediger MD, Lodge TP, *Macromolecules*, **36**, 9170 (2003)

[152]Lodge TP, Hanley KJ, Pudil B, Alahapperuma V, *Macromolecules*, **36**, 816 (2003)

[153]Ehlich D, Takenaka M, Hashimoto T, *Macromolecules*, **26**, 492 (1993)

[154]Dalvi MC, Lodge TP, *Macromolecules*, **27**, 3487 (1994)

[155]Fleischer G, Fujara F, Stuhn B, *Macromolecules*, **26**, 2340 (1993)

[156]Fleischer G, Ritting F, Stepanek P, Almdal K, Papadakis CM, *Macromolecules*, **32**, 1956 (1999)

[157]Ritting F, Karger J, Papadakis CM, Fleischer G, Stepanek P, Almdal K, *PCPP Phys. Chem. Chem. Phys.*, **1**, 3923 (1999)

[158]Anastasiadis SH, Ritting F, Chrissopoulou K, Fleischer G, Fytas G, Semenov AN, Karger J, Xenidou M, Pispas S, Hadjichristidis N, *Europhys. Lett.*, **51**, 68 (2000)

[159]Papadakis CM, Ritting F, Almdal K, Mortensen K, Stepanek P, *Eur. Phys. J.*, **E15**, 359 (2004)

[160]Shull KR, Kramer EJ, Bates FS, Rosedale JH, *Macromolecules*, **24**, 1383 (1991)

[161]Dalvi MC, Eastman CE, Lodge TP, *Phys. Rev. Lett.*, **71**, 2591 (1993)

[162]Fleischer G, Karger J, Stuhn B, *Colloid Polym. Sci.*, **275**, 807 (1997)

[163]Ritting F, Fleischer G, Karger J, Papadakis CM, Almdal K, Stepanek P, *Macromolecules*, **32**, 5872 (1999)

[164]Torikai N, Matsushita Y, Ebisawa T, *Physica B*, **248**, 284 (1998)

[165]Torikai N, Matsushita Y, Langridge S, Bucknall D, Penfold J, Takeda M, *Physica B*, **283**, 12 (2000)

[166]Torikai N, Noro A, Okuda M, Odamaki F, Kawaguchi D, Takano A, Matsushita Y, *Physica B*, **385-386**, 709 (2006)

[167]Cavicchi KA, Lodge TP, *Macromolecules*, **36**, 7158 (2003)

[168]Yokoyama H, Kramer EJ, *Macromolecules*, **31**, 7871 (1998)

[169]Yokoyama H, Kramer EJ, Fredrickson GH, *Macromolecules*, **33**, 2249 (2000)

Chapter 2 Viscoelastic Properties of Low Molecular Weight Symmetric Poly(styrene-*b*-2-vinylpyridine)s in the Ordered and Disordered States under Steady Shear Flow

2.1 Introduction

In the quiescent disordered states, it was reported that fluctuation effects were more pronounced on the viscoelastic properties than those on scattering data [1]. Both storage (G') and loss (G'') modulus were enhanced due to the fluctuation effects at lower frequency (ω) end while the enhancement of modulus by the fluctuation effects was more obvious for G' than for G'' [2, 3]. In a few studies, flow induced ordering was reported in the quiescent disordered states close to the order disorder transition (ODT) [4-6]. In the quiescent ordered states, G' and G'' showed power law dependence on ω (G', $G'' \sim \omega^{1/2}$) at the low ω end [1-2, 7]. It was observed that G' and G'' values in the power law region became smaller when lamellae were preferentially aligned parallel and perpendicular to the flow direction in which lamellar normals are parallel to shear gradient and vorticity directions, respectively [8-13]. The effect of alignment was more pronounced in the latter case. When the structure was well aligned, ω dependencies of G' and G'' became similar to those of uniform polymeric liquids.

In the disordered states [14], no fluctuation effect was observed on G'' and shear stress P_{21} so that the zero shear viscosity (η^0) values obtained by dynamic and steady

flow measurements were practically the same as those for components' solutions [15, 16] for symmetric poly(styrene-*b*-2-vinylpyridine)s (SP) copolymers with components having almost same physical properties. In contrast, steady state compliance (J_e) obtained by dynamic measurements were higher than those for components. Under steady shear flows, however, SANS intensities became lower than quiescent state and J_e became almost the same as those of components denoting the suppression of fluctuation effects. Even in the quiescent ordered states [14, 17], η^0 data can be obtained under steady flow, which were consistent with those for components. On the other hand, shear rate ($\dot{\gamma}$) dependence of first normal stress difference (N_1) changed from textured fluid like behavior ($\sim\dot{\gamma}$) to uniform polymeric liquid like behavior ($\sim\dot{\gamma}^2$) when the lamellae were well aligned similarly as polystyrene-*block*-polyisoprene (SI) solutions. When N_1 became proportional to $\dot{\gamma}^2$ at higher $\dot{\gamma}$, flow-SANS intensities showed strong anisotropy denoting perpendicular alignment of lamellar structure. The values of J_e obtained in well aligned states were practically the same as those of components.

In the above studies, it is shown that molecular weight and concentration dependencies of η^0 and J_e for SPs in disordered and well aligned ordered states are the same as those of component polymer solutions over wide ranges of molecular weight and concentration. However, all the data are in a very narrow range of effective χN close to ODT. In addition, it is observed that fluctuation effects in SP solutions are very weak compared to poly(styrene-d_8-*b*-2-vinylpyridine) (DP) solutions.

To further examine the viscoelastic properties of block copolymers, it is very interesting and essential to study SP diblocks in comparison with components in a wider range of χN at melt states, where stronger fluctuation effects are expected as shown by a previous study [18]. In this study, we examine viscoelastic properties of ordered and disordered symmetric SP diblocks having relatively low molecular weights at melt under steady shear flow based on the temperature dependence of χ obtained for the same DP sample in a previous study in a wider range of temperature.

2.2 Experimental

2.2.1 Samples

The SP diblock copolymers and polystyrenes (PS) were synthesized by anionic polymerization in *vacuo* as reported previously [19, 20]. Weight-averaged molecular weights M_w of the samples were determined by multi-angle laser light scattering (MALLS) method using DOWN EOS enhanced optical system of the Wyatt Technology at 35 °C in THF after optical purification with 0.2 μm PTFE filter. The wave length used was 690 nm and the reflective index increment, dn/dc, of PS in THF, 0.185 mL/g was used since the value for poly(2-vinylpyridine) (P2VP) is very close to the former.

Molecular weight heterogeneities, M_w/M_n, (M_n: number-averaged molecular weights) were determined in THF by a GPC system of Tosoh Ltd., equipped with RI-8012 differential refractive index detector using three GMH_{HR} columns and PSs as standards. Volume fractions of styrene in SP, ϕ_s, were determined by ^{1}H NMR spectra measured with a Varian unity-500 NMR spectrometer.

Table 2-1 Characteristics of poly(styrene-*b*-2-vinylpyridine)s and polystyrenes

Sample code	M_w [a]	M_w/M_n [b]	ϕ_s [c]	T_g [d] (°C)
SP106	0.47×10^4	1.02	0.51	87.0
SP105	0.81×10^4	1.02	0.52	88.0
SP107	1.25×10^4	1.02	0.51	89.8
SP29	1.52×10^4	1.03	0.52	90.2
SP27	2.10×10^4	1.03	0.50	
SP102	2.90×10^4	1.01	0.52	
SP101	4.69×10^4	1.04	0.51	
PS-19.6K	1.96×10^4	1.02		
PS-9.6K	0.96×10^4	1.02		

[a] by MALLS; [b] by GPC; [c] by ^{1}H-NMR; [d] by DSC.

ODT temperature, T_{ODT} of SP29 was determined as 135 ~ 138 ˚C by dynamic mechanical analysis (DMA) in a previous work [16]. Since T_{ODT} for other M_w samples cannot be determined by DMA, we determined temperature, T, dependence of χ parameter by SANS measurement using the same deutrated sample DP17 (M_n : 1.2×10^4, M_w/M_n : 1.05) in a much wider T range than previous work [18]. Using the T dependence of χ, ODT of other samples are estimated. Then the states of a few samples are confirmed by small angle X-ray scattering (SAXS) measurements at selected T. Molecular characteristics of SPs and PSs are tabulated in Table 2-1.

2.2.2 DSC Measurements

Glass transition temperature, T_g of SP samples were determined by DSC measurement using Seiko Instruments Inc., DSC6220 at heating rate of 5 ˚C/minutes from room temperature to 160 ºC. Two times scanning was used to clear the effect of thermal history on T_g.

2.2.3 SANS Measurements

DP17 was sealed into a 2 mm thick conventional quartz cell for liquid after evacuating it at melt state to prevent from producing bubbles during SANS measurements. The SANS measurement was performed on SANS-U spectrometer [21] of the Institute for Solid State Physics, the University of Tokyo, installed at the JRR-3 research reactor of JAEA, Tokai, Japan. The wavelength, λ, of neutrons used was 0.70 nm and the sample-to-detector distance was 3.0 m. Each measurement was conducted for 30 or 40 minutes in data acquisition period at different temperatures, T, ranging from 80 to 184 ˚C.

All the scattering patterns observed on a two-dimensional position-sensitive detector were isotropic, so that they were circularly averaged into the scattering intensity, $I(q)$, profiles as a function of the wave vector, q, defined as $(4\pi/\lambda)\sin\theta$, where 2θ is the scattering angle. All $I(q)$ profiles were corrected for incoherent

scattering using hydrogenous P2VP, and converted into the absolute intensity in the unit of cm^{-1} using standard Lupolen.

2.2.4 SAXS Measurements

SAXS measurements were performed by SAXSess mc^2 equipped with TCS120 thermo-control chamber at the show room of Anton Paar Japan. The X-ray beam generated by 3.5 kW generator was collimated by Kratky block collimator (Kα line, λ = 0.154 nm) and scattered beam was detected by an imaging plate [22]. Powder like samples of SP29, SP107 and SP105 were put into powder cell and measured at 117 ˚C for SP29 and SP107, and at 100 ˚C for SP105. The data acquisition time was 12 minutes for each sample. All the scattering patterns observed were isotropic so that circularly averaged $I(q)$ profiles were obtained after desmearing of the data and background (empty cell) subtraction [22].

2.2.5 Rheological Measurements

Disk shaped samples for rheological measurements were prepared by moulding at around 150 ^{o}C and annealed in vacuum oven to get rid of bubbles before the measurements. Steady shear flow measurements were carried out with a TA Instruments ARES rheometer using 15 mmϕ and 0.1 rad cone angle cone plates at 160 ^{o}C. First, transient behaviors were examined for each sample at a few selected shear rates. Steady state values of stresses were reached almost instantaneously for the samples in the disordered state, while it took about 3 to 7 minutes to reach steady values for those in the ordered states and the steady values showed relatively large irregular vibrations. Therefore, 10 minutes duration of the flow was employed before 5 minutes data acquisition to obtain steady state data in the ordered states.

DMA in linear region (maximum strain: 1%) were performed with an Anton Parr MCR300 rheometer using 8 mmϕ parallel plates in a temperature range of 170-120 ^{o}C for 4 lower M_w samples. All the measurements were carried out under N_2 gas after at least 10 minutes duration time before the measurement at each temperature.

2.3 Results and Discussion

2.3.1 DSC Results

Figure 2-1 shows DSC curves for four kinds of low molecular weight SP copolymers. It is found that all of the samples have an obvious transition near 90 °C and T_g depends on molecular weight, which is not observed for SP copolymers with high molecular weights. T_g for these samples are listed in Table 2-1 in detail.

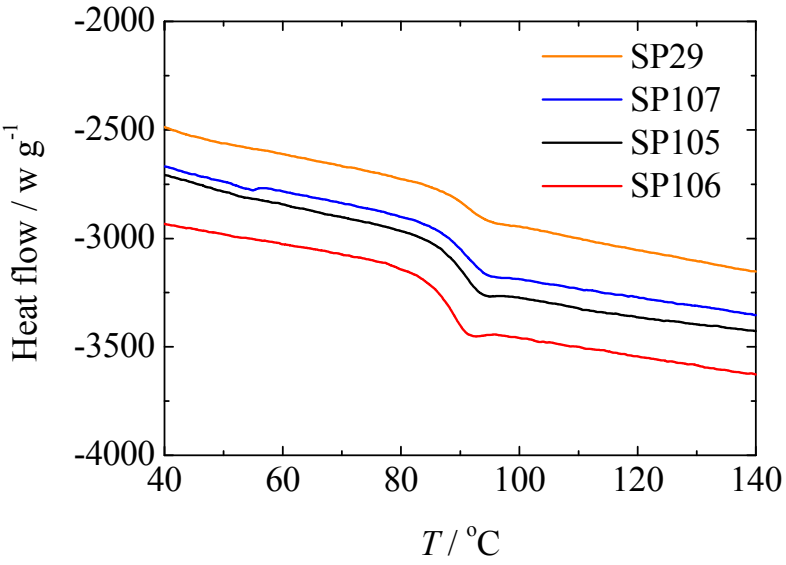

Figure 2-1 DSC curves for low molecular weight SP copolymers. Symbols are denoted in the figure.

2.3.2 *T* Dependence of *I(q)* for DP17

Figure 2-2 shows plots of $I(q)$ vs. q for DP17 at different T. All the profiles exhibit only one broad peak without any higher-order peaks from ordered structure. The peak intensity, I_m, first increased when T was increased up to 92 ˚C, which is close to T_g (91 ˚C), determined previously [18] and then decreased with further increasing T. The shape of $I(q)$ become broader, and the peak position, q_m, is slightly shifted to higher q with increase of T above T_g. The latter indicates that characteristic length, D, defined as $2\pi/q_m$ corresponding to chain dimension, decreases gradually with increase of T.

Sakamoto and Hashimoto [23] intensively examined ODT of SI with low molecular

weight by using SAXS. They characterized the phase behavior of SI at high temperature ($T > T_g$) by defining two characteristic temperatures: T_{ODT} and the critical temperature, T_{MF}, for the mean-field theory. At $T < T_{MF}$, thermal fluctuation effect cannot be ignored. To estimate the χ values as exactly as possible without the thermal fluctuation effect, T_{MF} was first determined for DP17, following the methods employed by Sakamoto and Hashimoto [23].

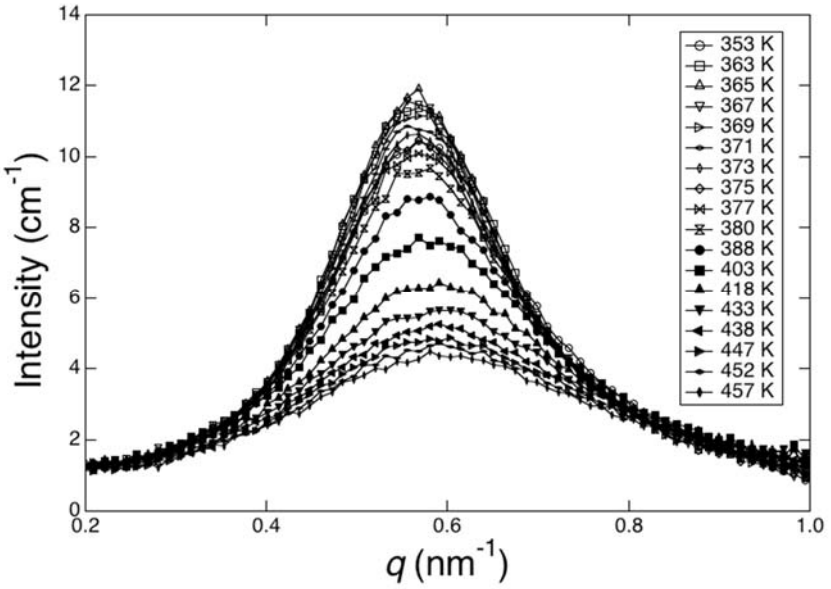

Figure 2-2 Plots of $I(q)$ against q for DP17. Symbols are denoted in the figure.

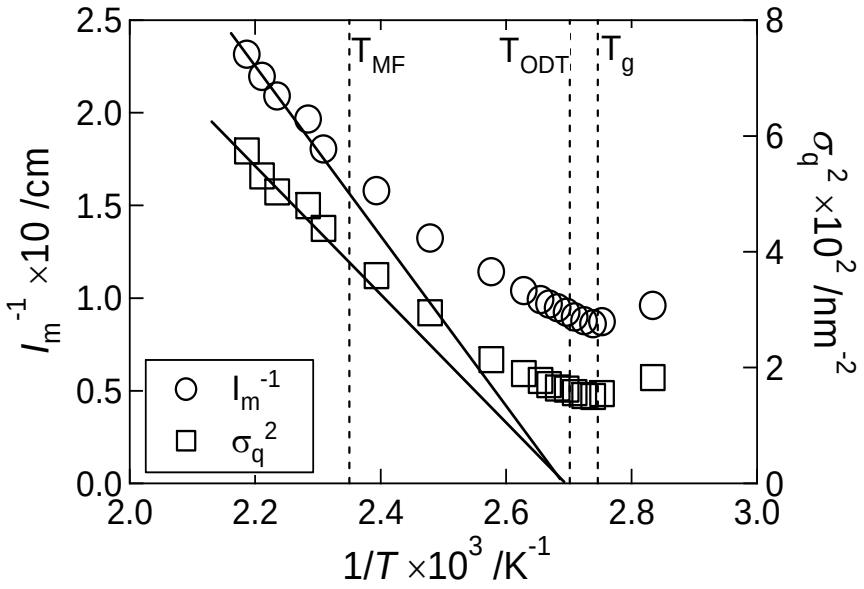

Figure 2-3 Plots of I_m^{-1} and σ_q^2 against T^{-1} for DP17. Symbols are denoted in the figure. T_{MF}, T_{ODT} and T_g are shown by vertical dotted lines. Solid lines are fitted to I_m^{-1} and σ_q^2 at $T^{-1} < T_{MF}^{-1}$

2.3.3 *T* Dependence of I_m and σ_q for DP17

Figure 2-3 shows plots of I_m^{-1} and the square of the half-width at half maximum, σ_q^2, of the observed peak as a function of T^{-1} for DP17. In this figure, T_g and median value of T_{ODT}, 93~102 ˚C for DP17, consistently determined with highly concentrated solutions of DP17 [18], are indicated by the vertical broken lines. Both I_m^{-1} and σ_q^2 exhibited linear relationship against T^{-1} as shown by respective straight lines at sufficiently low T^{-1}, that is, at sufficiently high T, according to the prediction of the mean-field theory. The deviations of I_m^{-1} and σ_q^2 from the straight lines due to the thermal fluctuation effect occur at almost the same T, corresponding to T_{MF} (around 152 ˚C). The extrapolated straight lines coincided on the abscissa at a T^{-1}, which corresponds to the mean-field spinodal temperature [23]. From these results, we can say that fluctuation effects are apparently observed in wide range of experimental window for low molecular weight samples at melt state, unlike the case of SP solutions.

2.3.4 *T* Dependence of χ for DP17

The value of χ was evaluated at each T by analyzing SANS profiles with the mean-field theory of Leibler [24] corrected for the polydispersity, M_w/M_n, of 1.05 in molecular weight. However, the asymmetry in segmental volume between PS and P2VP was not taken into account, since they possess the same statistical segment length [19, 20]. The evaluated values of χ and D are represented against T^{-1} in Figure 2-4. In this figure, T_{MF}, T_{ODT} and T_g determined above are indicated as the vertical broken lines together. Both χ and D gradually increase with increasing T^{-1} or decreasing T. The increment in D slightly changes at around T_{MF}, but it is not clearly observed as reported for PS-PI. The value of D increases with increase of T^{-1}, up to the value in the ordered state (lamellar spacing). The lamellar spacing at around room temperature is consistent with those for symmetric SPs in a previous work [25]. T dependence of χ was evaluated from the linear relationship observed below T_{MF}^{-1}, that is, above T_{MF}, for DP17 as $\chi = 0.0072 + 30/T$ (K).

Since molecular weights of SP105 and SP106 are lower than that of DP17, we can safely assume that T_{ODT} of these samples are below their T_g. Estimated mean field χN values for SP105 and SP106 at 160 ˚C are 5.7 and 3.3, respectively. For higher molecular weight samples, SP27, SP102 and SP101, it is expected that these samples are in the ordered states even at the highest experimentally accessible temperatures, say at 240˚C. For SP27, however, we may say that this sample is in weak segregation regime (mean field χN value: 14 at 160˚C). If we allow 10% experimental error, T_{ODT} for SP29 determined by DMA become consistent with the estimated value using above T dependence of χ. For SP107, it is expected that T_{ODT} is somewhere around 105 ~ 120 ˚C. This estimation was further examined by SAXS measurements.

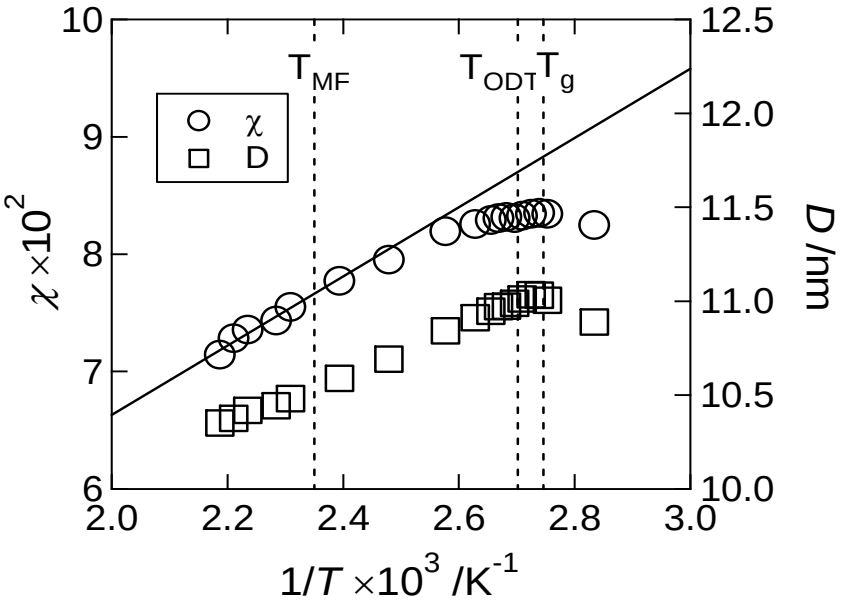

Figure 2-4 Plots of χ against T^{-1} for DP17. Solid line denotes fitting to the data in mean field region.

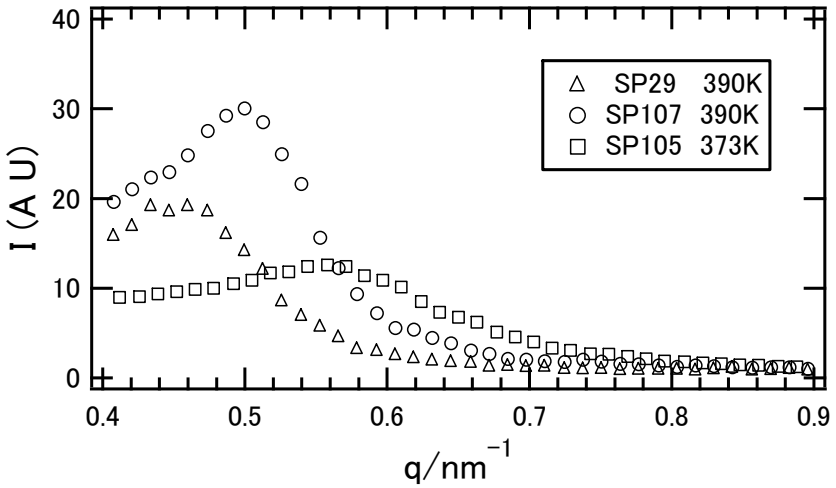

Figure 2-5 Plots of I vs q obtained by SAXS measurements for SP29 and SP107 at 117 ^{o}C and for SP105 at 100 ^{o}C. Symbols are denoted in the figure.

2.3.5 SAXS Results

Figure 2-5 shows plots of $I(q)$ vs q for SP29 and SP107 at 117 ˚C (390 K), the highest T reached by TCS120 chamber and for SP105 at 100 ˚C (373 K). It is clear that SP29 shows relatively narrower and stronger peak of $I(q)$ than SP105. From the difference in the shape of $I(q)$ peaks, we can confirm that SP29 is in the ordered state while SP105 is in the disordered state at respective temperatures. The $I(q)$ profile of SP107 resembles to that of SP29 so that we conclude that T_{ODT} of SP107 is slightly higher than 117 ˚C. Note that the lamellar spacing obtained from these data for SP29 and SP107 are consistent with the previous data for SPs [25].

2.3.6 Steady Shear Flow Behaviors

Figure 2-6 shows double logarithmic plots of σ and N_1 at steady states against $\dot{\gamma}$ for SP27, SP102 and SP101 at 160 ˚C. The values obtained by transient measurements for SP27 are also shown in Figure 2-6(a) by filled symbols. Note that the steady values cannot be approached at lower $\dot{\gamma}$ since stresses continuously decreased very gradually, while the sample became instable at higher $\dot{\gamma}$ so that the data are limited in narrow range of $\dot{\gamma}$ regimes. The data for SP27 (Figure 2-6(a))

shows transition from textured fluid like behavior to uniform polymeric liquid like behavior with increase of $\dot{\gamma}$, though the data are scarce at low $\dot{\gamma}$. From σ and N_1 data at higher $\dot{\gamma}$ regime, where polymeric liquid like behavior is observed, apparent η^0 and J_e for SP27 in the well aligned ordered states can be obtained. For SP102 and SP101, only textured fluid like behavior is observed as shown in Figure 2-6(b) and (c). We also tried to measure steady state values for higher molecular weight samples but steady state was not attained at all, say within 30 minutes.

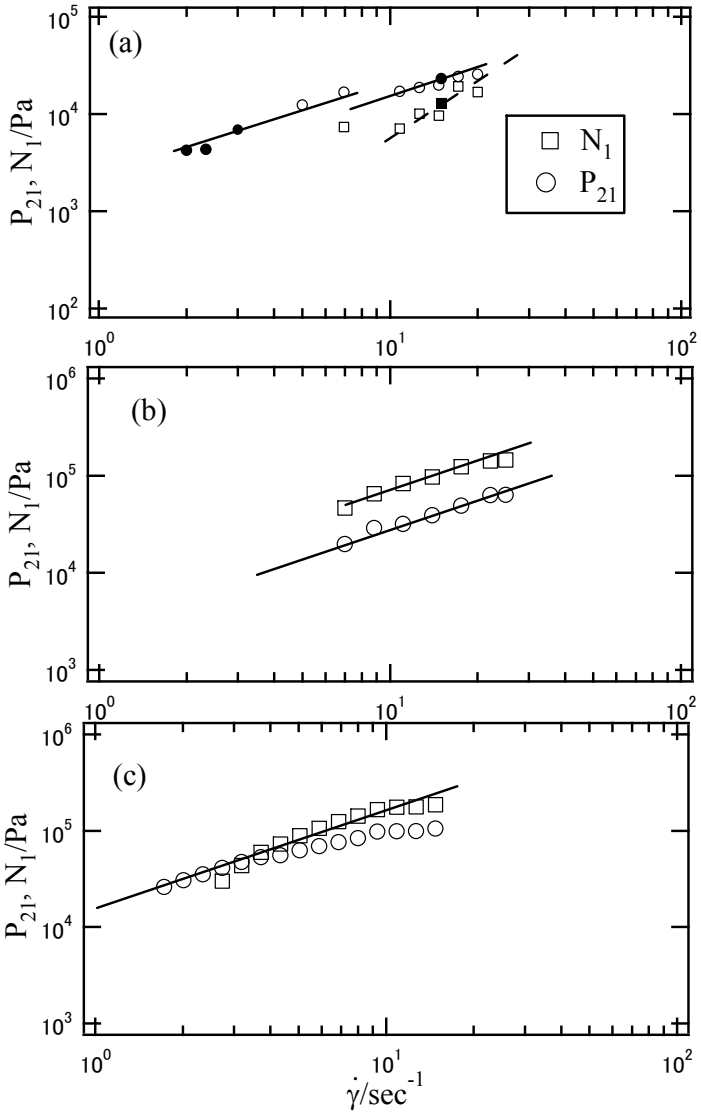

Figure 2-6 Double logarithmic plots of P_{21} and N_1 at steady states against $\dot{\gamma}$ for (a) SP27, (b) SP102 and (c) SP101 in the ordered state at 160 ˚C. Symbols are denoted in the figure. Slopes of solid and dashed lines are 1 and 2, respectively.

We could not succeed the steady flow measurement for the lowest molecular weight sample, SP106 due to its very low η. Figure 2-7 shows double logarithmic plots of η and J_e against $\dot{\gamma}$ for 3 other samples in the disordered states at 160 ˚C. The $\dot{\gamma}$ dependences of η and J_e for the second lowest molecular weight sample, SP105 shown in Figure 2-7(a) are similar to those of typical uniform polymeric liquids so that η^0 and J_e can be obtained by usual manner. With increase of molecular weight, or in other words approaching to ODT, striking features are observed for $\dot{\gamma}$ dependence of η. That is, two constant values for η can be obtained for SP107 and SP29. Hereafter, the constant η values at lower and higher $\dot{\gamma}$ are designated as η^0_1 and η^0_2 for simplicity. As clarified from SANS measurements for DP17, fluctuation effects apparently exist at melt state near the ODT so that we can attribute higher η^0_1 to fluctuation effects.

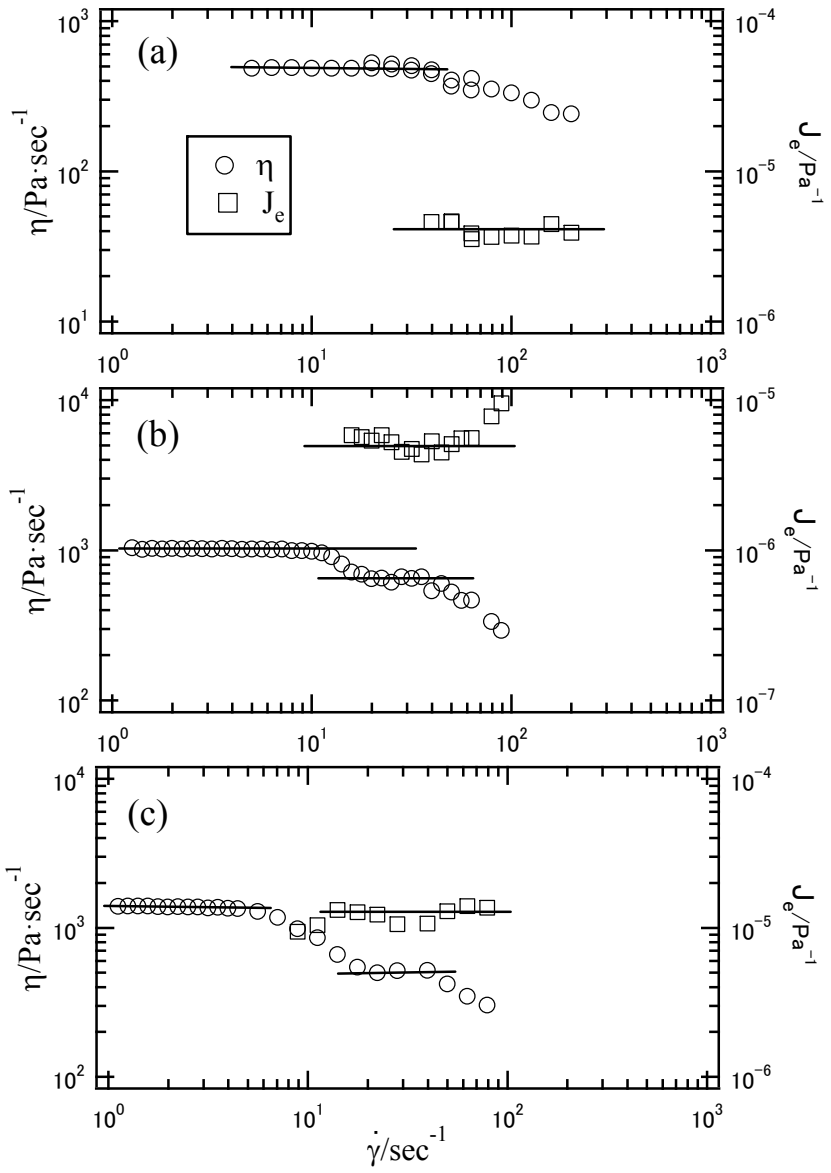

Figure 2-7 Double logarithmic plots of η and J_e against $\dot{\gamma}$ for (a) SP105, (b) SP107 and (c) SP29 in the disordered states at 160 ˚C. Symbols are denoted in the figure.

According to the previous studies, there are 2 possible understanding for the data at high $\dot{\gamma}$, that is, flow induced ordering and alignment or flow suppression of fluctuations. However, as pointed out in the previous work, flow induced ordering did not occur for SP solution having similar effective χN at which DP solution showed flow induced ordering. When viscoelastic contrast of block components is large, tentative domains induced by composition fluctuations results in hard and soft domains which tend to phase separate under the flow. On the other hand, when

viscoelastic contrast of block components is small, which is the case for SP, it can flow homogeneously so that composition fluctuation can be easily dissipated by the flow.

Together with the fact that the transient behaviors of these samples are different from those in the ordered states as mentioned in experimental section, and the fact that immediately repeated measurements are consistent with first ones, we speculate that there exists no ordered structure after the flow for these samples. Therefore, we tentatively conclude that the higher η^0_1 and the lower η^0_2 values are due to the fluctuation effects and their suppression by the flow with higher $\dot{\gamma}$, respectively. To get definite conclusion, it is essential to confirm the structure of corresponding deutrated sample at similar experimental conditions by flow SANS, which is unfortunately not available now. Even if flow induced ordering taking place at high $\dot{\gamma}$, the following discussions are not seriously affected. The constant values of J_e for SP107 and SP29 can be obtained at $\dot{\gamma}$ range where η^0_2 are obtained. These data are discussed with data obtained by DMA mentioned below.

2.3.7 Dynamic Rheological Behaviors

Figure 2-8 compares master curves of dynamic moduli ($G'(\omega)$ and $G''(\omega)$) for SP29 and SP105 with those of PS having similar N at 160 ˚C. It is clear that the data in the transition region for SP and PS are practically the same, while the data for SP are higher than those of PS in the terminal region which are more pronounced for G' than for G''. Note that M_w of SP29 is lower than that of PS-19.6K so that the higher values of G' and G'' cannot be attributed to residual difference of N. It is natural to conclude that enhancement of G' and G'' in terminal region is due to the fluctuation effects, which will be discussed later with the behaviors of other data.

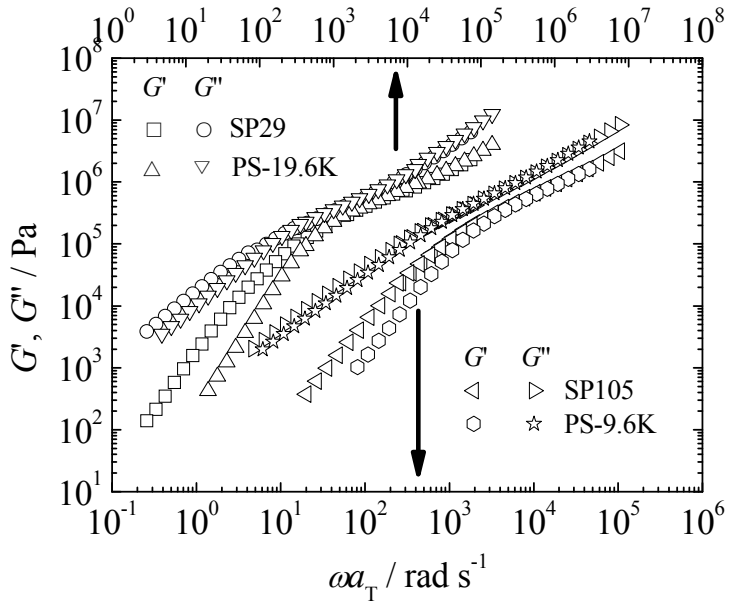

Figure 2-8 Double logarithmic plots of G' and G" against ωa_T for SP29 and SP105 in the disordered state at 160 ˚C. Data for PS having similar N are also shown for comparison. Symbols are denoted in the figure.

Figure 2-9 summarizes master curves of SP samples in the disordered states. Temperature dependences of shift factors a_T used to generate these master curves are almost the same as those for components, P2VP [15] and PS [26]. However, there are slight differences from the data for high molecular weight samples reflecting their lower T_g. Therefore, the data in Figure 2-9 are further shifted to iso-free volume states referring the data for PS-19.6K, though the shifts are small. From these data, η^0 and J_e are obtained by ordinary methods and compared with those obtained under steady shear flow.

Figure 2-10 shows double logarithmic plots of η^0 and J_e vs. M_w obtained from the data in Figures 2-6(a), 2-7 and 2-9. The data for PS, which are consistent with previous studies for PS and P2VP, are shown by thick solid lines. The dashed lines are guide for eyes. It is clear in Figure 2-10(a) that the η^0 for SP105 (M_w: 8.1K) obtained by DMA and steady flow coincide with each other. In addition, the η^0 for two low M_w samples by DMA are close to the data for PS. Since T_{MF} was 152 ˚C for DP17 (mean field χN: about 8), it may be reasonable to say that fluctuation effects become very weak for σ and G" for SP106 and SP105 having lower mean field χN at 160 ˚C. In

Figure 2-10(b), it is seen that J_e value for SP106 is close to that of PS. However, the J_e values obtained for 3 samples in the disordered state are all higher than those of PS, implying that fluctuation effects are more pronounced for elastic behaviors than for η, qualitatively consistent with previous studies.

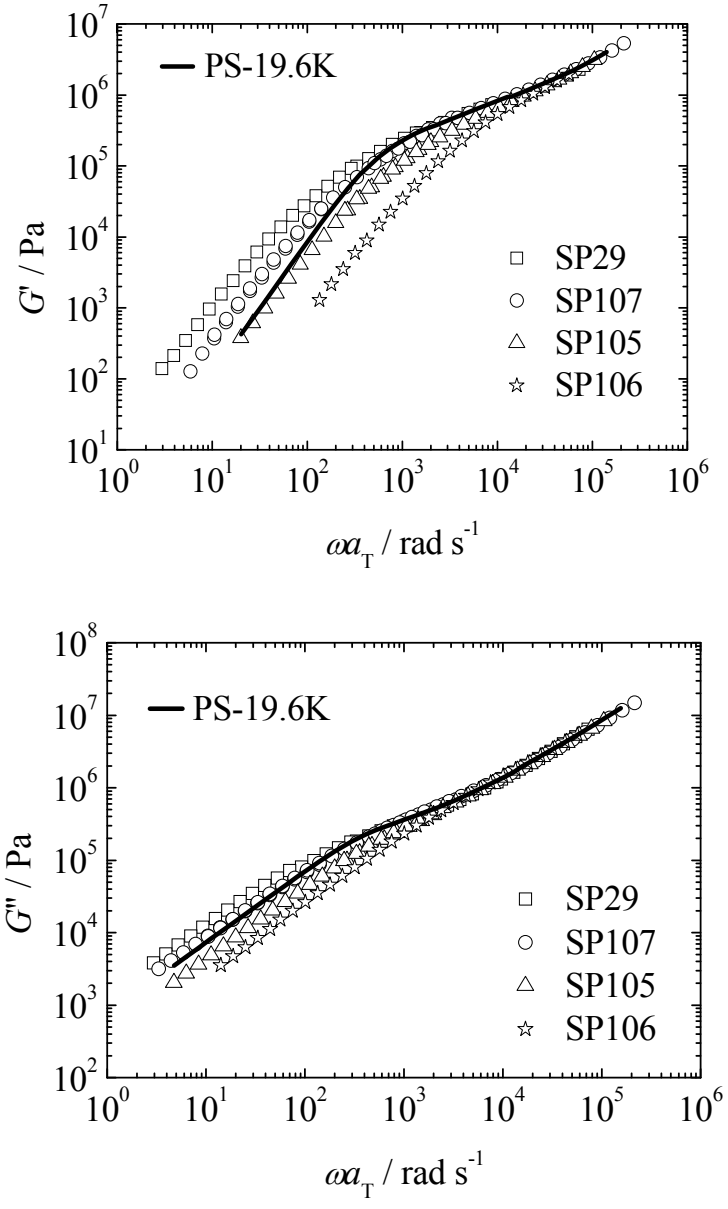

Figure 2-9 Comparison of master curves for SP29, SP107, SP105 and SP106 in the disordered state at 160 ˚C. Solid lines denote the data for PS-19.6K. Other symbols are denoted in the figure.

In the fluctuation regime near the ODT, chain conformation of block copolymer fluctuates between elongated one due to the repulsion of component chains of block copolymer and unperturbed one. Since the repulsion force becomes stronger by approaching ODT so that average chain length (D in Figure 2-4) increases, which

results in the higher values of elastic parameters than unperturbed polymer chain. Also the block copolymers tend to segregate so that tentative microdomains are formed, which are dissipated by the thermal motions of chains. The tentative structure sustains the stress and interface therein retards the dissipative motion of chains. The size of the tentative structure become larger and its life time become longer by approaching ODT. These characteristics are the reasons for broader distribution of relaxations for diblocks compared to corresponding PS (Figure 2-8), the enhancement of η^0 and J_e and their higher M_w dependencies compared to PS.

Since all the theoretical studies concerned with enhancement of viscoelastic parameters due to the fluctuation effects assumes entangled systems, whereas all the data in this study are those for non-entangled samples, we avoid direct comparison of the experimental results (such as slopes of dashed line) with theories and limit the discussion to the χN range of fluctuation effects and their suppression by the flow.

It is also clear in Figure 2-10(a) that η^0 obtained by DMA and η^0_1 fall on the dashed line, while η^0_2 are close to the solid line for SP107 and SP29. These results imply that η^0_1 and η^0 obtained by DMA are values with enhancement due to fluctuation effects, while the lower values of η^0_2 than η^0_1 and η^0 are due to the suppression of fluctuation effects by shear flow with high $\dot{\gamma}$. In addition, the J_e values from steady shear in Figure 2-10(b) are slightly higher than those from DMA. This feature may mean that N_1 is not so much suppressed as viscosity. However, concerning the difficulties of measurements with small geometries and larger error in G' and N_1, the difference between data from steady shear and DMA may be within the experimental error so that we cannot get definite conclusion about the flow suppression of fluctuation effects for N_1. From the overall features of Figure 2-10, we can at least conclude that fluctuation effects on viscoelastic properties completely disappear at around $\chi N < 2 \sim 3$ for SPs.

The data for SP27 (M_w: 21K) in the ordered state are also shown in Figure 2-10. The data obtained by separation method of grain/defect and chain responses in G' and G'' discussed in chapter 3 (open symbols) are consistent with the data in disordered

state. The data obtained at well aligned state are also consistent with other data in the disordered state. Therefore, we can conclude that no discontinuity of η^0 and J_e occur by ODT for SP melts, consistent with the results for SP solutions.

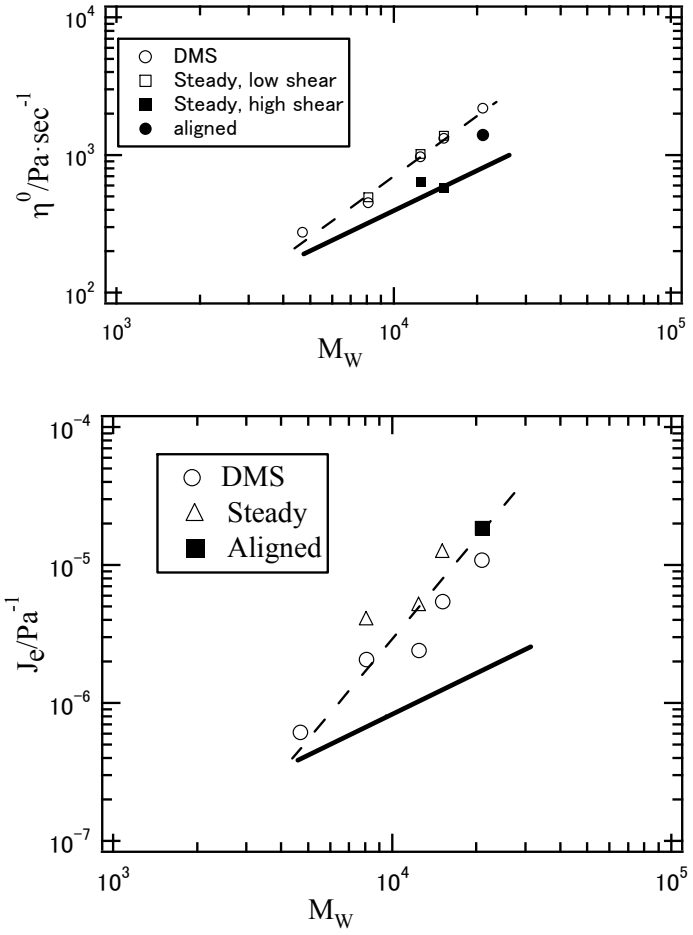

Figure 2-10 Double logarithmic plots of (a) η^0 and (b) J_e vs. M_w obtained from DMA and steady flow measurements in the disordered state. The data for ordered state (SP27) obtained at well aligned state and by subtraction method are also shown for comparison. Symbols are denoted in the figure. Solid line denotes data for components. Dashed lines are guide for eyes.

2.4 Summary

Viscoelastic properties of symmetric poly(styrene-*b*-2-vinylpyridine)s, having almost the same components' viscoelastic properties, in the ordered and disordered states under steady shear flow are examined for relatively low molecular weight samples at melt state based on the temperature dependence of χ. In the disordered

state near the ODT, two constant values for η, η^0_1 and η^0_2 at lower and higher $\dot{\gamma}$, respectively are obtained and η^0_1 coincided with the value obtained by DMA. The constant values of J_e are obtained at $\dot{\gamma}$ range where η^0_2 are obtained. It was concluded that higher η^0_1 and lower η^0_2 values are due to the fluctuation effects and their suppression by the flow with higher $\dot{\gamma}$, respectively. In the ordered state, well aligned state was only attained for the sample having lowest molecular weight. The values of η^0 and J_e obtained in well aligned state are consistent with those in disordered state, denoting that there is no discontinuity of data due to ODT. It can be also concluded that fluctuation effects on viscoelastic properties completely disappear at around $\chi N < 2 \sim 3$ for SPs.

References

[1]Bates FS, Rosedale JH, Fredrickson GH, *J. Chem. Phys.*, **92**, 6255 (1990)

[2]Bates FS, *Macromolecules*, **17**, 2607 (1984)

[3]Jin X, Lodge TP, *Rheol. Acta*, **36**, 229 (1997)

[4]Koppi KA, Tirrell M, Bates FS, *Phys. Rev. lett.*, **70**, 1449 (1993)

[5]Balsara NP, Hammouda B, Kesani PK, Jonnalagadda SV, Straty GC, *Macromolecules*, **27**, 2566 (1994)

[6]Balsara NP, Dai HJ, Kesani PK, Garetz BA, Hammouda B, *Macromolecules*, **27**, 7406 (1994)

[7]Bates FS, Rosedale JH, *Macromolecules*, **23**, 2329 (1990)

[8]Tepe T, Hajduk DA, Hillmyer MA, Weimann PA, Tirrell M, Bates FS, *et al.*, *J. Rheol.*, **41**, 1147 (1997)

[9]Winey KI, Patel SS, Larson RG, Watanabe H, *Macromolecules*, **26**, 2542 (1993)

[10]Kannan R, Kornfield JA, *Macromolecules*, **27**, 1177 (1994)

[11]Gupta VK, Krishnamoorti R, Kornfield JA, Smith SD, *Macromolecules*, **28**, 4464 (1995)

[12]Patel SS, Larson RG, Winey KI, Watanabe H, *Macromolecules*, **28**, 4313 (1995)

[13]Riise BL, Fredrickson GH, Larson RG, Pearson DS, *Macromolecules*, **28**, 7653 (1995)

[14]Takahashi Y, Noda M, Kitade S, Matsuoka K, Matsushita Y, Noda I, *Polym. J.*, **37**, 894 (2005)

[15]Takahashi Y, Ochiai N, Matsushita Y, Noda I, *Polym. J.*, **28**, 1065 (1996)

[16]Takahashi Y, Noda I, Nagasawa M, *Macromolecules*, **18**, 2220 (1985)

[17]Takahashi Y, Imaichi K, Noda M, Takano A, Matsushita Y, *Polym. J.*, **39**, 632 (2007)

[18]Takahashi Y, Kitade S, Noda M, Ochiai N, Noda I, Imai M, Matsushita Y, *Polym. J.*, **30**, 388 (1998)

[19]Matsushita Y, Nakao Y, Saguchi R, Choshi H, Nagasawa M, *Polym. J.*, **18**, 493, (1986)

[20]Matsushita Y, Nakao Y, Shimizu K, Noda I, Nagasawa M, *Macromolecules*, **21**, 2790 (1988)

[21]Ito Y, Imai M, Takahashi S, *Physica B*, **213&214**, 889 (1995)

[22]Schnablegger H, Singh Y, "The SAXS Guide Getting acquainted with the principles" 2nd ed. Anton Paar GmbH, Austria (2011)

[23]Sakamoto N, Hashimoto T, *Macromolecules*, **28**, 6825 (1995)

[24]Leibler L, *Macromolecules*, **13**, 1602 (1980)

[25]Matsushita Y, *J. Polym. Sci. Polym. Phys.*, **38**, 1645 (2000)

[26]Graessley WW, "*Polymer Liquids & Networks: Dynamics and Rheology*", London and New York: Talyor & Francis Group (2008)

Chapter 3 A Separation Method of Responses from Large Scale Motions and Chain Relaxations for Viscoelastic Properties of Symmetric Poly(styrene-*b*-2-vinylpyridine)s in the Ordered State

3.1 Introduction

Block copolymers have attracted much interest from researchers due to the characteristic phase separation behavior. The nanophase separated structures are basically determined by the Flory-Huggins segment-segment interaction parameter χ, degree of polymerization N, and composition of components ϕ as discussed by Leibler [1]. Even if the thermodynamic equilibrium of nanophase separated structure is achieved for block copolymer chains, the large scale structure is in frozen states of randomly oriented multi-grain structure containing many defects. Because of these structural characters and viscoelastic heterogeneity of component polymers, viscoelastic properties of block copolymers in the ordered states become very complicated even for the simplest ones, i.e., diblock copolymers. A huge number of experimental and theoretical studies have been carried out to understand the relationship among morphology, molecular characteristics, and rheological behavior of block copolymers [2-8].

Bates *et al* [9-11] first reported that frequency (ω) dependencies of storage modulus $G'(\omega)$ and loss modulus $G''(\omega)$ of lamellar forming diblock copolymers asymptote to $\omega^{0.5}$ at low frequency region. Kawasaki and Onuki [12] theoretically explained the above results as responses from large scale motions of grains/defects. Theoretical studies for rheological behaviors of block copolymers [13-16] are developed to include other morphologies and chain relaxations. Chain retraction mode for entangled systems also predicted the same power law behaviors. Despite of many experimental studies, however, chain relaxations of block component polymers have not been well studied due to the difficulties in separation and specification of relaxation modes in

dynamic viscoelastic properties of block copolymers. Note that, time temperature superposition is not valid for viscoelastic properties of nanophase separated block copolymers in principle. Different relaxation modes from different components are overlapped at a certain temperature and frequency for general diblock copolymer samples.

To overcome the above problem, viscoelatic properties of poly(styrene-*b*-2-vinylpyridine)s (SP) in common good solvents have been well studied by Takahashi *et al* [17-19], since polystyrene (PS) and poly(2-vinylpyridine) (P2VP) have the same Kuhn segment length [20-22], the same glass transition temperature and almost the same viscoelastic properties at melt states and in common good solvents [23, 24]. To further examine the relaxation process of block copolymer chains in nanophase separated structure, it is essential to have a new analysis method which enables us to separate the responses from grains/defects and polymer chains in the dynamic moduli of diblock copolymers.

Thus, in this chapter, we focus on the separation method of viscoelastic responses for symmetric poly(styrene-*b*-2-vinylpyridine)s including the effects of pre-shear and annealing in the ordered state in comparison with corresponding PS homopolymers.

3.2 Experimental

3.2.1 Samples

The SP diblock copolymers and PS homopolymers were synthesized by anionic polymerization in *vacuo* as reported previously [21, 22]. Weight-averaged molecular weights M_w of the samples were determined by multi-angle laser light scattering (MALLS) method using DOWN EOS enhanced optical system of the Wyatt Technology at 35 ºC in THF. THF solutions of samples were optically purified with 0.2 μm PTFE filter before the measurement. The wave length used was 690 nm. The reflective index increment, dn/dc, of PS and P2VP in THF are 0.185 mL/g and 0.180 mL/g, respectively. Since the both values are very close to each other, 0.185 mL/g

was used as *dn*/*dc* for all M_w measurements.

Molecular weight heterogeneities, M_w/M_n, where M_n being number-averaged molecular weights were determined in THF by GPC system of Tosoh Ltd., equipped with RI-8012 differential refractive index detector and with three GMH_{HR} columns with 7.8 mm inner diameter each. Standard polystyrenes were used for the calibration. Volume fractions of styrene in SP copolymers were determined by ^1H NMR spectra measured with a Varian unity-500 NMR spectrometer. Molecular characteristics of SP copolymers and PS homopolymers are listed in Table 3-1. According to the previous ODT measurements [25], we can safely assume that SP copolymers used in this study are in the ordered states. For SP27, however, it is in the weak segregation regime due to lower molecular weight.

Table 3-1 Molecular charateristics of SP diblock copolymers and PS homopolymers

Samples	M_w [a]	M_w/M_n [b]	ϕ_s [c]
SP27	2.1×10^4	1.03	0.50
SP103	9.86×10^4	1.02	0.50
SP44	22.4×10^4	1.01	0.51
PS-19.6K	1.96×10^4	1.02	
PS-113K	11.3×10^4	1.01	

[a] by MALLS; [b] by GPC; [c] by ^1H-NMR.

3.2.2 Samples Preparation

Disk shaped samples with 8 mm diameter and 1.1 mm thickness for rheological measurements were prepared by hot-press method at 150 °C for 5 mins. The samples were annealed in vacuum oven for 10 hrs at 110 °C before the measurements.

3.2.3 Ordinary Frequency Sweep

Rheological measurements were performed with an Anton Parr MCR300 rheometer using 8 mmϕ parallel plates in a temperature range of 120-220 ºC. First, ordinary frequency sweep measurements were carried out in the above temperature range for all samples in linear region (maximum strain: 1%), then the effects of pre-shear and annealing were examined as follows.

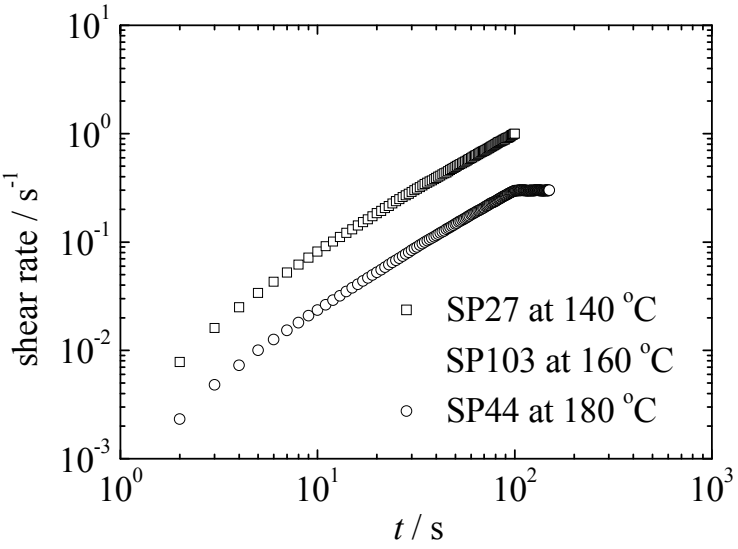

Figure 3-1 Relation between shear rate ($\dot{\gamma}$) and time (t) in pre-shear flow for SP27 at 140 ºC, SP103 at 160 ºC and SP44 at 180 ºC

3.2.4 The Effects of Pre-shear and Annealing

To avoid chain cessation by sudden flow with high shear rates [26], shear rate $\dot{\gamma}$ was increased from 0.01 to 1 sec^{-1} during 100 sec for SP27 at 140 ºC and for SP103 at 160 ºC, and from 0.01 to 0.3 sec^{-1} during 100 sec followed with 50 sec duration at 0.3 sec^{-1} for SP44 at 180 ºC in a stepwise pre-shear protocol as shown in Figure 3-1. Then frequency sweep measurements were carried out at 120-160 ºC for SP27, 120-200 ºC for SP103 and 120-220 ºC for SP44. The measurements were repeated 2 times for the same sample. The effect of annealing was also repeatedly examined 2 times by the same manner, after annealing the samples in parallel plates for 2 hrs at 140 ºC for SP27, 160 ºC for SP103 and 180 ºC for SP44.

All the measurements were carried out under N_2 gas after at least 10 minutes duration time before the measurement at each temperature. After the measurement, GPC measurement was conducted to confirm that no chain degradation occurred by the severe experimental condition in this study.

3.3 Results and Discussion

3.3.1 Viscoelastic Properties of SP27 in Comparison with PS-19.6K

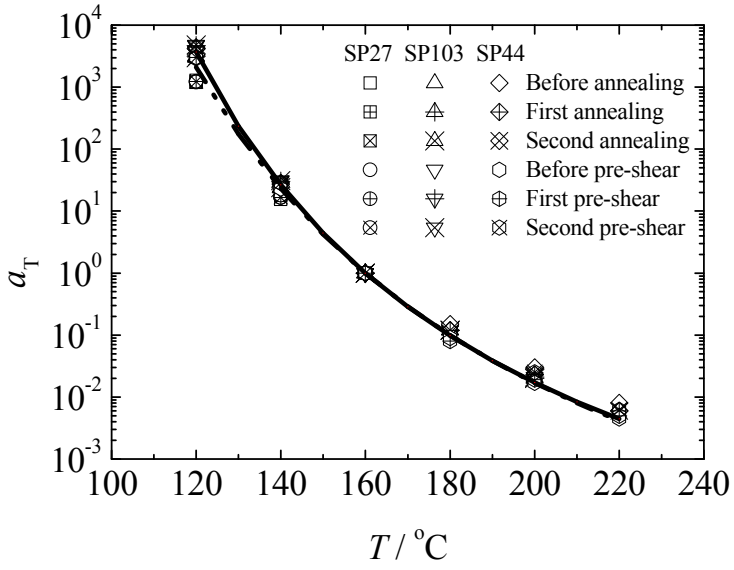

Figure 3-2 Semi logarithmic plots of shift factors a_T against T for SP27, SP103 and SP44 with different annealing or pre-shear times at T_r =160 °C. The dashed and solid lines denote WLF equation for P2VP [23] and PS [27], respectively. Symbols are denoted in the figure.

Master curves of dynamic moduli for SP diblocks (G^*_{SP}) and hPS (G^*_{hPS}) are generated from the data measured at each temperature by the general method. Figure 3-2 shows temperature dependence of shift factors a_T used to generate the master curves, which are almost the same as those for components, P2VP [23] and PS [27]. There exist small differences for a_T values of P2VP and PS and also for SP27 and SP103 at the lowest temperature, the main results in this paper are not affected by these facts.

Figure 3-3(a) shows double logarithmic plots of master curves of G^*_{SP} and G^*_{hPS} against ωa_T at a reference temperature, T_r = 160 °C, for SP27 and PS-19.6K, respectively, both having almost the same N. It is clear in Figure 3-3(a) that viscoelastic properties of SP27 are practically the same as those of PS-19.6K in the high ω region, while they deviate with decrease of ω and the data for SP27 asymptote to $\omega^{0.5}$ dependence in the low ω region due to the presence of lamellar structure.

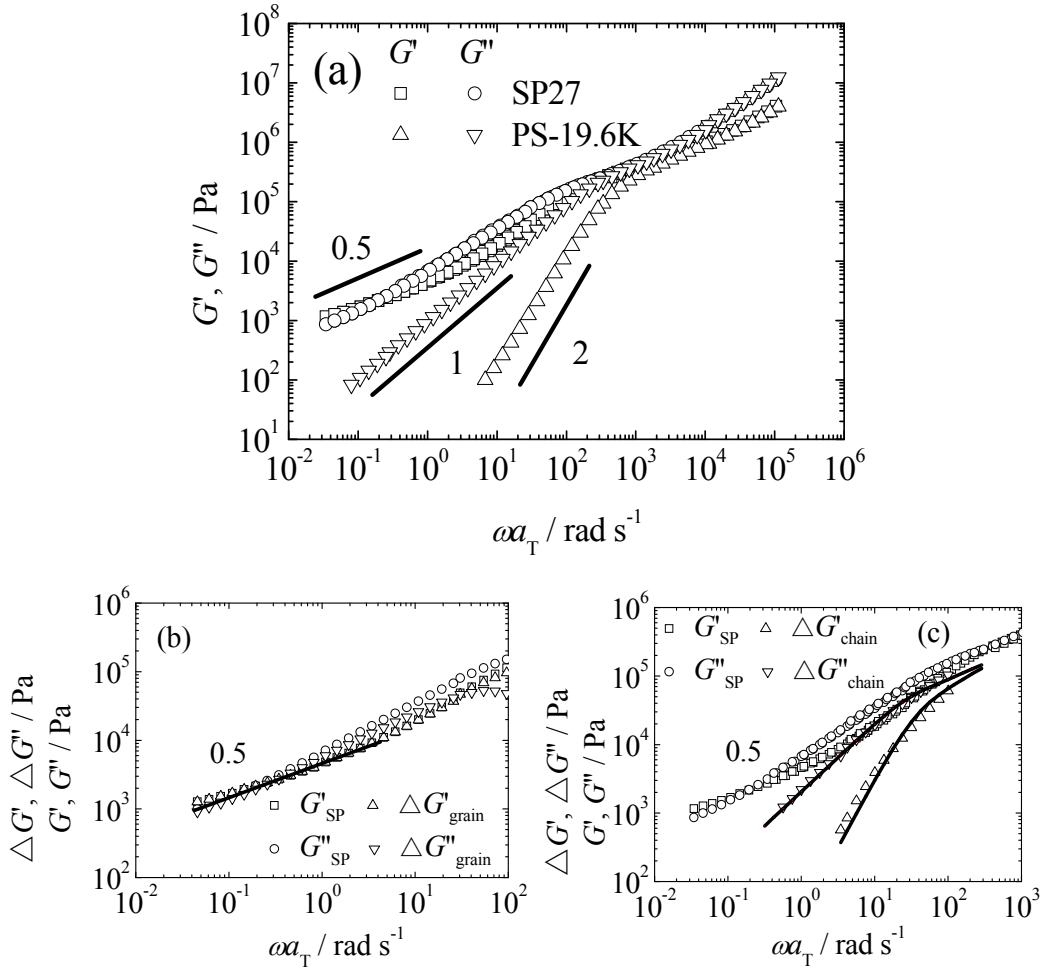

Figure 3-3 Double logarithmic plots of master curves of G^*_{SP}, G^*_{hPS} and ΔG^* against ωa_T for SP27 and PS-19.6K at T_r=160 °C. (a) Comparison between G^*_{SP} and G^*_{hPS}; (b) Comparison between G^*_{SP} and $\Delta G^*_{grain} = G^*_{SP} - G^*_{hPS}$; (c) Comparison between G^*_{SP} and ΔG^*_{chain}. Straight line with the slope of 0.5 in (b) denotes ΔG^*_{grain} used in evaluation of ΔG^*_{chain}. The solid lines in (c) denote results of fitting to equations (3.1) and (3.2) for ΔG^*_{chain}. Other symbols are denoted in the figures.

For SP27, there is no plateau region since the total molecular weight is only a little larger than entanglement molecular weight of PS (M_e = 18000). Thus, it is a natural expectation that relaxations attributable to chain motions appear in a frequency region between the high frequency region where response from local motion is dominant and the low frequency region where response from grains/defects is dominant. To examine this idea, the difference between the data for SP27 (G^*_{SP}) and PS-19.6K (G^*_{hPS}), ΔG^*_{grain} (= G^*_{SP} - G^*_{hPS}) is analyzed to observe the contribution from lamellar grains. Note that this analysis corresponds to subtracting contribution of chain relaxation process of block copolymer from overall viscoelastic responses of SP by assuming that the former is the same as homopolymer having the same N and assuming that the simple additivity holds for two kinds of contributions. There are other additivity rules such as inverse additivity and logarithmic additivity. As shown below, the simplest additivity rule is enough to analyze viscoelastic responses so that we omit discussions with other additivity rules.

Figure 3-3(b) shows double logarithmic plots of ΔG^*_{grain} vs ωa_T together with G^*_{SP} data for SP27. At low frequency end, ΔG^*_{grain} and G^*_{SP} almost coincide with each other, implying that the data in this region are dominated by the responses from lamellar grains/defects. The responses from lamellar grains/defects become more obvious as shown by solid lines with the slope of 0.5 in ΔG^*_{grain} data while G^*_{SP} data show slightly higher ω dependence in higher frequency region. Due to the restriction of chain motions in the ordered structure, it is expected that the chain relaxation process has longer relaxation time than the corresponding G^*_{hPS} [13-16]. Therefore, ΔG^*_{grain} data shown in Figure 3-3(b) may correspond to results with subtraction of somewhat underestimated chain relaxation. However, above result is still enough to assume that we can separate ΔG^*_{grain} and chain relaxation process by the subtraction method.

To extract chain responses from G^*_{SP}, we examine another subtracted data, $\Delta G^*_{chain} = G^*_{SP} - \Delta G^*_{grain}$. Figure 3-3(c) shows double logarithmic plots of ΔG^*_{chain} vs ωa_T for SP27. It is natural to think that the response from large scale motions does not largely affect the data in high frequency region so that ΔG^*_{grain} are expected to level

off or diminish at lower frequency end of high frequency region. Therefore, asymptotic solid lines with slope of 0.5 in Figure 3-3(c) are extended to the frequency where liquid like behavior is observed for G^*_{SP} ($G'_{SP} < G''_{SP}$) and used as ΔG^*_{grain}.

Concerning ΔG^*_{chain}, two extreme cases can be assumed, that is, one is the case with very strong restriction of chain motions due to ordered structure and the other is free from the restriction. Former case corresponds to non-entangled chain tethered on a flat wall and latter corresponds to Rouse chain. In reality, junction point of two components can defuse on the lamellar interface and free energy barrier for interpenetration of components is not so strong since SP27 is in weak segregation regime (mean field χN value: 14 at 160˚C), it is expected that ΔG^*_{chain} are similar to the Rouse type relaxations with equations (3.1) and (3.2) as shown in Figure 3-3(c).

$$G' = \sum_i \frac{\rho RT}{M} \frac{\omega^2 \tau_i^{\,2}}{(1+\omega^2 \tau_i^{\,2})} \tag{3.1}$$

$$G'' = \sum_i \frac{\rho RT}{M} \frac{\omega \tau_i}{(1+\omega^2 \tau_i^{\,2})} \tag{3.2}$$

Here, ρ is density, R is the gas constant and $\tau_i = \tau_1/i^2$, τ_1 being the longest relaxation time. The ρ value for PS [28] is used since PS and P2VP may have almost the same ρ. It seems that the fitting is not as good as hPS but still approximately represent the data implying that non entangled block chain has relaxation mode distribution similar to the Rouse model.

From the above ΔG^*_{chain} data, apparent η^0 and J_e of SP27 are obtained as 2.19×10^3 Pa·sec and 1.08×10^{-5} Pa^{-1}, respectively. The η^0 and J_e of SP27 obtained at well aligned states under steady shear flow in chapter 2 are 1.40×10^3 Pa·sec and 1.85×10^{-5} Pa^{-1}, respectively. Concerning the relatively large experimental error by using small geometries in these studies, we can say that the differences between η^0 and J_e obtained from two methods are consistent. They are higher than the values for corresponding hPS but consistent with the data for lower molecular weight SP samples in the disordered states, which are also higher than corresponding hPS data due to the fluctuation effects. This may imply that the chain relaxation process does not drastically change above and below ODT in the weak segregation regime.

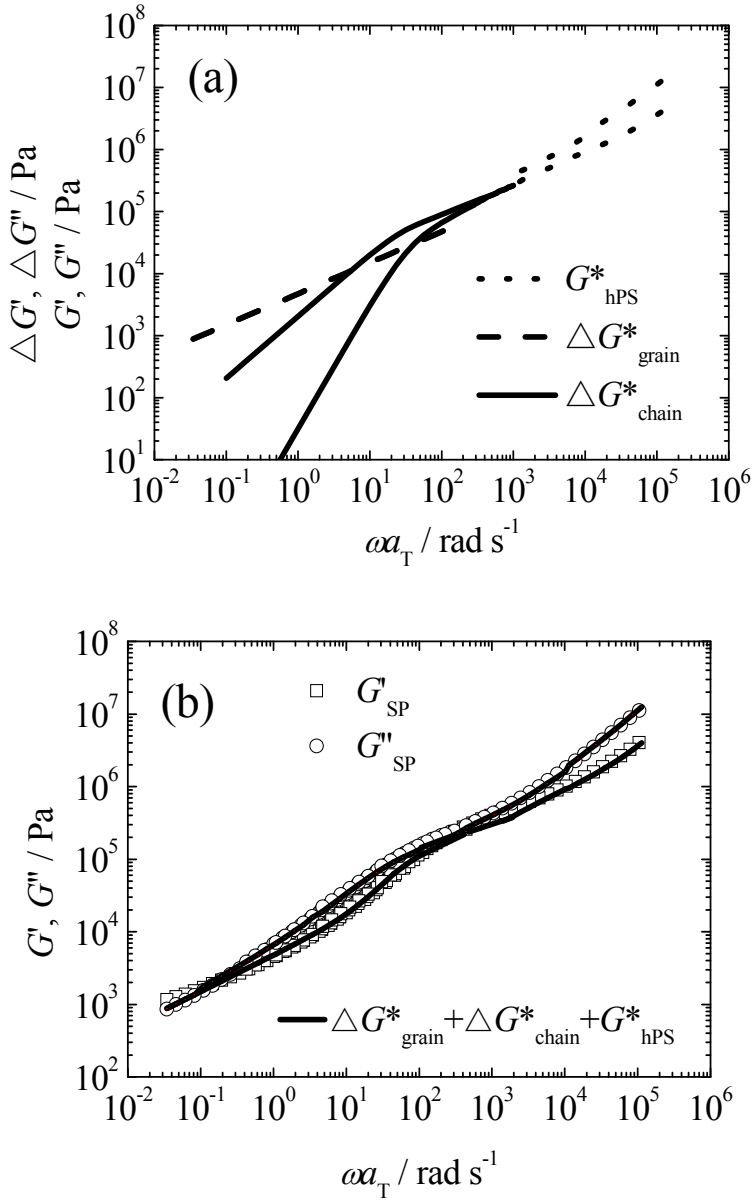

Figure 3-4 (a) Double logarithmic plots of the viscoelastic responses from lamellar grain, ΔG^*_{grain}, terminal portion of Rouse like modes from polymer chain, ΔG^*_{chain}, and responses at higher ω same as hPS, G^*_{hPS}, against ωa_T for SP27 at T_r=160 °C. (b) Comparison between the sum of ΔG^*_{grain}, ΔG^*_{chain} and G^*_{hPS}, and measured G^*_{SP} data. Symbols are denoted in the figures.

To confirm such separation method further, we compare measured G^*_{SP} with the sum of three specified viscoelastic responses, that is, ΔG^*_{grain}, terminal portion of Rouse like modes ΔG^*_{chain}, and responses at higher ω, which are assumed to be the same as G^*_{hPS} to check these three responses can well represent overall viscoelastic properties of symmetric SP diblock copolymers or not. Figure 3-4(a) show double

logarithmic plots of ΔG^*_{grain}, ΔG^*_{chain} for SP27, and G^*_{hPS} for PS-19.6K in high frequency region against ωa_T. Figure 3-4(b) compares the sum of ΔG^*_{grain}, ΔG^*_{chain}, and G^*_{hPS} and measured G^*_{SP} for SP27. Note that, ΔG^*_{grain} and ΔG^*_{chain} used are slightly extended to higher ω region to smoothly connect with G^*_{hPS}. It is clear that measured G^*_{SP} data can be well approximated by the sum of three different viscoelastic responses, ΔG^*_{grain}, ΔG^*_{chain} and G^*_{hPS} in the whole frequency region.

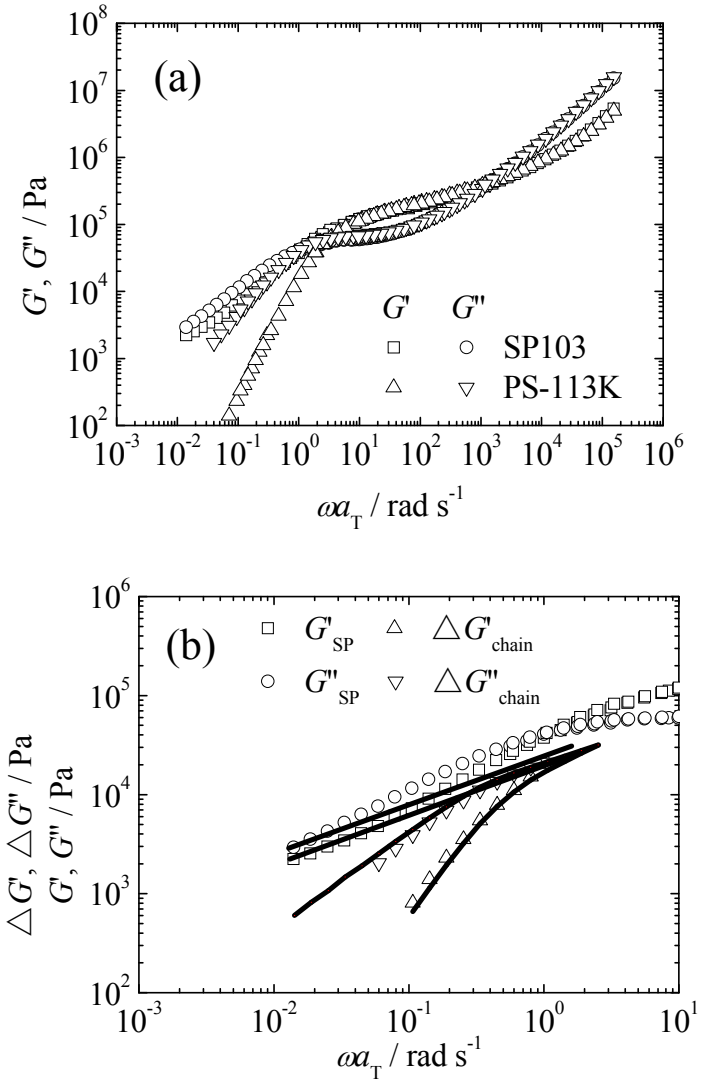

Figure 3-5 Double logarithmic plots of master curves of G^*_{SP}, G^*_{hPS} and ΔG^* against ωa_T for SP103 and PS-113K at T_r=160 °C. (a) Comparison between G^*_{SP} and G^*_{hPS}; (b) Comparison between G^*_{SP} and ΔG^*_{chain}. The straight lines in (b) with the slope of 0.5 denote ΔG^*_{grain} used in evaluation of ΔG^*_{chain}. The solid lines in (b) denote results of fitting to equations (3.1) and (3.2) for ΔG^*_{chain}. Other symbols are denoted in the figures.

3.3.2 Viscoelastic Properties of SP103 in Comparison with PS-113K

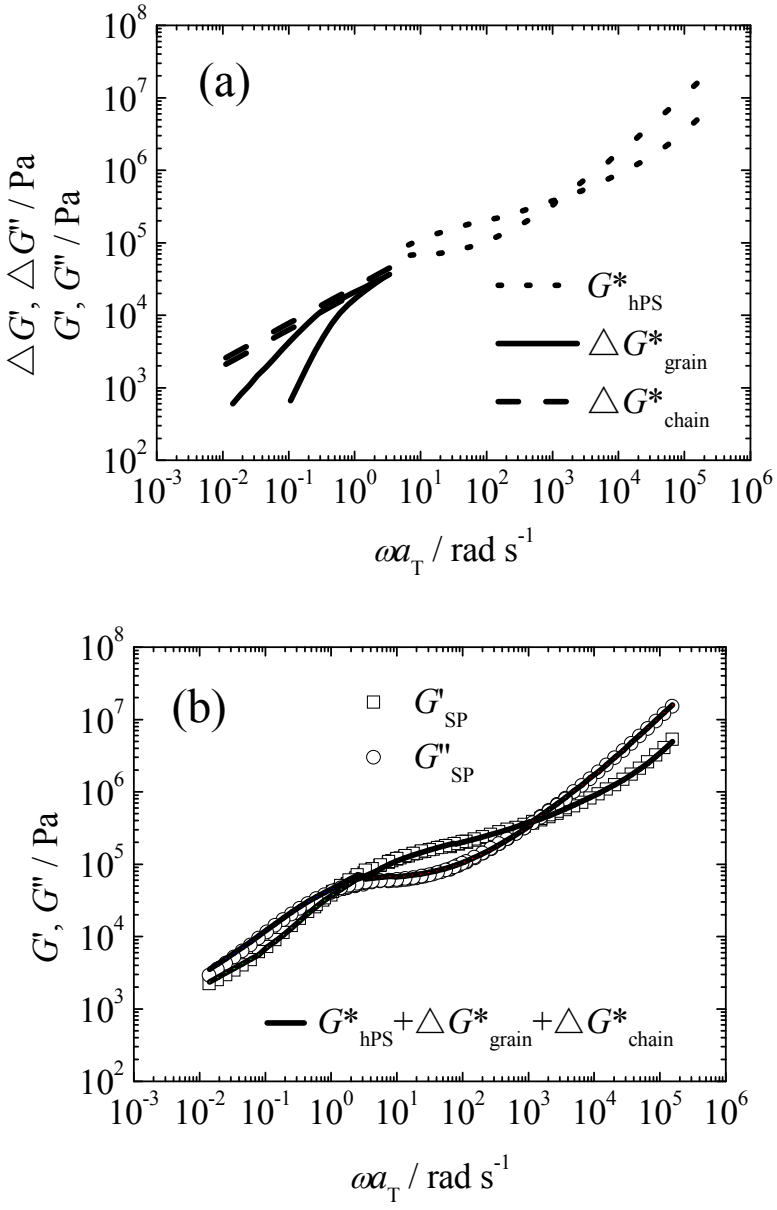

Figure 3-6 (a) Double logarithmic plots of the viscoelastic responses from lamellar grain, ΔG^*_{grain}, terminal portion of Rouse like modes from polymer chain, ΔG^*_{chain}, and responses at higher ω same as hPS, G^*_{hPS}, against ωa_T for SP103 at T_r=160 °C. (b) Comparison between the sum of ΔG^*_{grain}, ΔG^*_{chain} and G^*_{hPS}, and measured G^*_{SP} data. Symbols are denoted in the figures.

Figure 3-5(a) shows double logarithmic plots of master curves of G^* against ωa_T for SP103 and PS-113K with almost the same N. Compared with SP27, there is an obvious entanglement plateau region for SP103 due to larger molecular weight. It is

shown that viscoelastic responses of SP103 coincide with those of PS-113K both in high frequency region and plateau region, whereas viscoelastic responses of SP103 at lower frequency end become completely different from PS-113K due to the presence of lamellar grains. ΔG^*_{grain} are defined as asymptotic lines with the slope of 0.5 as shown in Figure 3-5(b). It is expected that the responses from lamellar grains/defects level off or diminish at the lower end of plateau region where entanglement effect dominates. Hence, ΔG^*_{chain} are attained by subtracting ΔG^*_{grain} till the lower end of plateau region and ΔG^*_{chain} can be approximately expressed by Rouse type relaxations with equations (3.1) and (3.2) as shown in Figure 3-5(b).

As the same with SP27, the three specified viscoelastic responses for SP103 are shown in Figure 3-6(a) including ΔG^*_{grain}, terminal portion of Rouse like modes ΔG^*_{chain}, and responses at higher ω. It is shown that measured G^*_{SP} for SP103 can be well represented by the three specified viscoelastic responses as shown in Figure 3-6(b).

Above all, it is found that master curves of symmetric SP copolymers can be formed by TTS principle as homopolymers and viscoelastic properties of SP are almost the same with those of corresponding PS homopolymers with almost same N in the high frequency region and plateau region. The difference of viscoelastic responses in the lower frequency end between SP and PS is attributable to the presence of lamellar grains. By subtracting ΔG^*_{grain}, ΔG^*_{chain} can be attained with showing Rouse type relaxations. By combining three specified viscoelastic responses, the measured G^*_{SP} can be well represented in the whole frequency region for non-entangled SP27 and entangled SP103.

3.3.3 The Effects of Pre-shear and Annealing on SP27

It is well known that the ΔG^*_{grain} data with the slope of 0.5 are subject to change their magnitudes depending on flow and thermal history [29-34]. That portion may not appear when alignment of lamellar structure is not enough. To examine whether the alignment degree of lamellar grains affects the chain motions or not, therefore, the

data obtained after pre-shear and annealing are discussed to further examine the above separation method for non-entangled SP27 with lower molecular weight, entangled SP103 with intermediate molecular weight and SP44 with higher molecular weight.

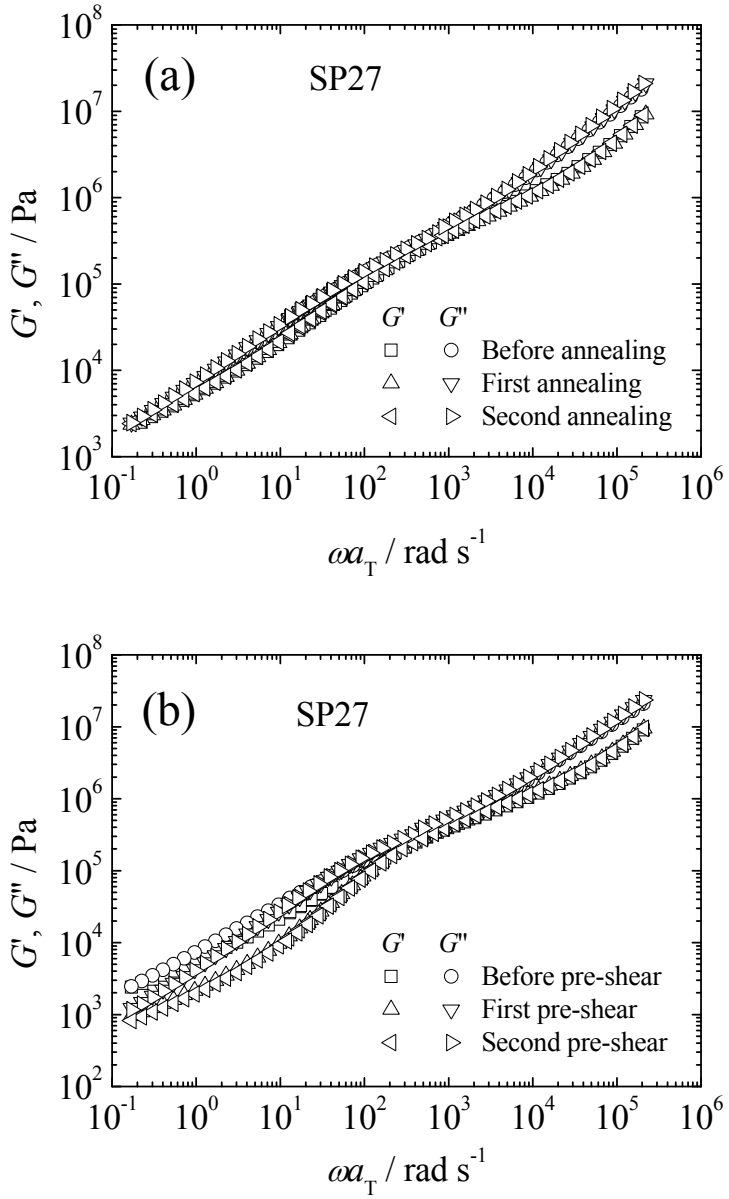

Figure 3-7 Double logarithmic plots of G^* against ωa_T after successive (a) annealing and (b) pre-shear for SP27 at 160 °C. Symbols are denoted in the figures.

Figure 3-7 show double logarithmic plots of G^*_{SP} vs ωa_T for SP27 obtained at 120-160 °C after successive annealing and pre-shear. It is shown that annealing has little effect on the viscoelastic properties in the whole frequency region. Pre-shear, however, results in large decreases at lower frequency region whereas there is no

change in the high frequency region. It has been examined that viscoelastic response in high frequency region is attributable to local motion and viscoelastic response at lower frequency region is resulted from lamellar grains/defects. Pre-shear can change the alignment degree of lamellar grains and consequently reduce the magnitude of *G*' and *G*'' at lower frequency region. However, viscoelastic response of local motion in high frequency region is independent of alignment degree of lamellar grains.

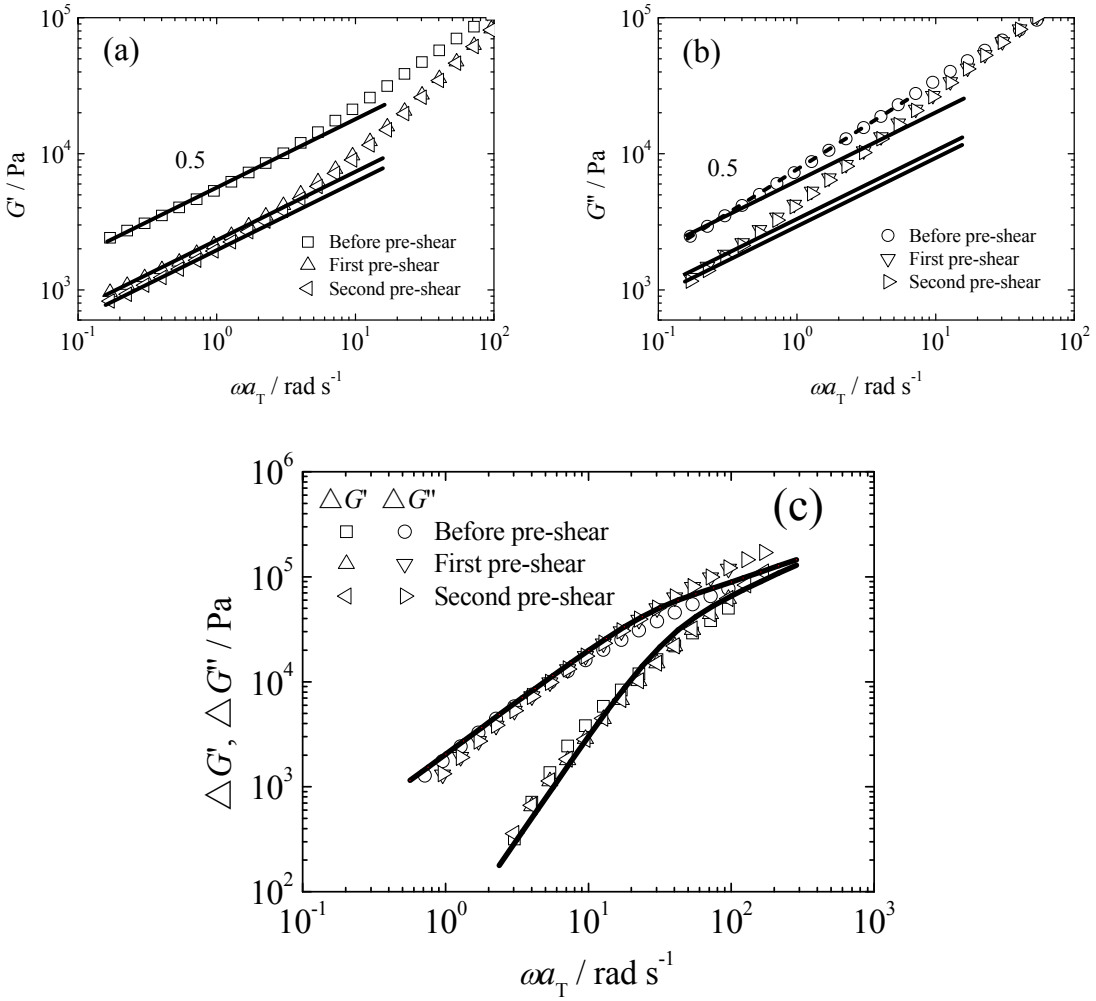

Figure 3-8 Double logarithmic plots of (a) *G*' and (b) *G*'' at lower frequency end against ωa_T after successive pre-shear for SP27 at 160 °C. (c) Double logarithmic plots of chain responses ΔG^*_{chain} against ωa_T after successive pre-shear for SP27 at 160 °C. The straight lines with the slope of 0.5 in (a) and (b) denote ΔG^*_{grain}. The asymptotic dashed line with steeper slope is also shown in (b). The solid lines in (c) denote results of fitting to equations (3.1) and (3.2) for ΔG^*_{chain}. Other symbols are denoted in the figure.

To examine further the effects of annealing and pre-shear on the chain relaxation, ΔG^*_{chain} of SP27 with different annealing and pre-shear times are attained by the same procedure as explained before. Since annealing has little effect on G^*_{SP} of SP27 in the whole frequency region, there is no necessary to analyze the effect of annealing on ΔG^*_{chain}. Figure 3-8 (a) and (b) show the enlarged G' and G'' at lower frequency end for SP27 after successive pre-shear. It is seen that the region where the data having $\omega^{0.5}$ dependence become clearer for G' and the data at lower frequency end decreases with the increase of pre-shear times, while G'' have somewhat higher ω dependence than $\omega^{0.5}$ even after 2 times pre-shear. When the asymptotic line with steeper slope as shown in Figure 3-8(b) is used as $\Delta G''_{grain}$ in the subtraction method, the obtained $\Delta G''_{chain}$ data become too small in comparison with $\Delta G'_{chain}$. As a result, $\omega^{0.5}$ dependence of ΔG^*_{grain} as shown in Figure 3-8(a) and (b) are used in evaluation of ΔG^*_{chain}. Figure 3-8(c) shows double logarithmic plots of chain responses ΔG^*_{chain} against ωa_T after successive pre-shear for SP27 at 160 °C. It is shown that pre-shear has a little effect on ΔG^*_{chain} in comparison with the change of G^*_{SP}, which implies that the chain relaxation of SP27 is almost independent of the alignment degree of lamellar grains.

3.3.4 The Effects of Pre-shear and Annealing on SP103

To investigate whether ΔG^*_{chain} of entangled SP103 depend on the alignment degree of lamellar grains or not, the effects of annealing and pre-shear are examined for SP103. Figure 3-9 show double logarithmic plots of G^*_{SP} vs ωa_T for SP103 obtained at 120-200 °C after successive annealing and pre-shear. It is shown that annealing has a little effect on viscoelastic properties of SP103 in the whole frequency region as the same with SP27. On the other hand, it is shown that G^*_{SP} coincide with each other in high frequency region after successive pre-shear, while G^*_{SP} at lower frequency end decreases obviously with the increase of pre-shear times as the same with SP27.

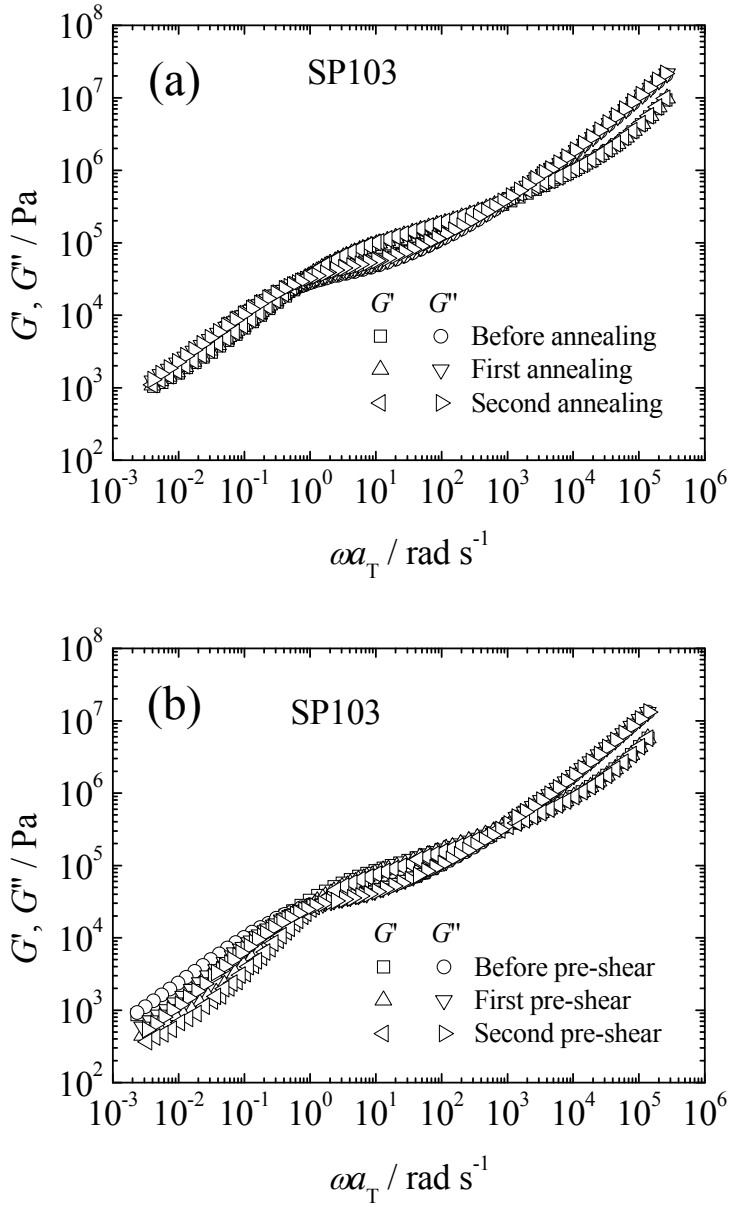

Figure 3-9 Double logarithmic plots of G^* against ωa_T after successive (a) annealing and (b) pre-shear for SP103 at 160 °C. Symbols are denoted in the figures.

Figure 3-10 shows double logarithmic plots of chain responses ΔG^*_{chain} attained by the same procedure against ωa_T after successive pre-shear for SP103 at 160 °C. Note that the evaluation method of ΔG^*_{chain} for SP103 after successive pre-shear is the same with that for SP27. Hence, the detailed subtraction method is skipped for SP103 after successive pre-shear. It is shown that pre-shear has a little effect on ΔG^*_{chain}, which may imply that pre-shear cannot affect chain relaxation even in the entangled state.

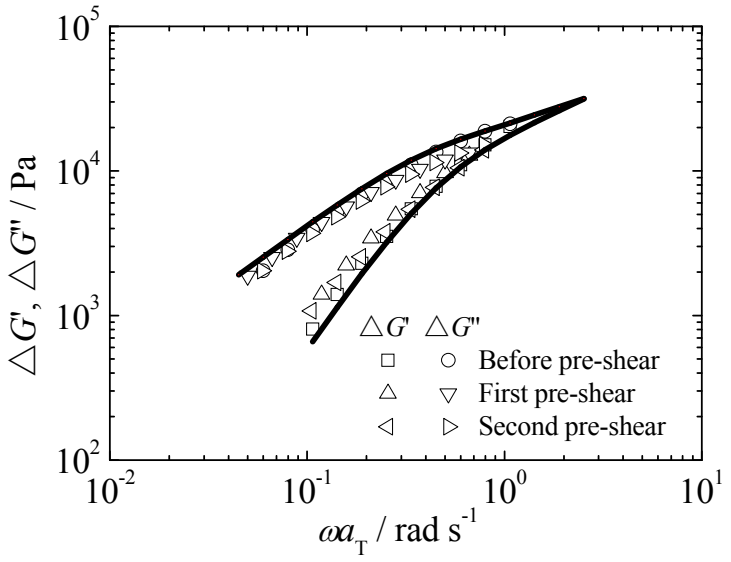

Figure 3-10 Double logarithmic plots of chain responses ΔG^*_{chain} against ωa_T after successive pre-shear for SP103 at 160 °C. The solid lines denote results of fitting to equations (3.1) and (3.2) for ΔG^*_{chain}. Other symbols are denoted in the figure.

3.3.5 The Effects of Pre-shear and Annealing on SP44

For SP44 with higher molecular weight, the separation method cannot be utilized since ΔG^*_{grain} is larger than G^*_{SP} in the low frequency region. However, pre-shear can reduce ΔG^*_{grain} at lower frequency end and result in the difference between G^*_{SP} and ΔG^*_{grain} as reported for SP103 and SP27. As a result, the effects of annealing and pre-shear are examined further for SP44. Figure 3-11 show double logarithmic plots of G^*_{SP} against ωa_T after successive annealing and pre-shear for SP44 at 160 °C. It is shown that annealing causes a little increase both in plateau region and lower frequency end whereas pre-shear results in an obvious decrease at lower frequency end as the same with SP27 and SP103. For SP44, ΔG^*_{grain} become lower than G^*_{SP} in the low frequency region after pre-shear and the difference between ΔG^*_{grain} and G^*_{SP} can be attained correspondingly. However, the separation method cannot be utilized due to large error for ΔG^*_{chain} and viscoelastic behaivor of SP44 will be examined further in chapter 4.

To investigate the effects of annealing and pre-shear on viscoelastic properties of SP103 and SP44 in detail, several rheological parameters are examined further,

including the frequency at the crossover of G' and G'' at the lower end of plateau region, $\omega_{\text{crossover}}$, and the frequency where $\tan\delta\,(=G''/G')$ has a minimum value, $\omega_{(\tan\delta)\text{min}}$, as well as plateau modulus G_N^0 which is defined as G' at $\omega_{(\tan\delta)\text{min}}$.

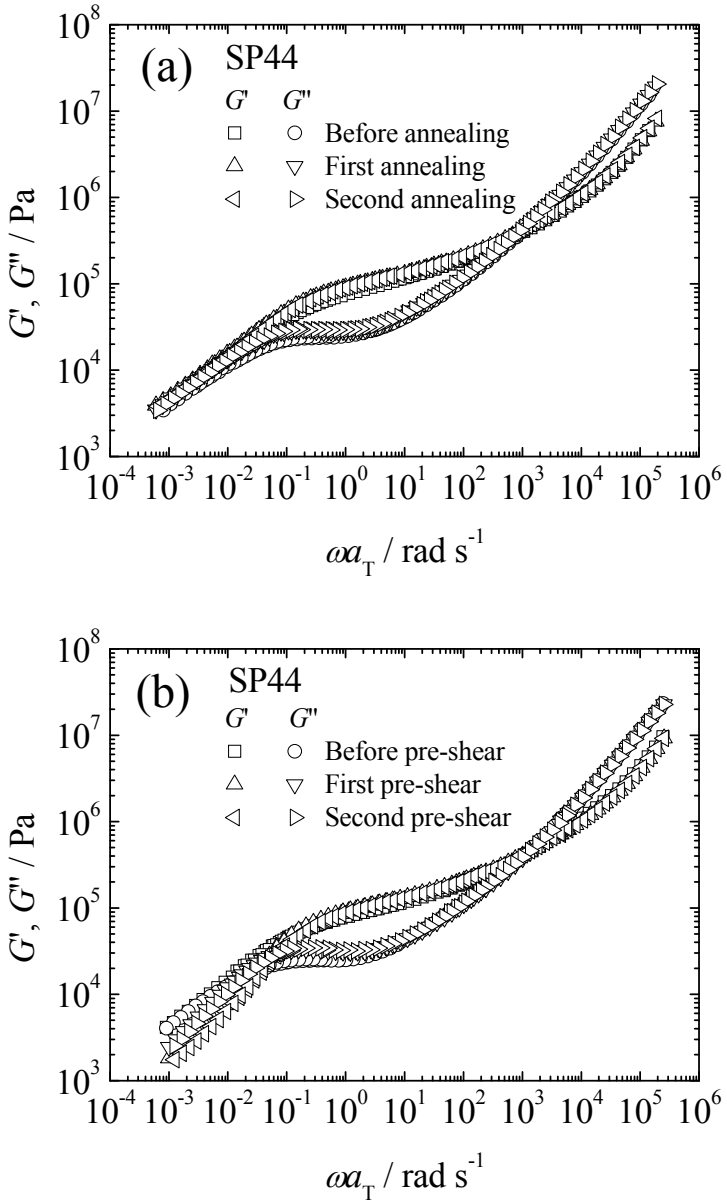

Figure 3-11 Double logarithmic plots of G^* against ωa_T after successive (a) annealing and (b) pre-shear for SP44 at 160 °C. Symbols are denoted in the figures.

Figure 3-12 show the effects of annealing and pre-shear on $\omega_{\text{crossover}}$, $\omega_{(\tan\delta)\text{min}}$ and G_N^0 for SP103 and SP44. Note that SP27 is not discussed due to lower molecular weight in the non-entangled state. It is shown that pre-shear and annealing can both

increase $\omega_{crossover}$ and $\omega_{(\tan\delta)min}$, while pre-shear has a larger effect on $\omega_{crossover}$ in comparison with annealing. Especially for SP44, there is no crossover of G' and G'' at the lower end of plateau region even after successive annealing, while $\omega_{crossover}$ comes out after pre-shear procedure, which may imply that viscoelastic responses of lamellar grains/defects become more obvious after successive pre-shear. Moreover, it is found that annealing causes a little increase in G_N^0 for both SP103 and SP44 since annealing can improve the alignment degree of lamellar grains. Pre-shear has the same effect with annealing for SP44 while it causes a little decrease in G_N^0 for SP103. In addition, the change of $\omega_{(\tan\delta)min}$ are not as much as $\omega_{crossover}$, which may imply that pre-shear has a larger effect on the viscoelastic responses in the low frequency region in comparison with plateau region where entanglement effect dominates.

Above all, annealing has little effect on non-entangled SP27 in the whole frequency region, while annealing causes a little increase both in plateau region and low frequency region for entangled SP103 and SP44. On the other hand, pre-shear results in large decreases in low frequency region while there is little effect on plateau region and high frequency region, where entanglement effects and local motions dominate, respectively. By subtracting ΔG^*_{grain}, however, annealing and pre-shear both have little effect on chain relaxations ΔG^*_{chain} for SP27 and SP103.

From these results, we conclude that when alignment degree of lamellar structure is appropriately controlled and hence responses due to grains/defects having lower magnitude than G^*_{SP} are asymptotically observed at the low frequency end, a new response attributable to chain motion ΔG^*_{chain} showing Rouse like behavior can be separated irrespective of pre-shear and annealing procedure, even when the ω dependencies of G^*_{SP} at low frequency end do not become precisely equal to $\omega^{0.5}$.

We speculate that the viscoelastic response ΔG^*_{chain} is either whole chain relaxation or independent motion of component chains. Even in the latter case, the fact that existence of only one major chain relaxation is understandable since two component chains should show practically the same responses due to almost the same

chain length and viscoelastic properties. We cannot discuss further the detail of ΔG^*_{chain} in this chapter but more systematic study by using a series of SP diblock copolymers with different molecular weights will be reported in the following chapter.

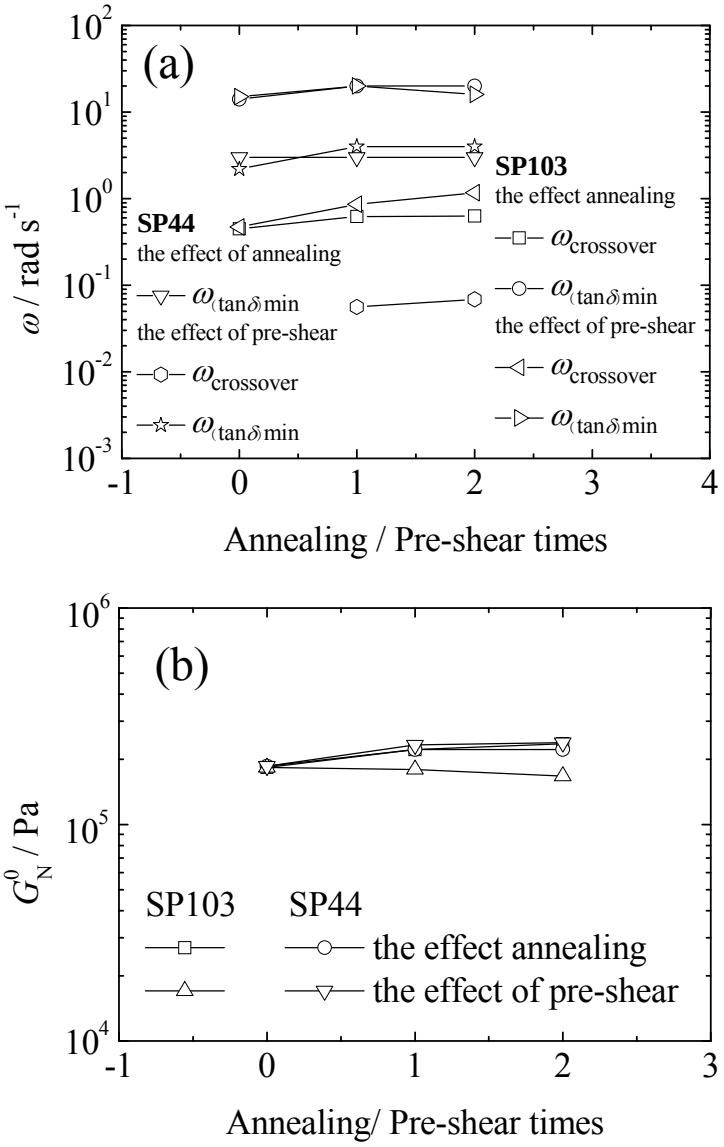

Figure 3-12 Semi logarithmic plots of several rheological parameters against annealing/pre-shear times for SP103 and SP44 at 160 °C. (a) $\omega_{crossover}$ and $\omega_{(\tan\delta)\min}$; (b) G^0_N. Symbols are denoted in the figures.

3.4 Summary

Due to the almost same thermo rheological properties of components, master curves of G^*_{SP} are obtained for symmetric poly(styrene-*b*-2-vinylpyridine)s. The

responses from large scale motions of lamellar grains/defects, ΔG^*_{grain}, becomes more apparent after appropriate pre-shear and/or annealing. When asymptotic $\omega^{0.5}$ dependence of ΔG^*_{grain} are observed at low frequency end and whose magnitude become lower than G^*_{SP}, the responses of components ΔG^*_{chain} having Rouse like modes can be successfully separated by subtracting method examined in this study, irrespective of pre-shear or annealing. By combining ΔG^*_{grain}, ΔG^*_{chain} and the data for hPS G^*_{hPS} at higher ω, G^*_{SP} data can be well approximated in a whole frequency range of the measurement.

References

[1]Leibler L, *Macromolecules*, **13**, 1602 (1980)

[2]Colby RH, *Curr. Opin. Colloid Interface Sci.*, **1**, 454 (1996)

[3]Watanabe H, "*Rheology of Multiphase Polymeric Systems*", In: Araki T, Qui TC, Shibayama M, "*Structure and Properties of Multiphase Polymeric Materials*", New York: Marcel Dekker (1998)

[4]Kossuth MB, Morse DC, Bates FS, *J. Rheol.*, **43**, 167 (1999)

[5]Spontak RJ, Patel NP, *Curr. Opin. Colloid Interface Sci.*, **5**, 334 (2000)

[6]Hamley IW, *Curr. Opin. Colloid Interface Sci.*, **5**, 342 (2000)

[7]Hamley IW, *J. Phys. Condens. Matter*, **13**, R643 (2001)

[8]Lodge TP, *Macromol. Chem. Phys.*, **204**, 265 (2003)

[9]Bates FS, *Macromolecules*, **17**, 2607 (1984)

[10]Bates FS, Rosedale JH, *Macromolecules*, **23**, 2329 (1990)

[11]Bates FS, Rosedale JH, Fredrickson GH, *J. Chem. Phys.*, **92**, 6255 (1990)

[12]Kawasaki K, Onuki A, *Phys. Rev. A*, **42**, 3664 (1990)

[13]Witten TA, Leibler L, Pincus PA, *Macromolecules*, **23**, 824 (1990)

[14]Rubinstein M, Obukov SP, *Macromolecules*, **26**, 1740 (1993)

[15]Ohta T, Enomoto Y, Harden JL, Doi M, *Macromolecules*, **26**, 4928 (1993)

[16]Doi M, Harden JL, Ohta T, *Macromolecules*, **26**, 4935 (1993)

[17]Yamaguchi M, Maeda N, Takahashi Y, Matsushita Y, Noda I, *Polym. J.*, **23**, 227

(1991)

[18]Takahashi Y, Noda M, Kitade S, Matsuoka K, Matsushita Y, Noda I, *Polym. J.*, **37**, 894 (2005)

[19]Takahashi Y, Imaichi K, Noda M, Takano A, Matsushita Y, *Polym. J.*, **39**, 632 (2007)

[20]Matsushita Y, Shimizu K, Nakao H, Choshi H, Noda I, Nagasawa M, *Polym. J.*, **18**, 361 (1986)

[21]Matsushita Y, Nakao Y, Saguchi R, Choshi H, Nagasawa M, *Polym. J.*, **18**, 493 (1986)

[22]Matsushita Y, Nakao Y, Shimizu K, Noda I, Nagasawa M, *Macromolecules*, **21**, 2790 (1988)

[23]Takahashi Y, Ochiai N, Matsushita Y, Noda I, *Polym. J.*, **28**, 1065 (1996)

[24]Takahashi Y, Noda I, Nagasawa M, *Macromolecules*, **18**, 2220 (1985)

[25]Takahashi Y, Kitade S, Noda M, Ochiai N, Noda I, Imai M, *et al.*, *Polym. J.*, **30**, 388 (1998)

[26]Takahashi Y, Ochiai N, Yanagida M, Kitade S, Noda I, *Polymer*, **39**, 4313 (1998)

[27]Graessley WW, "*Polymer Liquids & Networks: Dynamics and Rheology*", London and New York: Talyor & Francis Group (2008)

[28]Brandrup J, Immergut EH, "*Polymer Handbook*", 3rd ed., New York: Wiley Interscience (1989)

[29]Tepe T, Hajduk DA, Hillmyer MA, Weimann PA, Tirrell M, Bates FS, *et al.*, *J. Rheol.*, **41**, 1147 (1997)

[30]Winey KI, Patel SS, Larson RG, Watanabe H, *Macromolecules*, **26**, 2542 (1993)

[31]Kannan R, Kornfield JA, *Macromolecules*, **27**, 1177 (1994)

[32]Gupta VK, Krishnamoorti R, Kornfield JA, Smith SD, *Macromolecules*, **28**, 4464 (1995)

[33]Patel SS, Larson RG, Winey KI, Watanabe H, *Macromolecules*, **28**, 4313 (1995)

[34]Riise BL, Fredrickson GH, Larson RG, Pearson DS, *Macromolecules*, **28**, 7653 (1995)

Chapter 4 Molecular Weight Dependence of Viscoelastic Properties for Symmetric Poly(styrene-*b*-2-vinylpyridine)s in the Ordered State

4.1 Introduction

Lamellar domains are formed due to the repulsive interactions between A and B for symmetric AB diblock copolymers [1]. Viscoelastic properties of lamellar forming block copolymers have been investigated abundantly and it is shown that frequency (ω) dependencies of storage modulus $G'(\omega)$ and loss modulus $G''(\omega)$ asymptote to $\omega^{0.5}$ at low frequency region [2-4], which was regarded as the responses of large scale motions from grain/defects in theory [5]. Theoretical studies of viscoelastic behavior for block copolymers are developed to include other morphologies and other relaxation modes such as chain relaxations [6-9].

In chapter 3, we have checked a separation method of responses from large scale motions and chain relaxations for symmetric poly(styrene-*b*-2-vinylpyridine)s (SP) in the ordered state. It is found that master curves can be generated for SP copolymers since polystyrene (PS) and poly(2-vinylpyridine) (P2VP) have almost same thermo rheological properties [10, 11]. Moreover, it is found that molecular responses can be attained by subtracting large scale responses which are approximately described by the asymptotic lines with slope of 0.5 at lower frequency end. The attained molecular responses can be approximately expressed by Rouse type relaxations as polymer chains responses irrespective of pre-shear and/or annealing procedures.

However, block chain relaxation mechanisms have not been well understood despite of large numbers of experimental results [12-18]. Through diffusion experimental study for block copolymers with different ordered structures and different molecular weights, it is found that interface diffusion dominate in strong segregation regime (WSR) as discussed in chapter 1 [19]. In lamellar case, Rouse type relaxations are expected for block copolymers in the non-entangled state, whereas

block retraction relaxations are proposed when block copolymers are in the entangled state [20, 21]. The block chains have to first escape from interpenetration zones by gradual retraction motions toward junction points, which are similar to relaxation motions considered for long branched chains, resulting in power law like relaxations. With the progress of chain relaxations, the solid like viscoelastic response changes to liquid like response with Rouse like modes. In general, the "melting" of lamellae start for a component which is easier to escape from interpenetration zone followed by chain relaxations of the other component. However, those liquid like relaxation modes may be hidden by the responses from grains/defects.

In this chapter, dynamic viscoelastic properties are examined for symmetric SP diblock copolymers with randomly oriented lamellae over a wide range of molecular weight (M). It is expected for these samples that 2 component chains can be regarded as two equal but immiscible chains so that the situation is simplified. First, the data for lower, intermediate and higher molecular weight samples are compared with the data for corresponding PS with almost same N. A few characteristic parameters such as plateau modulus are directly obtained from the data. The responses from grains/defects and polymer chains in dynamic moduli are separated by subtraction method discussed in this study. The same procedure is used for other samples up to a certain critical M. From the molecular responses thus obtained, zero shear viscosity (η^0) and steady state compliance (J_e) are evaluated and discussed in comparison with those for PS.

4.2 Experimental

4.2.1 Samples

The SP diblock copolymers and PS homopolymers were synthesized by anionic polymerization in *vacuo* as reported previously [22, 23]. Weight-averaged molecular weights M_w of the samples were determined by multi-angle laser light scattering (MALLS) method using DOWN EOS enhanced optical system of the Wyatt

Technology at 35 ºC in THF. THF solutions of samples were optically purified with 0.2 μm PTFE filter before the measurement. The wave length used was 690 nm. The reflective index increment, *dn*/*dc*, of polystyrene and poly(2-vinylpyridine) in THF are 0.185 mL/g and 0.180 mL/g, respectively, being very close to each other. Therefore, 0.185 mL/g was used as *dn*/*dc* for all M_w measurements.

Table 4-1 Molecular characteristics of poly(styrene-*b*-2-vinylpyridine)s

Samples	M_w [a]	M_w/M_n [b]	ϕ_s [c]
SP27	2.10×10^4	1.03	0.50
SP102	2.90×10^4	1.01	0.52
SP28	3.03×10^4	1.16	0.54
SP22	3.80×10^4	1.01	0.52
SP101	4.69×10^4	1.04	0.51
SP20	6.83×10^4	1.04	0.52
SP103	9.86×10^4	1.02	0.50
SP34	10.9×10^4	1.05	0.51
SP55	13.5×10^4	1.04	0.46
SP104	20.9×10^4	1.03	0.51
SP44	22.4×10^4	1.01	0.51
SP24	38.6×10^4	1.15	0.51

[a] by MALLS; [b] by GPC; [c] by ^{1}H-NMR.

Table 4-2 Molecular characteristics of polystyrenes

Samples	M_w[a]	M_w/M_n [b]
PS-19.6K	1.96×10^4	1.02
PS-37.9K	3.79×10^4	1.01
PS-113K	11.3×10^4	1.01

[a] by MALLS; [b] by GPC.

Molecular weight heterogeneities, M_w/M_n, where M_n being number-averaged molecular weights are determined in THF by GPC system of Tosoh Ltd., equipped with RI-8012 differential refractive index detector and with three GMH_{HR} columns with 7.8 mm inner diameter each. Standard polystyrenes are used for the calibration. Volume fractions of styrene in SPs are determined by ^1H NMR spectra measured with a Varian unity-500 NMR spectrometer. Molecular characteristics of SPs and PSs are listed in Table 4-1 and Table 4-2 in detail. According to the previous ODT measurements [24], we can safely assume that SPs used in this study are in the ordered states.

4.2.2 Samples Preparation

Disk shaped samples with 8 mm diameter and 1.1 mm thickness for rheological measurements were prepared by hot-press method at 150 °C for 5 minutes. The samples were annealed in vacuum oven for 10 hrs at 110 °C before the measurements.

4.2.3 Dynamic Rheological Measurements

Dynamic rheological measurements were performed with an Anton Parr MCR300 rheometer using 8 mmϕ parallel plates in a temperature range of 200-120 °C except in the measurement for those with M_w more than 20×10^4, in which the data till 220 °C were also obtained. Frequency sweep measurements were carried out in the above temperature range for all samples in linear region (maximum strain: 1%).

All the measurements were carried out under N_2 gas after at least 10 minutes duration time before the measurement at each temperature. After the measurement, GPC measurement was conducted to confirm that no chain degradation occurred by the rheological measurements.

4.3 Results and Discussion

4.3.1 Comparison of Master Curves among SP Copolymers

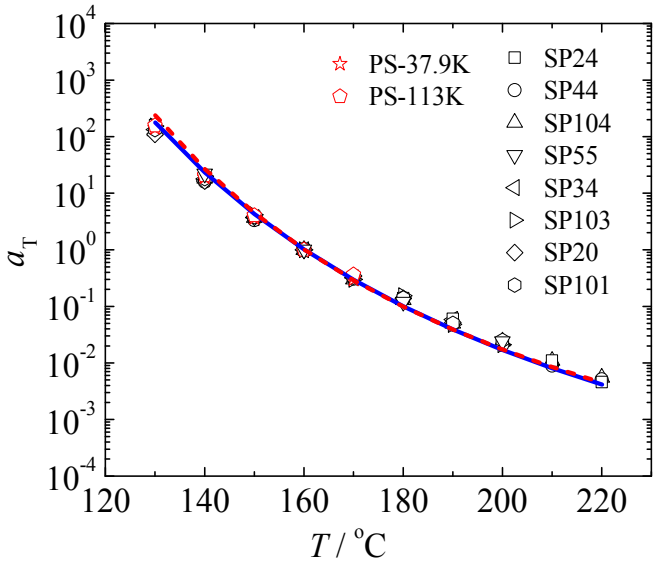

Figure 4-1 Semi logarithmic plots of shift factors a_T against T for entangled SPs and PSs at T_r=160 °C. The solid line for P2VP [10] and dashed line for PS [25] are shown in the figure. Symbols are denoted in the figure.

Figure 4-1 shows temperature T dependence of shift factors a_T used to generate the master curves of G^*_{SP} for higher M_w samples, which are almost the same as those for components, P2VP [10] and PS [25]. Note that there exist small deviations of data at lower and higher temperature ends and correction for iso-free volume state was needed for samples with lower M_w samples as discussed in previous works, main results in this study are not seriously affected by such differences in a_T.

To avoid severe overlap of data and clearly show their characteristics, master curves of G^*_{SP} and tanδ for SPs are separately shown in three groups. Figures 4-2 ~ 4-4 show double logarithmic plots of master curves of (a) G'_{SP}, (b) G''_{SP}, and (c) tanδ against ωa_T for non-entangled, slightly entangled and entangled SPs at T_r=160 °C, respectively. In these figures, data for PSs, PS-19.6K, PS-37.9K and PS-113K having almost the same N as SP27, SP22 and SP34, respectively, are shown for comparison.

It is clear in these figures that the SP data at higher ω are practically the same with each other and also as those of PSs. The data for SP and PS having almost the same N deviate at slightly higher ω than the ω where minimum of tanδ for PSs are observed.

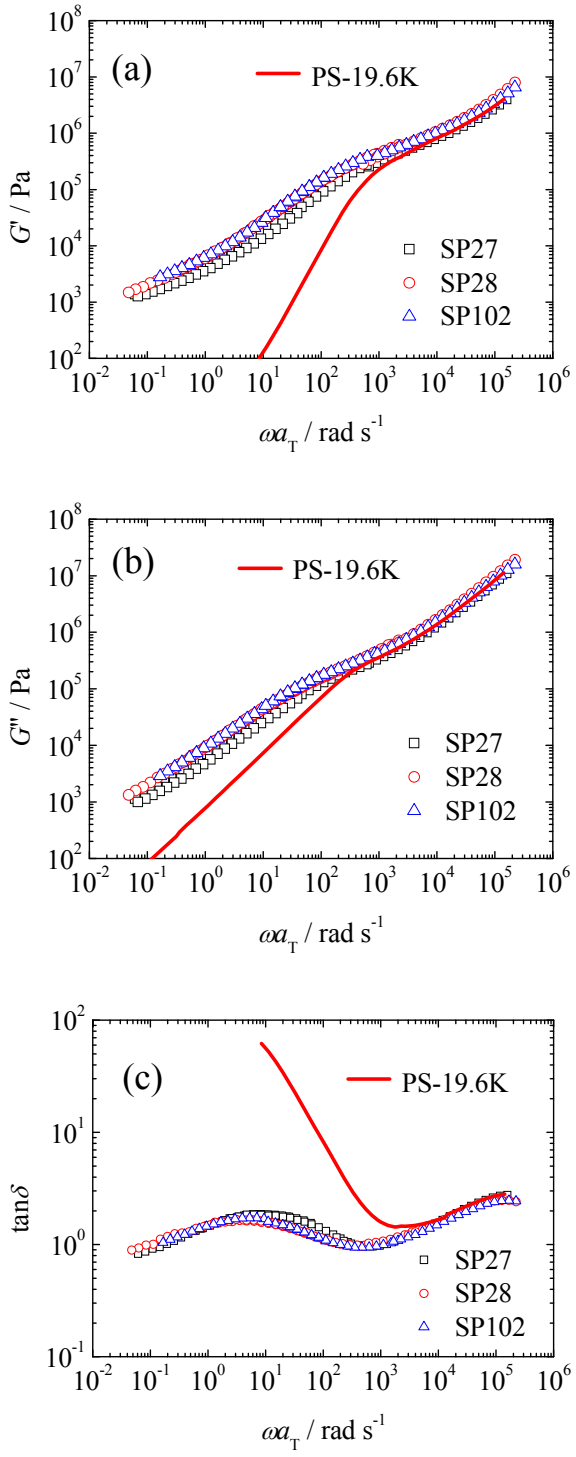

Figure 4-2 Double logarithmic plots of G' (a), G'' (b) and tanδ (c) against ωa_T for SPs with lower molecular weights and PS-19.6K at T_r=160 °C. Symbols are denoted in the figure.

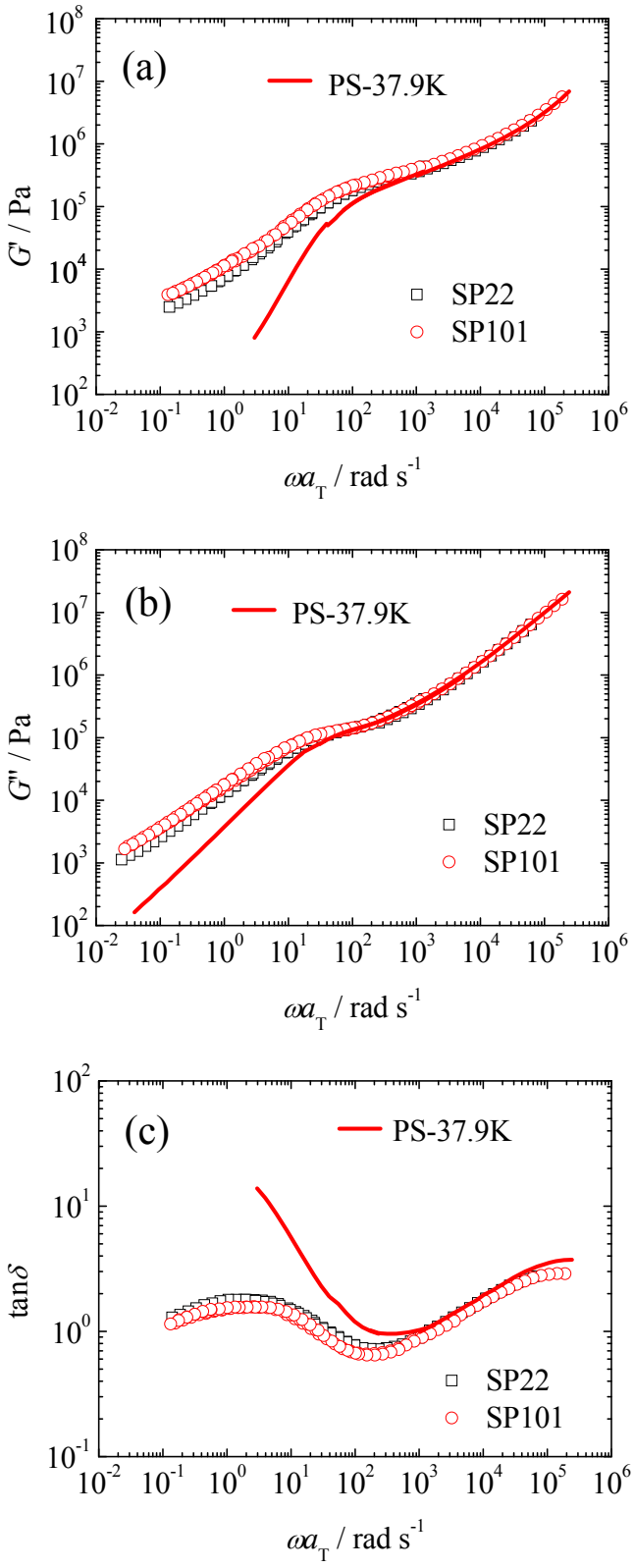

Figure 4-3 Double logarithmic plots of G' (a), G'' (b) and tanδ (c) against ωa_T for SPs with intermediate molecular weights and PS-37.9K at T_r=160 °C. Symbols are denoted in the figure.

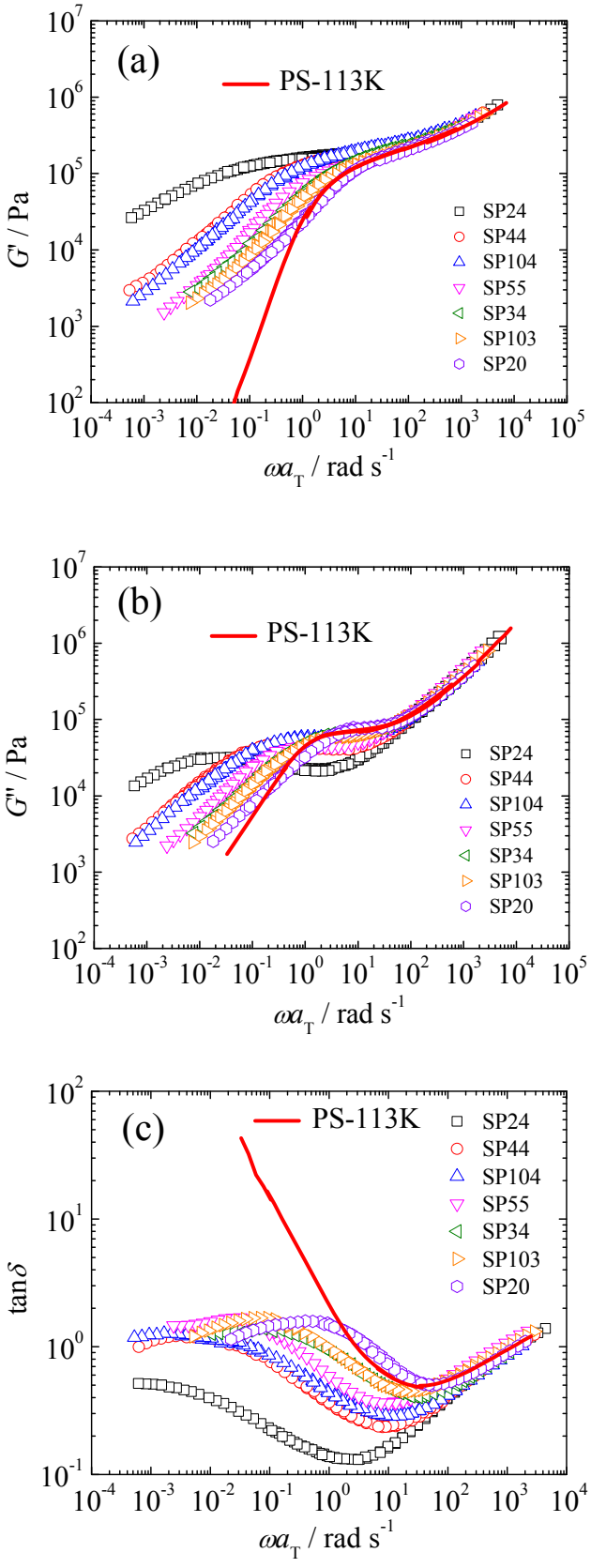

Figure 4-4 Double logarithmic plots of G' (a), G'' (b) and $\tan\delta$ (c) against ωa_T for SPs with higher molecular weights and PS-113K at T_r=160 °C. Symbols are denoted in the figure.

The SP data in Figure 4-2 are all similar with each other due to the small difference in M_w. From tanδ (Figure 4-2(c)), it is seen that there exist no solid like behavior in entire range of ω. The G^* data continuously decrease with decrease of ω showing small bumps, which corresponds to small and broad maximum of tanδ, and G^* asymptote to the power law like behavior at the lower ω end. As discussed for SP27 in previous study, the power law like behavior is attributed to the motions of grains/defects since these samples are not entangled and the responses from polymer chains can be obtained by the subtraction method, which will be discussed later. In Figures 4-3 and 4-4, apparent plateau region is observed for each sample as denoted by the minimum of tanδ < 1.

4.3.2 Molecular Weight Dependence of G_N^0, $G_{crossover}$ and $\omega_{crossover}$

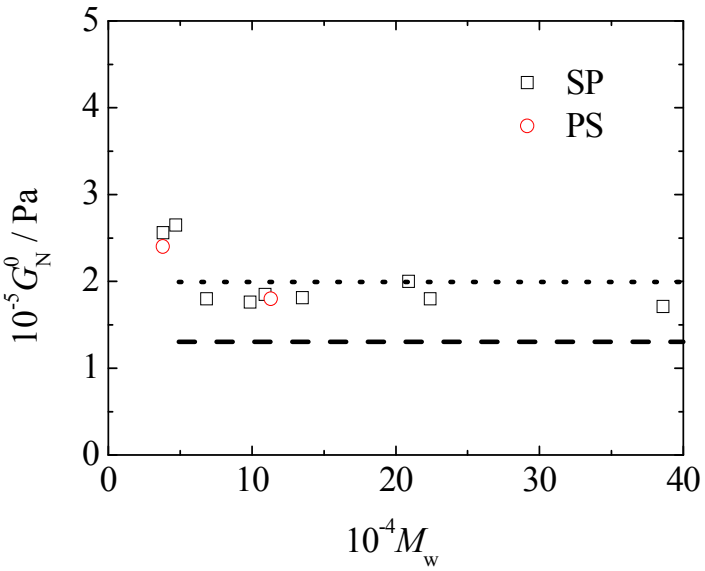

Figure 4-5 Linear plots of plateau modulus G_N^0 against M_w for entangled SPs and PSs at T_r=160 °C. The dotted line and dashed line denote G_N^0 for PS and P2VP, respectively. Symbols are denoted in the figure.

Plateau modulus G_N^0 for each sample is defined as the G' value where tanδ shows the minimum. Figure 4-5 shows double logarithmic plots of G_N^0 vs M_w for the

samples shown in Figures 4-3 and 4-4. The dotted line and dashed line in the figure denote the values for PS and P2VP, respectively. The G_N^0 values for SP samples with M_w > 60K locate between those for PS and P2VP and closer to that of PS. The data for slightly entangled samples (SP22, SP101 and PS-37.9K) have somewhat higher values than other entangled samples, which is artifact from narrow plateau region because of low M_w. As a whole, we conclude that there is no specific difference in the magnitude of plateau modulus for SP and PS. In other words, elongation of component chains perpendicular to lamellar interface does not affect entanglement density.

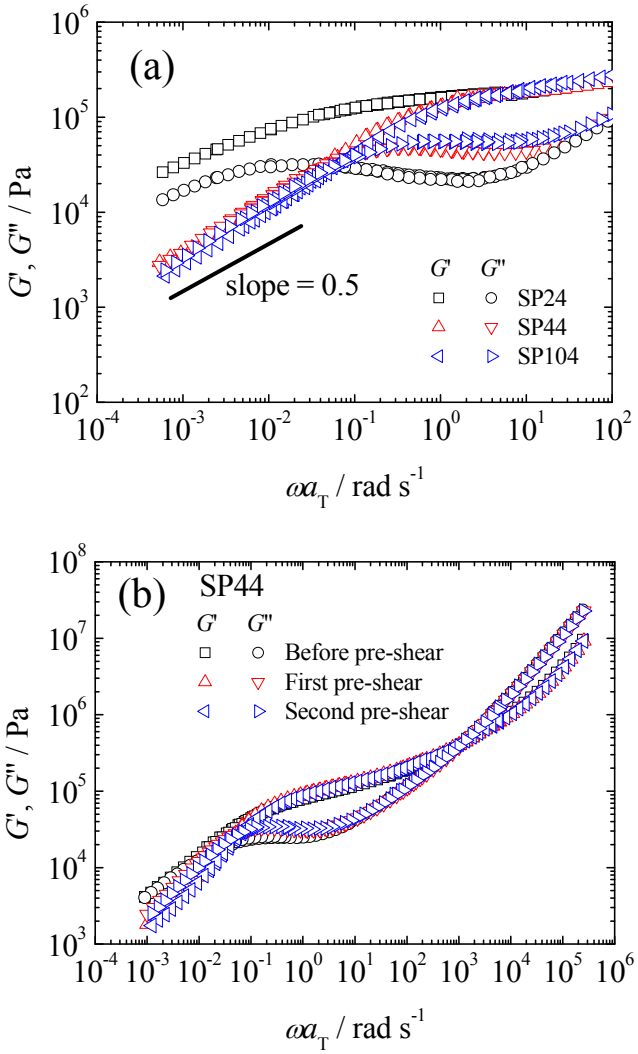

Figure 4-6 (a) Double logarithmic plots of G^*_{SP} against ωa_T for SP104, SP44 and SP24 at T_r=160 °C. (b) Comparison of G^*_{SP} data with and without pre-shear for SP44 at T_r=160 °C. The symbols are denoted in the figures.

It is seen in Figure 4-4 that the data for the three highest M_w samples are different from others. Figure 4-6(a) shows enlarged plots of G'_{SP} and G''_{SP} against ωa_T for the three samples at lower ω. It is seen that the data for SP44 and SP104 smoothly asymptote to the power law like behavior at the lower ω end. The data for SP24 seems to asymptote to the power law like behavior at significantly lower ω. By pre-shear, however, G'_{SP} and G''_{SP} are reduced gradually and power law like behavior appears in a higher frequency range as shown in Figure 4-6(b) for SP44. On the other hand, separation method cannot be applied even if large scale responses become lower than G^*_{SP} at lower frequency end for SP44 after pre-shear due to large error.

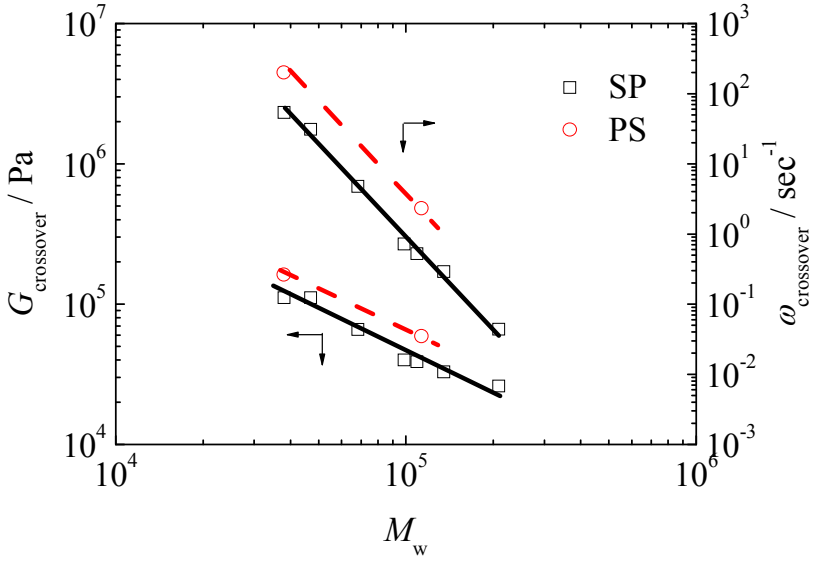

Figure 4-7 Double logarithmic plots of $G_{crossover}$ and $\omega_{crossover}$ against M_w for SPs and PSs at T_r=160 °C. Symbols are denoted in the figure.

For other entangled samples, transition from solid-like to liquid-like behavior is observed with decrease of ω as denoted by maximum in $\tan\delta$ (Figure 4-3(c) and 4-4(c)). With further decrease of ω the data asymptote to the power law like behavior at the lower ω end. To further examine these data, we employ reduced plot using the crossover point of G' and G'' ($G_{crossover}$) and corresponding ω ($\omega_{crossover}$) as the reference point. Figure 4-7 shows M_w dependences of $\omega_{crossover}$ and $G_{crossover}$. From these data, we can point out that plateau region for SP become much broader than PS, while the decrease of G' in plateau region is less significant.

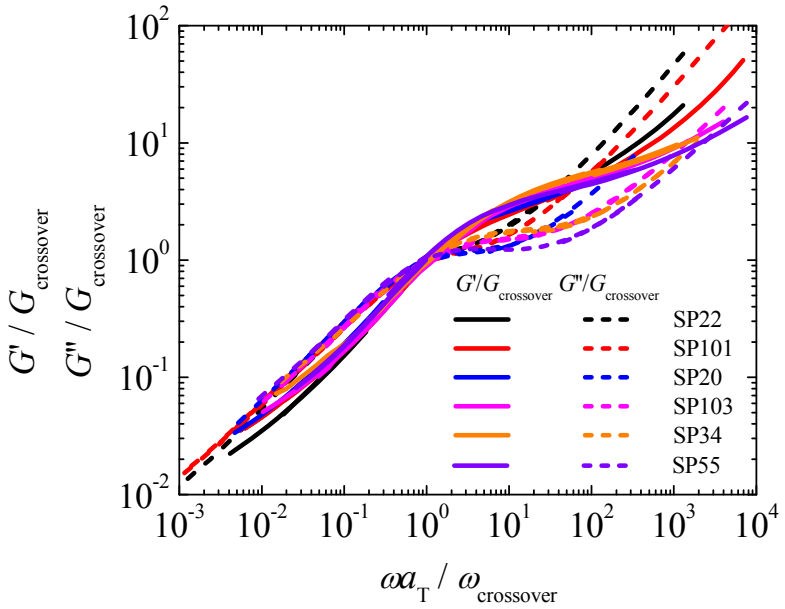

Figure 4-8 Double logarithmic plots of $G^*/G_{crossover}$ against $\omega a_T/\omega_{crossover}$ for entangled SPs copolymers at T_r=160 °C. Symbols are denoted in the figure.

Figure 4-8 shows plots of $G'/G_{crossover}$ and $G''/G_{crossover}$ vs $\omega a_T/\omega_{crossover}$ in double logarithmic scale. The data are different for sample by sample at $\omega a_T/\omega_{crossover} > 1$, while the data at $\omega a_T/\omega_{crossover} < 1$ show universalities in a certain ω region before asymptoting to the power law like behavior with respective magnitudes. These features are qualitatively similar to those reported for not well entangled linear homopolymers reported by Fetters *et al*. The universalities at lower ω can be attributed to terminal relaxation behavior of polymer chains.

An important point seen in this figure is that G'_{SP} asymptote to power law like behavior $\Delta G'_{grain}$ at higher ω than G''_{SP}, and G''_{SP} merge onto (extended) $\Delta G'_{grain}$ at lower ω. This is understandable since contribution of chain relaxation in this region diminish with decrease of ω and the contribution from G'_{chain} disappear at higher ω, since $G''_{chain} \sim \omega > G'_{chain} \sim \omega^2$. This fact suggests that even if asymptotic behavior is only observed for G'_{SP}, it is enough to separate the responses from grains/defects and chain motions, as long as G'_{SP} extended to higher ω is appropriately lower than G^*_{SP}.

4.3.3 Separation Method for SP Copolymers

As already mentioned in chapter 3, we discussed a separation method for responses from grains/defects motions (ΔG^*_{grain}) and the responses from component chains ΔG^*_{chain} in G^*_{SP} by subtraction method, $\Delta G^*_{chain} = G^*_{SP} - \Delta G^*_{grain}$ for SP27 and SP103, irrespective of pre-shear. In chapter 2, we examined viscoelastic properties of low M_w samples including SP27, SP102 and SP101 under steady shear flow, which are in the ordered state. For the highest molecular weight sample SP101, textured fluid like behavior (both shear stress and first normal stress difference are proportional to shear rate) was observed, implying that this sample undergo steady flow with multi grain structure changing with shear rate. From this fact we can conclude the separation method is valid for SPs having say, M_w < 47K. The applicability of the separation method is not clear from the previous work for higher molecular weight samples since we could not reach the steady flow (due to experimental difficulty).

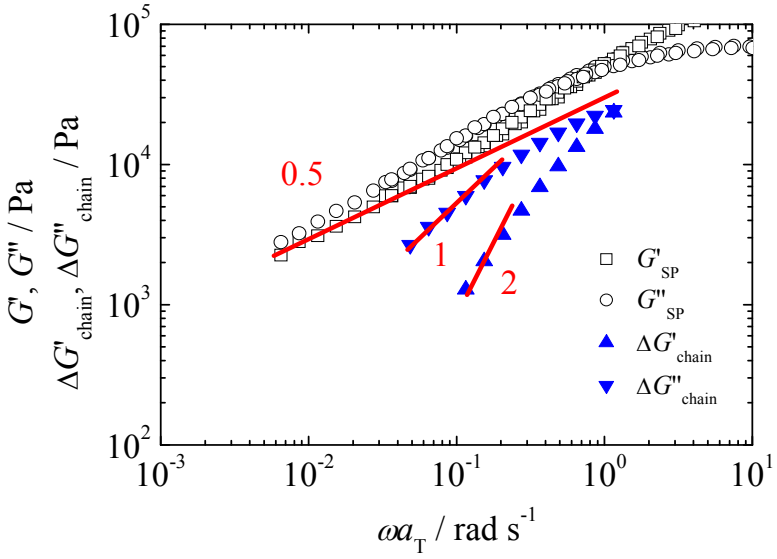

Figure 4-9 Double logarithmic plots of master curves of G^*_{SP} and ΔG^*_{chain} against ωa_T for SP34 at T_r=160 °C, respectively. The straight line with the slope of 0.5 denotes ΔG^*_{grain} used in evaluation of ΔG^*_{chain}. The lines with slope of 1 and 2 are shown in the figure. Other symbols are denoted in the figures.

Figure 4-9 shows an example of subtraction procedure for SP34. In this figure, master curves at lower ω range are shown with $\Delta G'_{grain}$ data (solid line) defined as an asymptotic line with slope of 0.5 fitted to G'_{SP} at low ω end and extended to the lower ω end of plateau region. In this figure, G''_{SP} data do not asymptote to $\Delta G'_{grain}$. Therefore, $\Delta G'_{chain}$ and $\Delta G''_{chain}$ data are obtained by subtracting $\Delta G'_{grain}$ from G'_{SP} and G''_{SP}, respectively, and thus obtained data are also shown in Figure 4-9 (not all but by selected points). There exist ambiguity for the upper limit of ΔG^*_{grain}, but the important point is the fact that ΔG^*_{chain} data at lower ω, where terminal region behavior is observed as denoted by solid lines, are independent of the choice of the upper limit of ΔG^*_{grain}.

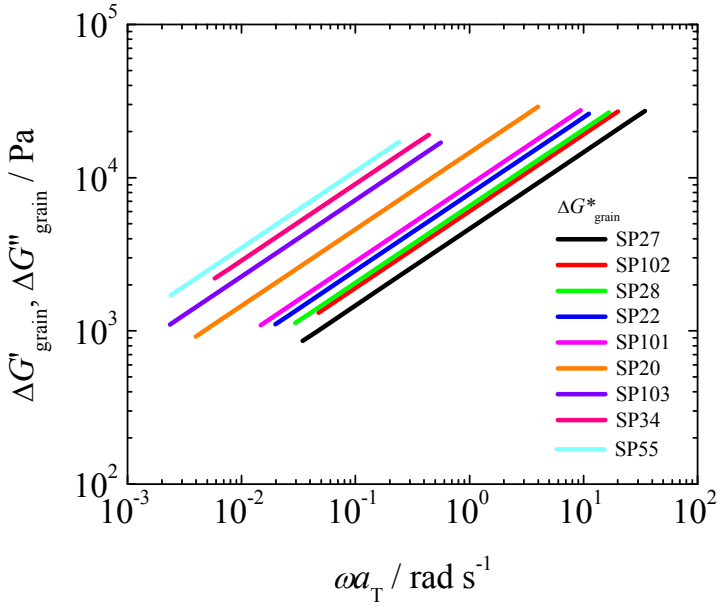

Figure 4-10 Double logarithmic plots of ΔG^*_{grain} against ωa_T for SPs at T_r=160 °C. Symbols are denoted in the figure.

Figure 4-10 shows G'_{grain} data used for the subtraction method. The $\Delta G'_{grain}$ and $\Delta G''_{grain}$ data for 5 lower molecular weight samples (from SP27 to SP101 in Table 4-1) coincided with each other but not for SP20, SP103, SP34 and SP55. If the coincidence of $\Delta G'_{grain}$ and $\Delta G''_{grain}$ becomes criterion for validity of the separation method, we cannot analyse the data for those 4 samples precisely. However, as pointed out in Figure 4-8, we can safely assume that G''_{SP} merge onto (extended)

$\Delta G'_{grain}$ at lower ω. Therefore, we apply the subtraction method to all SP data except for SP104, SP44 and SP24, which did not show liquid-like behavior. Note for SP103 examined in chapter 3, different magnitudes for $\Delta G'_{grain}$ and $\Delta G''_{grain}$ are used to analyze the separation method, which is a little different from ΔG^*_{grain} ($\Delta G'_{grain}$ = $\Delta G''_{grain}$) used in Figure 4-10.

4.3.4 Molecular Weight Dependence of η^0 and J_e

Figure 4-11 show double logarithmic plots of $\Delta G'_{chain}$ and $\Delta G''_{chain}$ against ωa_T. From these data, η^0 and J_e for SP are evaluated by ordinary methods. Note that $\Delta G''_{chain}$ for SP103 in Figure 4-11 is different from that examined in chapter 3 since $\Delta G''_{grain}$ for SP103 in chapter 3 is different from that in Figure 4-10. As a result, the attained η^0 and J_e for SP103 have a little difference. However, such difference is not so serious (say within 20%) and it will not affect the overall discussions about the chain relaxation mechanisms.

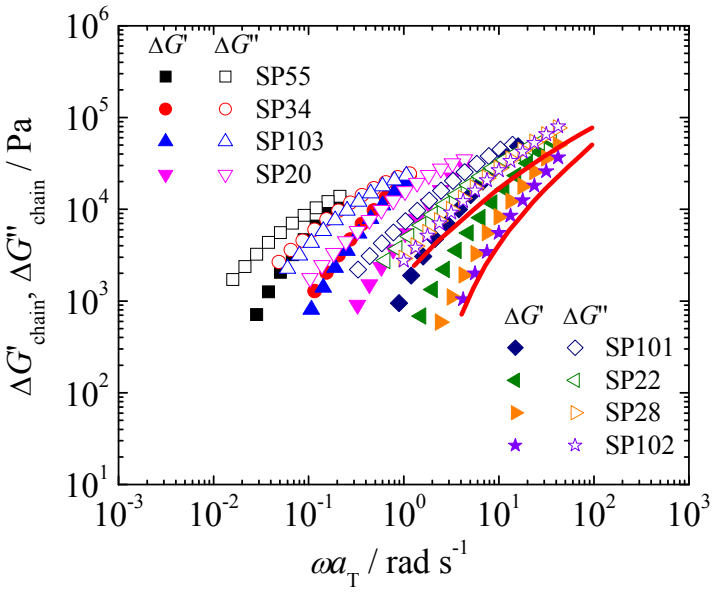

Figure 4-11 Double logarithmic plots of ΔG^*_{chain} against ωa_T for SPs at T_r=160 °C. Symbols are denoted in the figure. The data of ΔG^*_{chain} for SP27 in previous study are also shown with solid lines.

Figure 4-12 and 4-13 respectively show M_w dependences of η^0 and J_e, together with the data obtained for disordered SPs. The data for linear PS are shown by lines in these figures for comparison. The lowest datum of η^0 and J_e in disordered state almost coincide with those of PS. With increase of M_w, η^0 and J_e increase more steeply than those for PS due to the fluctuation effects. The datum for the lowest M_w in the ordered state (SP27) can be smoothly connected with those in disordered state. The absolute values of η^0 and J_e are about a few times and almost one order higher than those for PS at around ODT.

With further increase of M_w, η^0 and J_e become proportional to M_w and then M_w dependence of η^0 become steeper, similar to that of PS but at a higher characteristic M_w than PS. Note that M_w of PS chain in SP does not exceed characteristic molecular weight for J_e, at which entanglement effect appears on J_e.

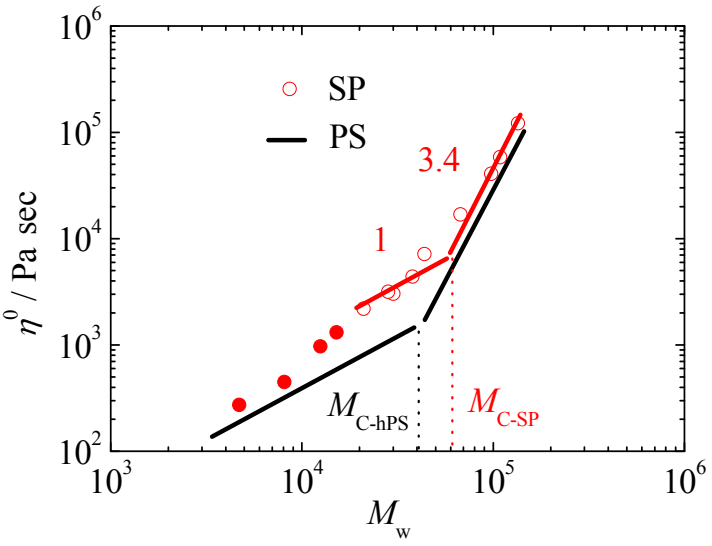

Figure 4-12 Double logarithmic plots of η^0 against M_w for SPs (circle symbols) and PSs (solid lines) at T_r=160 °C. Solid lines with slope of 1 and 3.4 are shown in the figure. The filled symbols are the data for SPs in the disordered state in previous study. Other symbols are denoted in the figure.

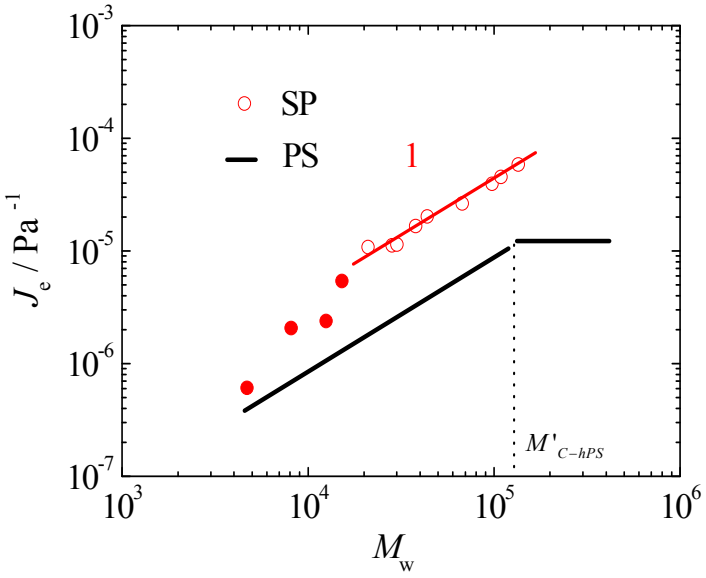

Figure 4-13 Double logarithmic plots of J_e against M_w for SPs (circle symbols) and PSs (solid lines) at T_r=160 °C. Solid line with slope of 1 is shown in the figure. The filled symbols are the data for SPs in the disordered state in previous study. Other symbols are denoted in the figures.

From above results, one might imagine similarity between relaxation process for component chain of SP and star polymers. In contrast to the difference in η^0 between SP and PS, however, η^0 of non-entangled star are not so much different from linear polymers. This fact implies that the relaxation processes of them are significantly different. We further examine the difference between relaxation process of SP and star polymer from distribution of relaxation time.

Products of G_N^0 and J_e can be used as a parameter to examine broadness of relaxation times for entangled polymers. It is known that the value for linear polymer asymptote to limiting value, say 2 ~ 3.5, with increase of number of entanglements, while star polymers have higher $J_eG_N^0$ values which slightly increase with increase of number of entanglements per arm. Figure 4-14 compares $J_eG_N^0$ values for SPs and star polymers [26]. It is clear that the values for SPs are much higher than those of star polymers, denoting much more broad distribution of relaxation time.

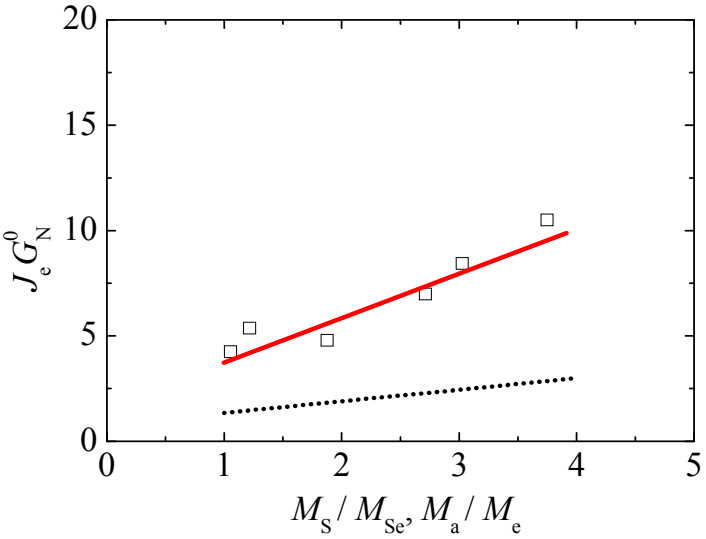

Figure 4-14 Double logarithmic plots of $J_e G_N^0$ against M_S/M_{Se} for entangled SPs at T_r=160 °C. The data for star polymers are also shown in the figure with dotted line. Other symbols are denoted in the figure.

4.3.5 Molecular Weight Dependence of $<\tau>_w$

To summarize all results, we use double logarithmic plots of $<\tau>_w$ against M_w as shown in Figure 4-15, where $<\tau>_w$ ($=\eta^0 J_e$) is an averaged relaxation time close to the longest relaxation time. The data for PS are shown by 3 dotted lines having slopes of 2, 4.4 and 3.4.

At the lowest M_w, the data for SP and PS coincide with each other. With increase of M_w, $<\tau>_w$ steeply increase for SP due to the fluctuation effects. The data for disordered and ordered SP are connected smoothly but the relaxation process changes from relaxation of whole chain for disordered state to independent relaxation of components. The relaxation of component chain is much slower than corresponding linear and star homopolymers since the junction point of components is confined in the interface of domain and the movement are restricted along the interface. However, when there is no entanglement effect for component chains of the same species, they can relax independently so that the M_w dependence of $<\tau>_w$ is the same as non-entangled homopolymers as denoted by solid line in Figure 4-15. When component chains are entangled, M_w dependence of $<\tau>_w$ becomes steeper. In Figure

4-15, two lines are drawn to fit the M_w dependence of $<\tau>_w$. Broken line is parallel to the line for PS, while blue line denotes exponential type equation for $<\tau>$, $<\tau> \sim \exp(\nu M/M_e)$ with $\nu = 2$ as a fitting parameter. It is impossible to judge from the data that which is better representation. However, the fact that higher molecular weight samples (M_w > 200K) showed power law like behavior without showing liquid-like behavior strongly suggests exponential type is close to the behavior of SP diblocks. When the number of entanglements is low, the entanglements between the chains from opposite interface may be rare so that chain relaxation can be observed. Power law like behavior due to the responses from grains/defects motions are overlapped with chain relaxation in a certain range of time scale. With increase of number of entanglements, relaxation time increases exponentially and finally another power law like behavior, which is qualitatively the same as predictions of theories, become dominant.

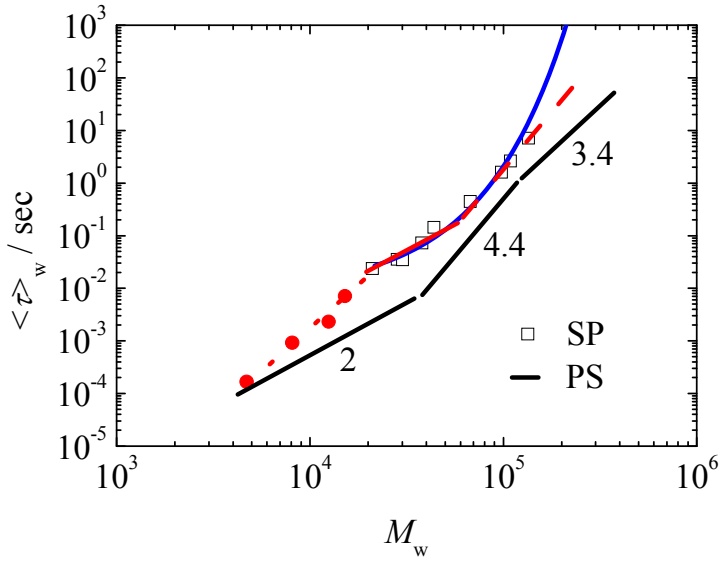

Figure 4-15 Double logarithmic plots of $<\tau>_w$ against M_w for all SP samples at T_r=160 °C. The filled symbols show the data for SP in the disordered state in previous study. The data for PS are shown by solid lines with slope of 2, 4.4 and 3.4, respectively. Other symbols are denoted in the figure.

4.4 Summary

In this chapter, viscoelastic properties of a series of symmetric SP copolymers

with different molecular weights are examined in the ordered state in comparison with corresponding PS. By using separation method of responses from large scale motions of grains/defects and molecular responses, chain relaxation of component chains in lamellar structure are studied as a function of molecular weight.

In combination with the data in previous chapter, the data for disordered and ordered SP are connected smoothly but the relaxation process changes from relaxation of whole chain for disordered state to independent relaxation of components. The relaxation of component chain is much slower than corresponding linear and star homopolymers since the junction point of components is confined in the interface of domain and the movement are restricted along the interface. When the number of entanglements is low, the entanglements between the chains from opposite interface may be rare so that chain relaxation can be observed. Power law like behavior due to the responses from grains/defects motions are overlapped with chain relaxation in a certain range of time scale. With increase of number of entanglements, relaxation time increases exponentially and finally another power law like behavior, which is qualitatively the same as predictions of theories, become dominant.

References

[1]Bates FS, Fredrickson GH, *Annu. Rev. Phys. Chem.*, **41**, 525 (1990)

[2]Bates FS, *Macromolecules*, **17**, 2607 (1984)

[3]Bates FS, Rosedale JH, *Macromolecules*, **23**, 2329 (1990)

[4]Bates FS, Rosedale JH, Fredrickson GH, *J. Chem. Phys.*, **92**, 6255 (1990)

[5]Kawasaki K, Onuki A, *Phys. Rev. A*, **42**, 3664 (1990)

[6]Witten TA, Leibler L, Pincus P A, *Macromolecules*, **23**, 824 (1990)

[7]Rubinstein M, Obukov SP, *Macromolecules*, **26**, 1740 (1993)

[8]Ohta T, Enomoto Y, Harden JL, Doi M, *Macromolecules*, **26**, 4928 (1993)

[9]Doi M, Harden JL, Ohta T, *Macromolecules*, **26**, 4935 (1993)

[10]Takahashi Y, Ochiai N, Matsushita Y, Noda I, *Polym. J.*, **28**, 1065 (1996)

[11]Takahashi Y, Noda I, Nagasawa M, *Macromolecules*, **18**, 2220 (1985)

[12]Colby RH, *Curr. Opin. Colloid Interface Sci.*, **1**, 454 (1996)

[13]Watanabe H, "*Rheology of Multiphase Polymeric Systems*", In: Araki T, Qui TC, Shibayama M, "*Structure and Properties of Multiphase Polymeric Materials*", New York: Marcel Dekker (1998)

[14]Kossuth MB, Morse DC, Bates FS, *J. Rheol.*, **43**, 167 (1999)

[15]Spontak RJ, Patel NP, *Curr. Opin. Colloid Interface Sci.*, **5**, 334 (2000)

[16]Hamley IW, *Curr. Opin. Colloid Interface Sci.*, **5**, 342 (2000)

[17]Hamley IW, *J. Phys. Condens. Matter*, **13**, R643 (2001)

[18]Lodge TP, *Macromol. Chem. Phys.*, **204**, 265 (2003)

[19]Yokoyama H, *Mater. Sci. Eng. R*, **53**, 199(2006)

[20]Ball RC, McLeish TCB, *Macromolecules*, **22**, 1911 (1989). Yurasova TA, McLeish TCB, Semenov AN, *Macromolecules*, **27**, 7205 (1994)

[21]Doi M, Edwards SF, "*The Theory of Polymer Dynamics*", 2nd ed., Oxford: Oxford University Press (1988)

[22]Matsushita Y, Nakao Y, Saguchi R, Choshi H, Nagasawa M, *Polym. J.*, **18**, 493 (1986)

[23]Matsushita Y, Nakao Y, Shimizu K, Noda I, Nagasawa M, *Macromolecules*, **21**, 2790 (1988)

[24]Takahashi Y, Kitade S, Noda M, Ochiai N, Noda I, Imai M, *et al.*, *Polym. J.*, **30**, 388 (1998)

[25]Graessley WW, "*Polymer Liquids & Networks: Dynamics and Rheology*", London and New York: Talyor & Francis Group (2008)

[26] Watanabe H, *Prog. Polym. Sci.*, **24**, 1253 (1999)

Chapter 5 Conclusions

Viscoelastic properties of symmetric SP diblock copolymers with wide M_w range are examined in the disordered and ordered states. For SP with relatively lower M_w in the disordered state, fluctuation effects are observed by combination of dynamic and steady shear flow measurements based on the temperature dependence of χ. The fluctuation effects on viscoelastic properties can be suppressed by high shear rate and completely disappear at around $\chi N < 2 \sim 3$ for SP copolymers. As M_w increases, $<\tau>_w$ steeply increases for SP due to the fluctuation effects. The data for disordered and ordered SP can be connected smoothly but the relaxation process changes from relaxation of whole chain for disordered state to independent relaxation of components for ordered state.

For SP with lower M_w in the ordered state, the responses from large scale motions of lamellar grains/defects, ΔG^*_{grain}, becomes more apparent after appropriate pre-shear and/or annealing. When asymptotic $\omega^{0.5}$ dependence of ΔG^*_{grain} are observed at low frequency end and whose magnitude become lower than G^*_{SP}, the responses of components ΔG^*_{chain} having Rouse like modes can be successfully separated by subtracting method examined in this study, irrespective of pre-shear or annealing. By combining ΔG^*_{grain}, ΔG^*_{chain} and the data for hPS, G^*_{hPS} at higher ω, G^*_{SP} data can be well approximated in a whole frequency range of the measurement. For SP with higher M_w in the ordered state, however, power law like behavior without showing liquid-like behavior is observed.

The relaxation of component chain is much slower than corresponding linear and star homopolymers since the junction point of components is confined in the interface of domain and the movement is restricted along the interface. When the number of entanglements is low, the entanglements between the chains from opposite interface may be rare so that chain relaxation can be observed. Power law like behavior due to the responses from grains/defects motions are overlapped with chain relaxation in a certain range of time scale. With increase of number of entanglements, relaxation time

increases exponentially and finally another power law like behavior, which is qualitatively the same as predictions of theories, become dominant.

Publications

1. Long Fang, Yoshiaki Takahashi, Atsushi Takano, Yushu Matsushita. A Separation Method of Responses from Large Scale Motions and Chain Relaxations for Viscoelastic Properties of Symmetric Poly(styrene-*b*-2-vinylpyridine)s in the Ordered State. *Nihon Reoroji Gakkaishi (Journal of the Society of Rheology, Japan)* vol.41(2), pp77-85 (2013).
2. Yoshiaki Takahashi, Long Fang, Atsushi Takano, Naoya Torikai, Yushu Matsushita. Viscoelastic Properties of Low Molecular Weight Symmetric Poly(styrene-*b*-2-vinylpyridine)s in the Ordered and Disordered States under Steady Shear Flow. *Nihon Reoroji Gakkaishi (Journal of the Society of Rheology, Japan)* vol.41(2), pp87-93 (2013).
3. Long Fang, Yoshiaki Takahashi, Atsushi Takano, Yushu Matsushita. Molecular Weight Dependence of Viscoelastic Properties for Symmetric Poly(styrene-*b*-2-vinylpyridine)s in the Ordered State. (To be submitted)

Acknowledgment

How time flies! The time has come for me to say goodbye with Japan. During the three years in Kyushu University, I am extremely grateful to **Associate Prof. Yoshiaki Takahashi**. He is wealthy in knowledge and friendly in manner. I cannot graduate on time without his help and he taught me a lot in professional knowledge and creative thoughts. I was deeply influenced by his accuracy and strict method, which is of vital importance for my career in future. I also want to thank **Assistant Prof. Akihiko Takada**, who was very kind and helped me a lot not only in research but also in daily life. He helped me improve Japanese and encouraged me to speak more.

As the collaborators of this study, I want to express my sincere thanks to **Prof. Yushu Matsushita** and **Associate Prof. Atsushi Takano** in Nagoya University, who helped me polymerize and characterize all of the samples. Without them, I cannot carry out any experiment. I also want to thank Mr. Nao Yamada and other staff in Anton Paar Japan for their assistance in SAXS measurements.

Thanks for all of the students in this lab. I felt very glad to stay with all of you during the three years and I learned a lot with the students from different countries. I miss the days we went to travel and play together. At last, I want to thank my family for supporting and helping me finish this thesis successfully. Without their help, I cannot insist on moving forward.

Above all, please allow me to express my sincere thanks to all of you.